

# **Identification of a core gene-regulatory trajectory to terminal T cell dysfunction in human tumors and discovery of potential target genes involved in this process**

Dissertation zur Erlangung des Doktorgrades der  
Naturwissenschaften (Dr. rer. nat.) der Fakultät für  
Biologie und Vorklinische Medizin der Universität  
Regensburg

vorgelegt von

**Dania Riegel**

aus

Bonn

im Jahr

2022



# **Identification of a core gene-regulatory trajectory to terminal T cell dysfunction in human tumors and discovery of potential target genes involved in this process**

Dissertation zur Erlangung des Doktorgrades der  
Naturwissenschaften (Dr. rer. nat.) der Fakultät für  
Biologie und Vorklinische Medizin der Universität  
Regensburg

vorgelegt von

**Dania Riegel**

aus

Bonn

im Jahr

2022



Das Promotionsgesuch wurde eingereicht am:  
**24.02.2022**

Die Arbeit wurde angeleitet von:  
**Prof. Dr. rer. nat. Michael Rehli**

Unterschrift:



Parts of the here presented data are taken from a manuscript draft which shall be published in the future:

Integrated single-cell profiling dissects cell-state-specific enhancer landscapes of human tumor-infiltrating T cells. **Dania Riegel\***, Elena Romero Fernández\*, Malte Simon\*, Akinbami Raphael Adenugba, Katrin Singer, Roman Mayr, Florian Weber, Charles D. Imbusch, Marina Kreutz, Benedikt Brors, Ines Ugele, Jens M. Werner, Peter J. Siska, Christian Schmidl.

\*Equally contributing first authors.

For the manuscript draft I established single-cell ATAC-seq and performed single-cell ATAC-seq of primary TILs and PBMCs. Further, I performed FACS analysis and restimulation assays of primary TILs and PBMCs. Christian Schmidl performed bioinformatic analysis of the single-cell ATAC-seq, and bulk ATAC-seq data, respectively.

For the thesis I conducted research about putative target genes and selected putative target genes together with Christian Schmidl. I expanded human melanoma TIL209 with the help of Jasmin Mühlbauer (AG Beckhove, LIT). Further, I established CRISPR/Cas9 in TIL209 cells using the Neon™ transfection system, and with help of my Bachelor student Meike Neureither using the Nucleofector™ system, respectively. I performed target knock-out for validation assays. I further established, performed and analyzed killing assays and FACS analysis of genome-edited TILs. I performed flow cytometry based analysis of targets in TIL209 and primary TILs and I performed bulk ATAC-seq of TIL209. Furthermore, I conducted all FACS analysis and performed respective statistical analysis. Yvonne-Natascha-Susanne Weiss (AG Jantsch, UKR) performed Ca<sup>2+</sup> flux assays. The FACS Sort Facility of our institute conducted cell sorting and the NGS Core Facility performed sequencing and demultiplexing.



# Contents

<b>1 Abstract</b>	<b>1</b>
1.1 Abstract . . . . .	1
1.2 Zusammenfassung . . . . .	2
<b>2 Introduction</b>	<b>5</b>
2.1 The immune system fighting cancer . . . . .	5
2.1.1 The concept of T cell exhaustion in cancer . . . . .	9
2.1.2 Immunotherapy and its limits . . . . .	14
2.2 Epigenetics and chromatin remodeling as determinants of cell identity and function . . . . .	18
2.2.1 Epigenetic regulation of T cell differentiation and function . . .	20
2.3 Studying and manipulating cell states . . . . .	22
2.3.1 Open chromatin profiling on the single cell level . . . . .	23
2.3.2 CRISPR/Cas9 based genome editing . . . . .	25
2.4 Aim of the thesis . . . . .	27
<b>3 Material and Methods</b>	<b>29</b>
3.1 Material . . . . .	29
3.1.1 Laboratory consumables and equipment . . . . .	29
3.1.2 Reagents and media . . . . .	31
3.1.3 Solutions, buffer and media . . . . .	34
3.1.4 Cell lines . . . . .	35
3.1.5 Primary human samples for scATAC-seq . . . . .	35

## Contents

---

3.1.6	Antibodies and fluorescent molecules . . . . .	36
3.1.7	Commercial assays . . . . .	38
3.1.8	Oligonucleotides . . . . .	39
3.1.9	Software and Algorithms . . . . .	41
3.2	Methods . . . . .	43
3.2.1	Ethics . . . . .	43
3.2.2	Cell culture . . . . .	43
3.2.3	Sample collection and cell preparation . . . . .	44
3.2.4	FACS staining, acquisition and cell sorting for ATAC-seq experiments . . . . .	45
3.2.5	Establishment of scATAC using a species mixing experiment . . . . .	47
3.2.6	Optimized scATAC-seq protocol for primary samples . . . . .	49
3.2.7	Bulk ATAC-seq . . . . .	50
3.2.8	Pre-processing and analysis of bulk ATAC-seq . . . . .	51
3.2.9	Pre-processing and analysis of scATAC-seq . . . . .	52
3.2.10	TIL209 expansion and cell culture . . . . .	55
3.2.11	CRISPR/Cas9-based genome editing via electroporation . . . . .	56
3.2.12	TIDE assay for determination of INDEL mutations after CRISPR/Cas9 . . . . .	59
3.2.13	Quantification of CRISPR/Cas9 KO efficiency via flow cytometry . . . . .	59
3.2.14	Ca <sup>2+</sup> influx assay . . . . .	60
3.2.15	Image-based killing assay . . . . .	61
3.2.16	Target staining in primary TILs . . . . .	62
3.2.17	Statistical analysis . . . . .	63
<b>4</b>	<b>Results</b>	<b>65</b>
4.1	Establishment of plate based single-cell ATAC sequencing . . . . .	65

---

4.2	Single-cell open chromatin profiling and functional analysis of human CD8 <sup>+</sup> TILs and controls . . . . .	67
4.2.1	Improvement of plate based single-cell ATAC sequencing for primary samples . . . . .	68
4.2.2	Single-cell ATAC sequencing of human CD8 <sup>+</sup> TILs and peripheral blood derived CD8 <sup>+</sup> T cells worked reliably . . . . .	69
4.2.3	Implementation of controls and public available data . . . . .	70
4.2.4	FACS-based phenotypical and functional characterization of TILs . . . . .	71
4.3	Unbiased analysis reveals heterogeneity and distinct IT relevant cell states among human CD8 <sup>+</sup> TILs . . . . .	74
4.3.1	Different cell states can be identified by gene activity of marker genes . . . . .	74
4.3.2	CD8 <sup>+</sup> TIL states can be annotated by projection of public T cell signatures . . . . .	77
4.4	Dissection of gene-regulatory cues, differential gene regulation and the tissues' influence on human CD8 <sup>+</sup> TILs . . . . .	78
4.4.1	CD8 <sup>+</sup> TIL states are driven by differential gene-regulatory mechanisms . . . . .	79
4.4.2	The specific tumor tissue might influence the chromatin landscape of CD8 <sup>+</sup> TILs . . . . .	82
4.5	Identification of an entity-shared trajectory to terminal dysfunction of human TILs . . . . .	84
4.6	Selection of novel, entity-shared target genes that might influence T cell (dys)function . . . . .	91
4.7	Establishment of CRISPR/Cas9 based genome editing in TIL209 cells	95
4.7.1	Comparison of knock-out efficiency using different electroporation devices and programs . . . . .	97

4.7.2	gRNA screening is necessary to receive adequate knock-out efficiency . . . . .	101
4.7.3	Genome editing does not reflect target protein degradation . .	103
4.8	Target validation in TIL209 cells and primary TILs . . . . .	104
4.8.1	VDR and EOS knock-out decrease Ca <sup>2+</sup> flux in TIL209 cells .	105
4.8.2	Target knock-out might change killing capacity of TIL209 cells .	107
4.8.3	VDR and EOS are co-expressed with TOX in primary TILs . . .	109
<b>5</b>	<b>Discussion</b>	<b>111</b>
5.1	Heat or hypoxia as well as the tumor tissue could influence chromatin remodeling of TILs . . . . .	112
5.2	A core trajectory to terminal T cell dysfunction can be defined exclusively by profiling multiple entities . . . . .	114
5.3	Chromatin profiling of human TILs creates a resource of potential immunotherapeutically relevant targets . . . . .	116
5.4	Challenges and pitfalls of a CRISPR/Cas9 based target screening using <i>in vitro</i> expanded TILs . . . . .	122
5.5	Limitations of the study . . . . .	123
5.6	Conclusion and Outlook . . . . .	124
<b>6</b>	<b>REFERENCES</b>	<b>127</b>
<b>7</b>	<b>Appendix</b>	<b>157</b>
7.1	List of Abbreviations . . . . .	157
7.2	List of Units . . . . .	160
7.3	List of Dimensions . . . . .	160
7.4	List of Figures . . . . .	161
7.5	List of Tables . . . . .	163
7.6	Acknowledgments . . . . .	164

# 1 Abstract

## 1.1 Abstract

Diseases such as cancer are often associated with suppression of the immune system. Thereby, cytotoxic CD8<sup>+</sup> T cells, originally meant to kill the cancerous cells, tend to become dysfunctional, as they are struggling with long term exposure to antigens and the immunosuppressive tumor microenvironment. As a consequence, tumor-specific CD8<sup>+</sup> T cells often fail to fully eliminate cancer cells. Much research has been conducted on T cell exhaustion in the context of chronic viral infection. However, it remains unknown, whether gene-regulation patterns causing terminal T cell exhaustion in cancer are specific to cancer type or tumor microenvironment or, whether they are governed by a universal exhaustion program. ATAC-seq (Assay for Transposase-Accessible Chromatin using sequencing) is a great tool to identify cell states based on their open chromatin landscape. Therefore, we used this method to investigate chromatin states of CD8<sup>+</sup> tumor-infiltrating lymphocytes, isolated from HCC (Hepatocellular Carcinoma), RCC (Renal Cell Carcinoma), and HNSCC (Head and Neck Squamous Cell Carcinoma) patients, on the single cell level. This approach enables unbiased identification of discrete TIL (tumor-infiltrating lymphocytes) subpopulations as well as key transcription factors and gene-regulatory elements that determine different cell states.

Bioinformatic analysis verified terminal exhausted TIL populations in every cancer type except HNSCC and revealed candidate determinants of exhaustion common to RCC and HCC, as well as to BCC (Basal Cell Carcinoma, integrated data from a

## 1. ABSTRACT

---

published study). Further, we sought to determine the role of these candidates using CRISPR (Clustered Regularly Interspaced Short Palindromic Repeats) knock-out in expanded TILs from melanoma patients.

We anticipate that our findings will improve understanding gene-regulatory mechanisms leading to terminal T cell dysfunction in different human cancer types and help to identify factors, which could improve immunotherapies such as CAR T-cell therapy.

## 1.2 Zusammenfassung

Krankheiten wie Krebs stehen oft im Zusammenhang mit einer Unterdrückung des Immunsystems. Es wurde beobachtet, dass zytotoxische CD8<sup>+</sup> T-Zellen, die eigentlich entartete Krebszellen zerstören sollen, dysfunktionell werden. Als Grund dafür werden die langanhaltende Tumor-Antigenpräsentation und das immunsupprimierende Tumormikromilieu genannt. Infolgedessen gelingt es tumorspezifischen CD8<sup>+</sup> T-Zellen oft nicht, Krebszellen vollständig zu eliminieren. Es wurde bislang schon intensiv an der sogenannten "Erschöpfung" von T-Zellen im Zusammenhang mit einer chronischen Virusinfektion geforscht. Es konnte bisher jedoch nicht beantwortet werden, ob Genregulationsprogramme, die eine terminale T-Zell-Erschöpfung im Zusammenhang mit Tumorerkrankungen verursachen, spezifisch für die Krebsart bzw. für die Mikroumgebung des Tumors sind oder, ob sie universell einheitlich sind. ATAC-seq (Test für Transposase-zugängliches Chromatin durch Sequenzierung) ist ein großartiges Werkzeug, um Zellzustände anhand ihrer unterschiedlichen Chromatin-Zugänglichkeit zu identifizieren. Daher haben wir diese Methode verwendet, um Chromatinzustände von CD8<sup>+</sup> tumorinfiltrierenden Lymphozyten, die aus Patienten mit Hepatozellulärem Karzinom, Nierenzellkarzinom oder Kopf-Hals-Plattenepithelkarzinom isoliert wurden, auf Einzelzellebene zu untersuchen. Dieser Ansatz ermöglicht eine unvoreingenommene Identifizierung spezifischer Zell-Subpopulationen sowie wichtiger Transkriptionsfaktoren und genregula-

torischer Elemente, die die unterschiedlichen Zellzustände bestimmen.

Unsere bioinformatische Analyse dieses Datensatzes ergab, dass dysfunktionelle CD8<sup>+</sup> tumorinfiltrierende Lymphozyten in allen Krebsarten außer Kopf-Hals- Plattenepithelkarzinomen vorzufinden sind. Desweiteren entdeckten wir mögliche bestimmende Faktoren, die der T-Zell-Dysfunktion in Nieren-, Leber-, sowie Basalzellkarzinomen (publizierte Daten, die in unseren Datensatz integriert wurden) zugrundeliegen könnten. Darüberhinaus versuchten wir, die Rolle dieser Faktoren (Kandidatengene) mithilfe von CRISPR (Clustered Regularly Interspaced Short Palindromic Repeats) basierten Gen-Knockouts in expandierenden tumorinfiltrierenden Lymphozyten von Melanompatienten zu bestimmen.

Wir gehen davon aus, dass unsere Ergebnisse das Verständnis von Genregulationsmechanismen, die zu einer terminalen T-Zell-Dysfunktion bei verschiedenen menschlichen Krebsarten führen, verbessern werden. Wir glauben desweiteren, dass unsere Ergebnisse dazu beitragen können, Faktoren zu identifizieren, die Immuntherapien wie die CAR-T-Zelltherapie verbessern könnten.



## 2 Introduction

### 2.1 The immune system fighting cancer

Cancer is a term for a very diverse group of deadly, genetic diseases in which cells acquire mutations, grow aberrantly and gain the ability to spread in the body, which is then referred to as metastasis [136]. Although major breakthroughs in cancer therapy have been achieved in the past decade [73], cancer is still the leading cause of death worldwide [195].

In 2000, Douglas Hanahan and Robert A. Weinberg proposed the first six hallmarks of cancer, which they extended over time to ten hallmarks [76, 77, 75] that refer to the biological capabilities, which drive malignant growth. They include independence of external growth signals, evading growth suppressors, resisting cell death, sustained angiogenesis, replicative immortality, tissue invasion and metastasis, genome instability, deregulated metabolism, escape from the immune response, tumor promoting inflammation, phenotypic plasticity as well as cell senescence (Figure 2.1). Furthermore, nonmutational epigenetic reprogramming and polymorphic microbiomes have just recently been mentioned to be characteristics that enable these hallmarks. The acquisition of all these capabilities allows cancer to grow uncontrolled and overcome the bodies' incorporated protection mechanisms.

## 2. INTRODUCTION

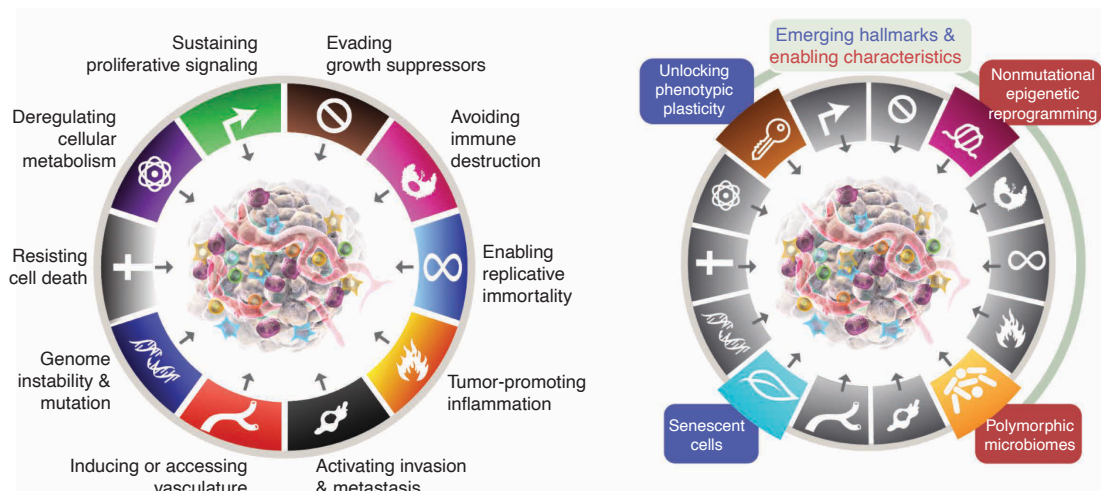


**Figure 2.1: The hallmarks of cancer**

The hallmarks of cancer (left) and further emerging hallmarks and enabling characteristics (right) as proposed by Douglas Hanahan and Robert A. Weinberg in 2022. Reprinted from [75] with permission from AACR.

Our immune system protects us from foreign pathogens, is composed of a variety of effector cells and molecules and can be divided into two main parts. The innate immune system is responsible for an immediate response [22], whereby the adaptive immune system concertedly time-delayed but very specific and powerful antigen-specific T- and B lymphocytes. This includes both cell-mediated as well as humoral immunity components and creates immunological memory to serve protection even upon future encounters with pathogens [134]. T cells develop in the thymus, carry an antigen-specific T cell receptor (TCR) and are divided into two major subtypes: CD4<sup>+</sup> T helper cells, which express the co-receptor cluster of differentiation (CD) 4 and recognize antigens via major histocompatibility complex (MHC) class II and CD8<sup>+</sup> cytotoxic T lymphocytes (CTLs), which are specific for intracellular antigens presented on MHC class I molecules [134, 20]. Once activated, CTLs can induce apoptosis in infected cells. Sufficient T cell priming requires at least two signals: the first one is acquired by engagement of the TCR with its cognate antigen presented by MHC molecules on antigen presenting cells (APCs), the second one is applied by encounter of the T cells' co-stimulatory receptors, for example of CD28 T cells

with its ligands expressed on APCs. Third, specific cytokines stimulate differentiation into effector T cell subsets [134]. To maintain self-tolerance and a consistent but not over-reactive T cell activation, a negative feedback mechanism is needed. Co-inhibitory receptors, so-called immune checkpoints, are upregulated on T cells after their activation [137]. Upon binding to their ligands, downstream signaling dampens the T cell response, thereby preventing potential tissue damage or autoimmune reactions [169]. CTLA4 (cytotoxic T-lymphocyte-associated protein 4) and PD1 (Programmed cell death protein 1) are two of the best known co-inhibitory receptors expressed by T cells [145, 141, 140, 142]. CTLA4 fine-tunes T cell activation mainly in lymph nodes, since the ligands are expressed by APCs, whereby PD1 plays a role in the periphery where tissue cells express the ligands PD-L1 and PD-L2 (Programmed death-ligand 1 and 2).

Already In 1909, Paul Ehrlich proposed that the immune system is also able to recognize and eliminate nascent transformed cells, not only pathogens [84]. Later on, Frank MacFarlane Burnet and Lewis Thomas formulated the theory of cancer immunosurveillance [26, 200]. The so called “cancer-immunity cycle” is a framework, which describes how the immune response against cancer is initiated and maintained (Figure 2.2, [30]). This cycle consists of seven major steps and starts with dying tumor cells, which release antigens. These antigens are often mutated due to the transformation from normal to cancer cells (so called neoantigens) and therefore can be recognized as foreign from the adaptive immune system. APCs take up these neoantigens and present them to antigen specific T cells in the lymph nodes, which subsequently become activated. After activation, CD8<sup>+</sup> T cells differentiate into cytotoxic effector cells and infiltrate the tumor (then referred to as tumor-infiltrating lymphocytes, TILs) where they kill the target tumor cells via cytolytic activity and secretion of inflammatory cytokines. The tumor cell killing leads to additional antigen release and can further promote the immune response.

However, research has been shown that this process is more complex and protective immunity can barely be maintained long-term. Indeed, it became clear that the

## 2. INTRODUCTION

---

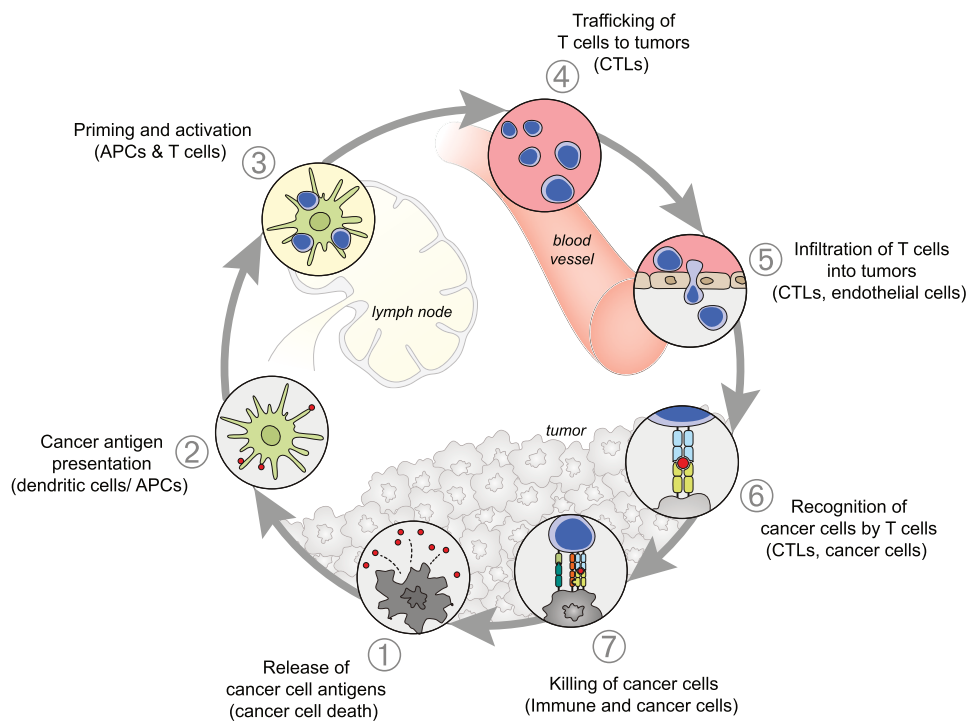


### Figure 2.2: The cancer immunity cycle

Cancer immunity is generated and ideally amplified in a cyclic process, here pictured for the cytotoxic T cell immune response. The cyclic process consists of seven major steps, which are depicted and described above. Abbreviations are as follows: APCs, antigen presenting cells; CTLs, cytotoxic T lymphocytes. Reprinted from [30] with permission from Elsevier.

immune system not only prevents tumor growth, but also edits the tumors immunogenicity in an unfavorable manner. This process is called cancer immunoediting and consists of three phases: elimination, equilibrium and escape [211]. In the first phase, tumor cells are eliminated by cells of the innate and adaptive immune system. The nature of cancer with its constant genetic alterations eventually leads to tumor cell variants, which evade the immune system and subsequently enter the equilibrium phase. Within this phase, not all cells can be recognized by the immune system, thus tumor growth and destruction is in balance. Over time the selection pressure from the immune response leads to dominance of tumor cell clones with decreased immunogenicity. In the escape phase, tumor cells develop mechanisms to evade and inhibit anti-tumor immunity, for example via fostering an immunosuppressive tumor microenvironment (TME). One of the mechanisms tumor cells hijack to evade the immune attack is the expression of inhibitory ligands, which by binding to the co-inhibitory receptors on CD8<sup>+</sup> T cells suppress the latter [48, 225].

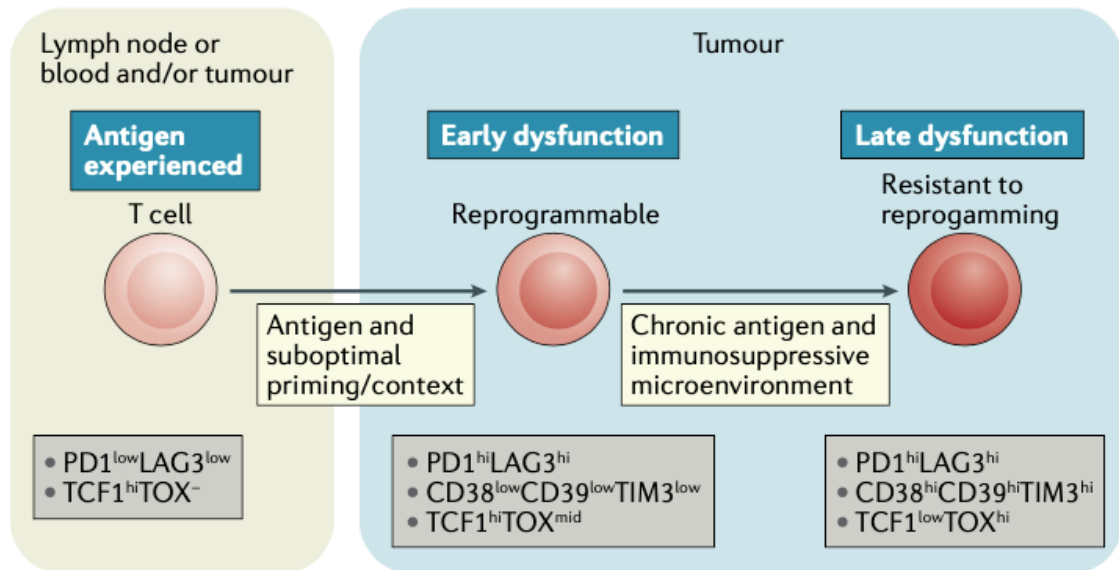
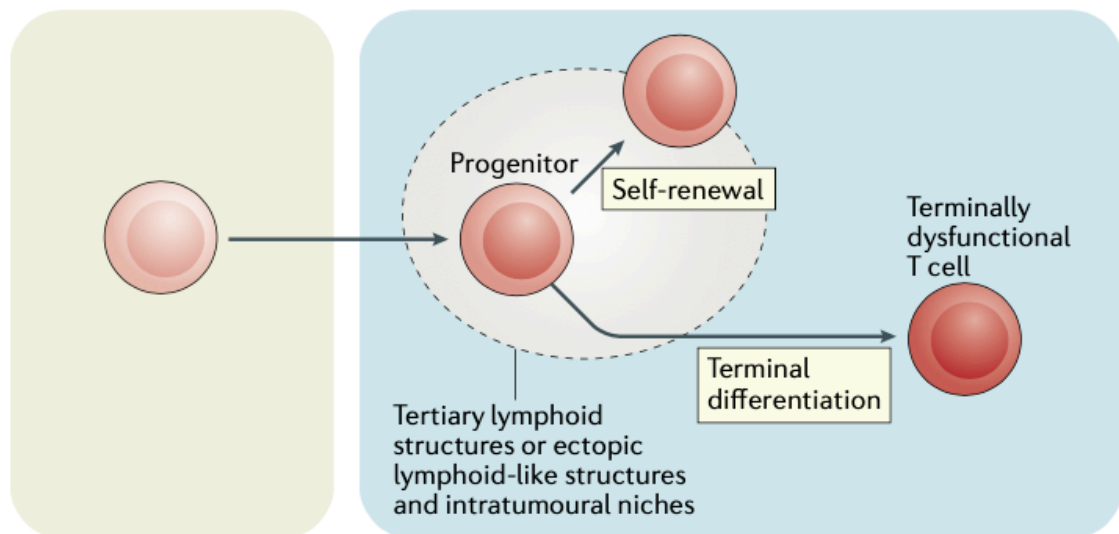
### 2.1.1 The concept of T cell exhaustion in cancer

Tumor-reactive cytotoxic CD8<sup>+</sup> T cells are considered to be the main cell type exerting tumor cell killing in solid cancers [134, 145, 17, 69, 185]. However, despite their presence, tumors progress. This so called 'Hellstrom paradox' was first described in 1968 by Ingegerd and Karl Erik Hellstrom [82]. They suggested that intratumoral CD8<sup>+</sup> T cells become dysfunctional during tumor progression. Indeed, multiple studies have shown that CD8<sup>+</sup> TILs are often in a so called dysfunctional or 'exhausted' state, characterized by reduced cytotoxic effector function (failure to produce IFN $\gamma$ , TNF $\alpha$ , granzymes or perforin) and impaired proliferative capability. A further hallmark is sustained expression of inhibitory receptors (such as PD1, CTLA4, TIM3 (T-cell immunoglobulin and mucin-domain containing-3), LAG3(Lymphocyte-activation gene 3)) and metabolic enzymes CD38 (cyclic ADP ribose hydrolase) and CD39 (ecto-nucleoside triphosphate diphosphohydrolase) on the cell surface

## *2. INTRODUCTION*

---

[232, 230, 110, 226, 36, 113, 35, 184, 98, 4, 181].

**a Tumour: linear differentiation model****b Tumour: branched differentiation model****Figure 2.3: Differentiation models of CD8+ TILs**

(A) Model of linear differentiation to dysfunctional CD8+ T cells. Suboptimal T cell activation induces early dysfunction, which is a plastic cell state still reprogrammable by therapeutic intervention. Chronic antigen encounter and a suppressive TME lead to late dysfunction, a fixed cell state resistant to interventions. The different cell states are driven by epigenetic mechanisms and can be distinguished by differential expression of cell surface markers and transcription factors. (B) Model of branched differentiation of dysfunctional CD8+ T cells. In this model, progenitor-like dysfunctional T cells reside in special intratumoural niches, likely lymphoid structures, which facilitate maintenance of the progenitor state. Progenitor-like cells are thought to give rise to terminal differentiated dysfunctional cells. Reprinted by permission from Springer Nature Customer Service Centre GmbH: Springer Nature, CD8 T cell differentiation and dysfunction in cancer by Mary Philip et al., Copyright© 2021 [150].

## 2. INTRODUCTION

---

The term 'T cell exhaustion' refers to a CD8<sup>+</sup> T cell state originally detected in chronic viral infection, where persistence of the pathogen leads to a stalemate situation between host and pathogen [218]. Since dysfunctional TILs share key features with the exhausted T cells found in chronic infections, 'T cell exhaustion' is used in the context of cancer to describe TIL dysfunction in progressive tumors [150]. It is thought that chronic TCR stimulation via persistent antigen exposure in the tumor as well as the immunosuppressive TME (which includes among others regulatory T cells [174], myeloid derived suppressor cells (MDSCs), M2 macrophages [139], co-inhibitory receptor signaling [11], suppressive cytokines and unfavorable metabolic conditions [63, 17]) trigger differentiation into this cell state.

Due to technological advancement in single cell transcriptional and open chromatin profiling, researchers were able to begin dissecting the molecular mechanisms underlying T cell dysfunction [131, 177, 231, 192, 172, 9]. This research uncovered that dysfunctional T cells are heterogeneous and consist of a spectrum of cell states, ranging from plastic pre-dysfunctional to fixed terminally differentiated dysfunctional states [110, 226, 172]. Whether differentiation into late or terminal dysfunctional TILs is a linear or a branched differentiation process is still under debate (Figure 2.3), but it is thought that it is a progressive differentiation towards terminally exhausted cell states [110, 172, 202, 150], since TCR tracing revealed that terminal dysfunctional CD8<sup>+</sup> TILs exhibited the strongest clonal expansion [231, 73, 172, 110, 226]. Furthermore, exhausted CD8<sup>+</sup> TILs possess chromatin accessibility patterns, which are distinct from pattern of functional CD8<sup>+</sup> T cell states [151] and differ between precursor and terminally exhausted TILs. This observation could be confirmed so far in mouse tumor models as well as in human skin-, lung-, basal cell- and breast cancer patients [130, 172, 232, 131], suggesting that T cell dysfunction is a general phenomenon in tumorigenesis.



## 2. INTRODUCTION

---

mediate induction of the exhaustion program (Figure 2.4) [35, 113, 184]. TOX and NR4A1 both promote upregulation of inhibitory receptors and sustain themselves in a positive feedback loop [184, 181]. It was shown that TOX is required for the formation of exhausted T cells as it is involved in chromatin remodeling and alters their transcriptome [98].

It is still under debate why the differentiation into an exhausted state seems inevitable for CD8<sup>+</sup> T cells in the TME and whether it is favorable or not. It seems, that this developmental process reflects gradual adaptation to the TME, and frequent stressful stimulation. It is hypothesized that the T cell exhaustion program is needed to counteract overstimulation and thereby facilitates survival and persistence of TILs in the TME [181]. Researchers argue, that T cell exhaustion is further needed to prevent immunopathology in healthy tissues [40, 233]. Moreover, the precursor exhausted T cell subset is thought to proliferate and give rise to terminal exhausted T cells, which still maintain tumor control, although on a low level, as only the presence of the latter correlated with limited tumor growth [218, 201]. In addition, it has been observed that precursor exhausted T cells respond to checkpoint inhibition via proliferation [172]. It is believed that improved understanding of the role and function of the heterogeneous exhausted TIL states could facilitate successful cancer immunotherapy.

### 2.1.2 Immunotherapy and its limits

During the last decade, immunotherapy (IT) has become the fourth pillar of cancer treatment, besides surgery, radiotherapy and chemotherapy, thanks to advances in tumor immunology research. The ultimate goal of cancer immunotherapy is to induce, support, and maintain the immune systems ability to fight cancer. Immunotherapies can be subdivided into active or passive IT. While active IT targets on tumor cells directly, for example via chimeric antigen receptor T cells (CAR T cells) [95], which are engineered to detect and kill tumor cells, passive immunotherapy

enhances the pre-existing ability of the immune system to fight cancer, for example via checkpoint inhibitors [168]. Notably, these therapies can treat and even cure previously untreatable malignancies and metastatic disease. On the reverse side, often resistance or relapse occur and responses are restricted to a subset of patients [171, 145].

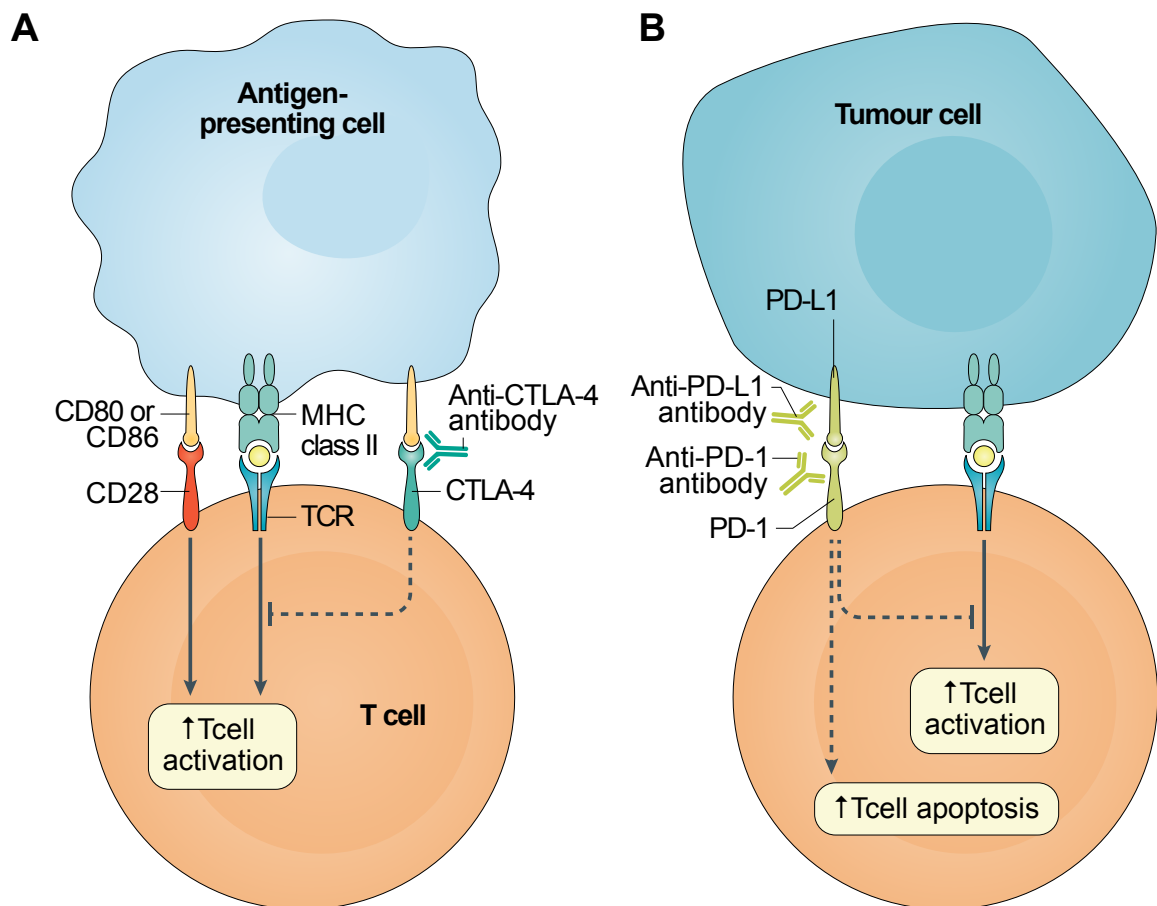


**Figure 2.5: Schematic of immune checkpoint therapy**

Immune checkpoint therapy uses antibodies, which are given to the patients and either block CTLA-4 (left) or PD1 or PD-L1 (right), respectively. Blockade prevents inhibition of T cells in lymphoid organs via signals from antigen-presenting cells, or in the tumor via signals from tumor cells, thereby facilitating anti-tumor immune response via cytotoxic T cells. Reprinted by permission from Springer Nature Customer Service Centre GmbH: Springer Nature, Immune-related adverse events of checkpoint inhibitors by Manuel Ramos-Casals et al. Copyright© 2020 [161].

Immune checkpoint blockade (ICB) or immune checkpoint therapy (ICT) uses anti-

## 2. INTRODUCTION

---

bodies targeting checkpoint molecules like CTLA4, PD1 or PD-L1 and thereby supports and preserves the anti-tumor immune response by cytotoxic T cells (Figure 2.5, [228, 161]). The development of checkpoint blocking antibodies, such as ipilimumab (targeting CTLA-4, [168]), pembrolizumab (targeting PD1, [52, 59]) or atezolizumab (targeting PDL1) has revolutionized immunotherapy in the past 10 years, as it is also effective in solid cancers and improves survival of many patients. Checkpoint inhibitors have proven to be effective against multiple cancer entities and are currently approved for the treatment of over 15 solid cancer types [203]. Since checkpoint inhibitors represent a great improvement in the fight against cancer, James P. Allison and Tasuku Honjo have been awarded with the Nobel Prize in Physiology or Medicine for their discovery of the immune checkpoints [73].

However, the vast majority of patients experience resistance to ICT [32, 179]. It is hypothesized that one of the reasons for this occurrence is T cell dysfunction, as growing evidence suggests that terminal exhausted CD8<sup>+</sup> TILs are in an epigenetically fixed state, do not respond and cannot be reinvigorated via ICT [151, 65, 146, 60, 116]. Indeed, studies, which investigated specimen from basal cell carcinoma (BCC), squamous cell carcinoma (SCC), lung cancer and melanoma patients found that PD1 blockade acts rather via expansion of precursor exhausted TILs or by recruiting peripheral T cells to the tumor site [226, 172, 115]. Nonetheless, this occurred only in PD1 blockade responsive patients.

Another novel approach for immunotherapy is the creation of CAR T cells. For the generation of this cell therapeutic product, the patients' T cells are extracted, genetically modified via viral transduction, *ex vivo* expanded and readministered to the patient (Figure 2.6A). The T cells are engineered in a way that they express an artificial T cell receptor, which recognizes a preferential tumor antigen (Figure 2.6B). The introduced chimeric antigen receptors combine an extracellular tumor antigen-recognition domain and an intracellular signaling domain. This enables tumor cell recognition and killing in an MHC-independent manner, and therefore represents a solution for cases where either the patients' immune system does not mount a

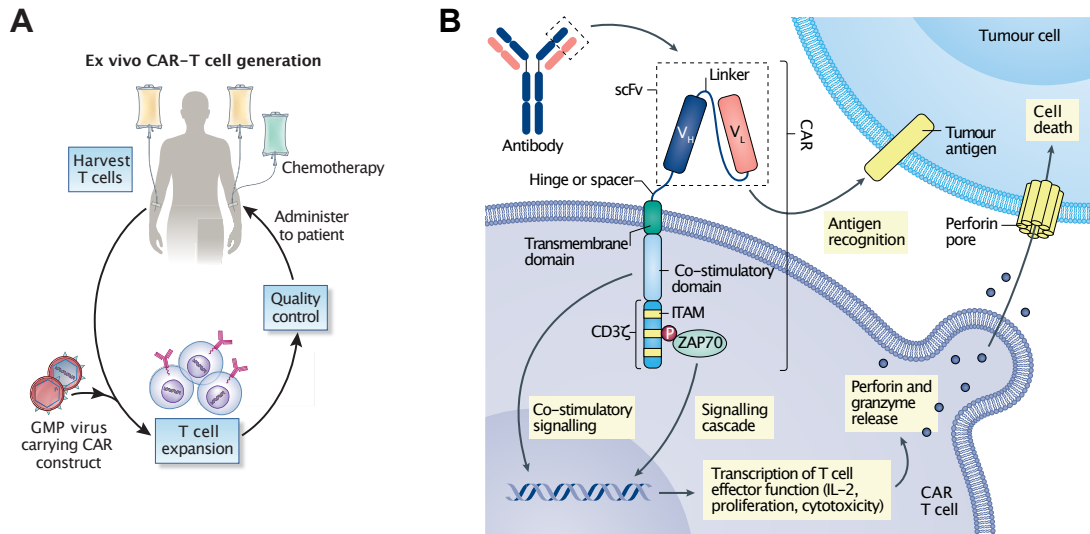


**Figure 2.6: CAR T cell therapy**

(A) CAR T cells are generated via ex vivo approaches. First, the patients' T cells are harvested and activated, followed by integration of the CAR via viral transduction. After expansion and quality control, the generated CAR T cells are infused back to the patients. In the case of hematological malignancies the endogenous blood cells are depleted via chemotherapy. Reprinted by permission from Springer Nature Customer Service Centre GmbH: Springer Nature, Manufacture of CAR-T cells in the body by Johanna Olweus, Copyright© 2017 [114]. (B) Schematic of a basic second-generation CAR T cell. The extracellular part of the CAR molecule typically resembles parts of a monoclonal antibody directed against the target tumor antigen. The extracellular, antigen-specific region of the CAR typically consists of a variable heavy (VH) and a variable light (VL) chains, also known as the single-chain variable fragment (scFv), which are adapted from monoclonal antibodies. This part is connected via a linker to a transmembrane region, which anchors the CAR in the cell membrane. Upon antigen-recognition the intracellular co-stimulatory domain and the CD3zeta domain become phosphorylated on ITAM (immunoreceptor tyrosine-based activation motif) motifs, which induces downstream signaling cascades leading to transcription of cytotoxic molecules (e.g. perforin and granzyme), which upon release lead to tumor cell death. Reprinted by permission from Springer Nature Customer Service Centre GmbH: Springer Nature, Recent advances and discoveries in the mechanisms and functions of CAR T cells by Rebecca C. Larson et al. Copyright© 2021 [107].

sufficient anti-tumor immune response or tumor cells lose MHC expression due to selection pressure during tumorigenesis [216]. CAR T cell therapeutics such as Tisagenlecleucel (Kymriah), a CD19-targeting CAR T cell product, which was first approved in 2017 by the FDA (United States Food and Drug Administration), mediate high response rates in B cell malignancies [129], even in refractory cases. In fact, it was observed that CAR T cell therapy can even cure hematological malignancies [127].

However, the success of CAR T cell therapy is mainly limited to haematological ma-

## 2. INTRODUCTION

---

lignancies and often fails in the case of solid tumors [162, 61, 217]. This could be at least partly due to the establishment of exhaustion in CAR T cells, which might, likewise to TILs, be induced by excessive antigen exposure and an immunosuppressive TME [118]. Notably, reduced proliferative and cytotoxic capacities as well as persistence of CAR T cells has been associated with an exhaustion-like phenotype and gene regulatory pattern [184, 155, 61]. Another study observed that this exhaustion program is at least partly driven by tonic CAR signaling [118, 116]. Thus, dysfunctional cell states represent a major hurdle for successful CAR T cell therapy. Further, until CAR T cell therapy for solid cancer is as successful as for hematological malignancies, a long way of improvements has to be faced.

To conclude, the progress in immunotherapy enabled major improvements in the fight of cancer. Still, there are hurdles to overcome, as T cell exhaustion limits the success of CAR T cell and immune checkpoint therapy and it is still unclear why only a subset of patients responds to ICT. As specific epigenetic and transcriptional programs driven by concerted action of gene regulators direct T cell differentiation programs, these should be unraveled and targeted to improve immunotherapy in the future.

## **2.2 Epigenetics and chromatin remodeling as determinants of cell identity and function**

All of our body's cells' share identical DNA sequences but nonetheless they are manifold in their phenotype and function. Changes in phenotype without modifications of the genotype are enabled by 'epigenetics', a term first established by C.H. Waddington in 1942 [213, 214, 5]. Epigenetic mechanisms allow cells to respond to changes in their environment by altering gene regulation and transcription. Epigenetic mechanisms facilitating these changes include structural and chemical modifications of chromatin and nucleic acids [15, 54].

Eukaryotic cells contain DNA in the form of chromatin, which is the tightly packed form composed of nucleosomes, the structural subunits of chromatin [5, 13]. One nucleosome consists of around 146 bp of DNA wrapped around a histone octamer, consisting of two copies of each of the four different core histones (H3, H4, H2A and H2B). The additional linker histone H1 is important for chromatin condensation [101]. Hence, this and further compaction steps enable fitting the approximately 3 meters of DNA into the nucleus [210]. This 3D organization of chromatin does not only ensure DNA packaging and protection but is of utmost importance for gene regulation.

Notably, only DNA not wrapped around nucleosomes, resulting in a so-called open chromatin state, allows gene transcription. In more detail, open chromatin facilitates gene expression as it enables binding of the transcription machinery to the promoter and of regulatory factors to regulatory DNA regions [50, 105]. Thus, chromatin remodeling, the modification of the chromatin architecture, needs to be actively regulated, for example via histone modifications [5, 163]. Amongst others, histones can be acetylated, methylated, phosphorylated or ubiquitinated [153, 154]. Histone acetylation can activate transcription, as it leads to dissociation of the DNA from the nucleosome, due to reduced DNA-nucleosome binding affinity. Depending on the specific region of methyl group attachment to histones, histone methylation does either increase or decrease the aforementioned binding affinity. Involved in histone modifications are special enzymes, so called 'writers', 'erasers' and 'readers', which either establish, delete or recognize the modifications, respectively. Readers can influence gene expression as they can, for example, interact with the transcriptional machinery or recruit further chromatin-remodelers [47, 135].

In addition to the more general gene regulation facilitated by structural and chemical modifications of chromatin, enhancers can facilitate cell type-specific transcription. Enhancers are non-coding gene regulatory elements that can be bound by transcriptional regulators, mostly transcription factors, in order to loop the DNA and bring the bound proteins in physical proximity to the initiation complex at the promoter of the

## 2. INTRODUCTION

---

target gene. Thereby, enhancers can activate and modulate cell-lineage specific gene expression in a distance independent manner [10]. Genome-wide analysis of different cell types found that cell type-specific enhancer activity matched with cell type-specific gene expression [219, 207, 81]. Even though there are hundreds of thousands of enhancers in the human genome [148], only distinct sets of enhancers are made accessible on the chromatin level, depending on the cell identity. This enables cell type specific gene expression even though many cells share the same signal transduction pathways and TF families.

The proteins that are involved in the process of gene transcription are called transcription factors. These proteins contain sequence-specific DNA binding domains, which bind to their respective transcription factor motif on the DNA. Furthermore, they possess a transactivation domain to bind to further proteins involved in transcriptional or gene-regulatory processes [122]. They become activated via environmental factors, which initiate specific signaling pathways and as a result can establish cell-type specific transcriptional networks. Thereby, all of the above-described mechanisms are somehow involved in gene regulation, which together ensure appropriate gene expression in a context- and time-dependent manner.

### **2.2.1 Epigenetic regulation of T cell differentiation and function**

During an immune response, the adaptive immune system undergoes extensive changes, whereby the cells have to exert a wide range of phenotypical and functional roles. Upon activation, CD8<sup>+</sup> T cells experience extensive chromatin remodeling in response to environmental signals, which, for instance, alters their transcriptome and metabolism [83, 178]. Depending on the signals, naïve CD8<sup>+</sup> T cells differentiate into other cell states with distinct functions, such as effector cells or memory cells. Thus, epigenetic mechanisms are very important for the control of T cell responses. CD8<sup>+</sup> T cell state-specific transcriptional programs are orchestrated by specific gene-regulatory networks, which work in conjunction of epigenetic mech-

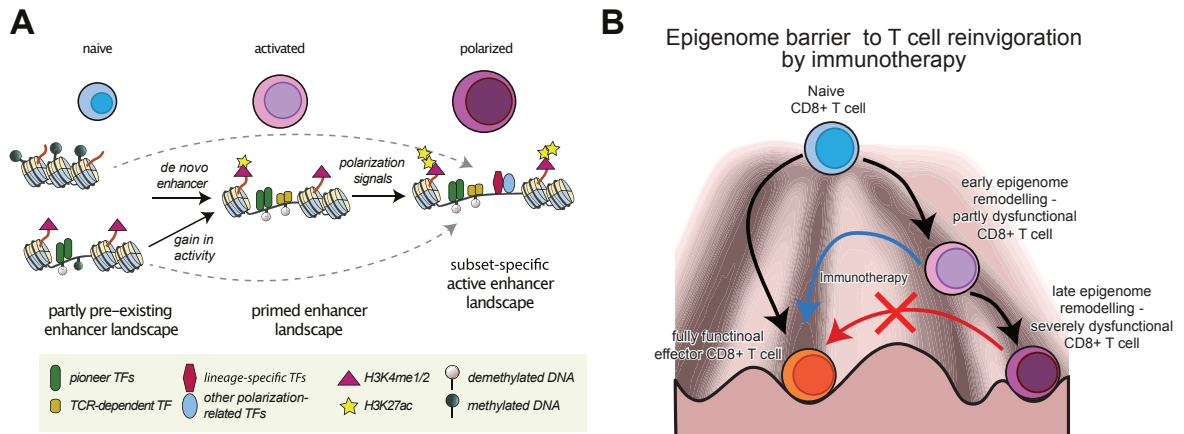


**Figure 2.7: Epigenetic mechanisms driving T cell dysfunction**

(A) Schematic of epigenetic mechanisms leading to T cell activation and differentiation. Upon cell activation, epigenome remodeling changes the enhancer accessibility. Further, environmental signals lead to activation of specific transcription factors, which can then use the prepared gene-regulatory landscape to facilitate and maintain specific gene-regulatory programs, which change the phenotype and effector functions of the cell. (B) Schematic of the epigenetic landscapes of TIL states. It is thought that prolonged antigen exposure in the tumor induces epigenome remodeling leading to dysfunctional cell states. The early dysfunctional cell states are still plastic and might be reinvigorated via checkpoint therapy, whereas the terminal dysfunctional cell states are epigenetically fixed and cannot be reinvigorated. Adapted from *Journal of Allergy and Clinical Immunology: Epigenetic mechanisms regulating T-cell responses*, Schmidl et al. Copyright© 2018, with permission from Elsevier [178].

anisms and transcription factors (Figure 2.7). These mechanisms ensure, that the establishment and maintenance of specific cell states is strictly controlled. Research investigating exhausted T cells unveiled a distinct exhaustion-specific chromatin landscape, which mirrored exhaustion-specific gene expression [146, 151, 177]. Furthermore, exhaustion-specific enhancers, likely regulating genes associated with exhaustion such as PDCD1, were found in different studies [131, 183, 146, 67, 66]. Motif analysis of differentially accessible chromatin sites in exhausted T cells identified enrichment of binding sites for transcription factors (TFs) such as NR4A1, NFAT and nuclear factor kappa B (NF- $\kappa$ B) [131, 67, 112]. Indeed, blockade of NFAT activity reduced expression of co-inhibitory receptor PD1 and enhanced expression of precursor exhaustion-associated TCF1 in exhausted TILs of a murine tumor model [151]. Moreover, NR4A changes expression of exhaustion related genes via establishing histone modifications close to their loci [113], further corroborating involve-

ment of specific epigenetic and gene-regulatory mechanisms in the establishment of T cell exhaustion. Therefore, better understanding epigenetic mechanisms involved in the establishment and maintenance of T cell exhaustion, especially in the case of human tumors, could help to optimize immunotherapeutic approaches.

### 2.3 Studying and manipulating cell states

Chromatin states and gene-regulatory mechanisms can be studied with specific methods. Transcription factor binding sites and histone modifications can be studied using ChIP-seq (chromatin immunoprecipitation with parallel DNA-sequencing). Chromatin accessibility can be studied via MNase-seq (micrococcal nuclease digestion with deep sequencing), DNase-seq (DNase I hypersensitive sites sequencing) or ATAC-seq (Assay for Transposase-Accessible Chromatin using sequencing). ATAC-seq is a method to survey genome-wide chromatin accessibility. In 2013, the technique was first described by Buenrostro et al. as a faster and more sensitive alternative to DNase-seq and MNase-seq [24]. ATAC-seq is a tool to define cell types and states based on their epigenome. With this method:

1. cell-state specific gene regulators can be defined
  - a) via their gene locus accessibility, which is referred to as being likely transcriptionally active
  - b) via their TF motif enrichment at accessible 'open' chromatin sites
2. cell-state specific enhancers can be defined
3. gene-regulatory networks can be inferred

Bulk ATAC-seq captures accessible DNA regions by probing chromatin of 500-50,000 cells with a mutated, hyperactive Tn5 transposase, which is loaded with sequencing adaptors [167]. In more detail, the transposase cleaves only accessible, nucleosome- and transcription factor-free DNA and tags the cleaved DNA fragments with the se-

quencing adaptors in a process called ‘tagmentation’ [152, 24]. The tagged DNA fragments are then purified, whereby the transposase is released, followed by PCR amplification, which inserts barcodes to discriminate the fragments from different samples after sequencing. The so-called library is then sequenced using next-generation sequencing. The sequencing reads will be mapped to the respective genome, followed by annotation of accessible chromatin sites to gene loci, mapping of transcription factor binding regions and dissection of non-coding gene regulatory elements using bioinformatic methods [7].

### **2.3.1 Open chromatin profiling on the single cell level**

Modified versions of ATAC-seq enable analysis of chromatin accessibility on the single cell level (single cell ATAC-seq or scATAC-seq), providing insights into cell states and regulomes in an unprecedented depth (Figure 2.8, [25, 173, 33]). ScATAC-seq allows to study heterogeneous cell populations containing very few cells in a specific cell-state that were impossible to assess via bulk ATAC-seq. Further, even whole tissue samples containing many different cell populations can be studied. Microfluidics [25], single nuclei sorting [33] or a droplet-based technique [173] can be used to separate single nuclei. Moreover, scATAC-seq has several advantages over scRNA-seq. First, transcription factors are mostly expressed on a low level and hard to be detected via scRNA-seq in a reliable way. The stability of the chromatin landscape is higher and describes the cells’ true state, whereas gene transcription is timely restricted or can change over time, thus scRNA-seq might just capture a ‘snapshot’. To study functional regulation of individual cells within a complex system, scATAC-seq is the current gold standard as it enables to identify genes which are likely active, gene regulators and their binding sites as well as cell-state specific enhancers at the same time. Thus, with scATAC-seq we can investigate the root cause of a cells’ identity better than with using scRNA-seq.

## 2. INTRODUCTION

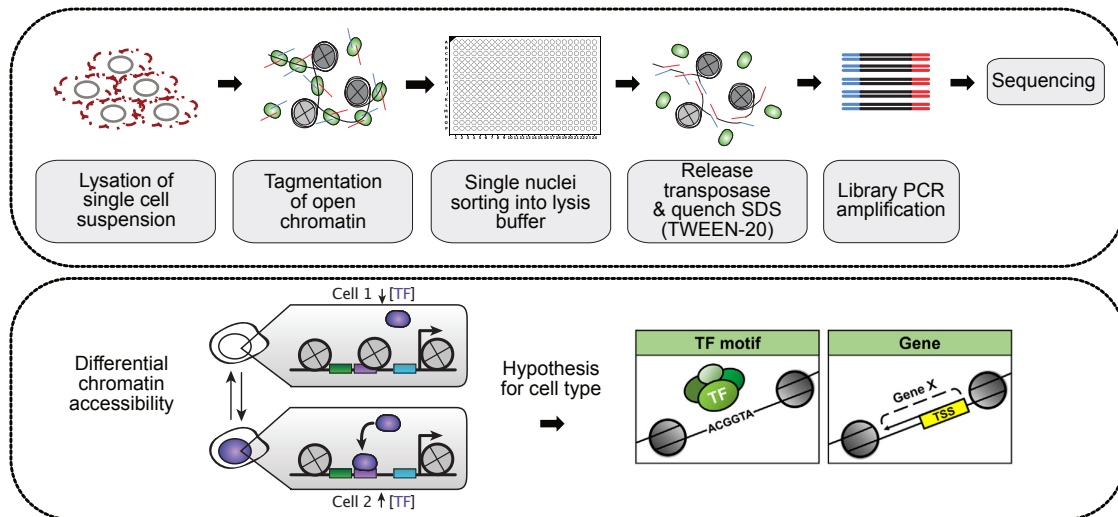


**Figure 2.8: Representative workflow and output of plate-based single cell ATAC-seq** (Top panel) Schematic overview of a single cell ATAC-seq workflow. First, cells are lysed in bulk followed by tagmentation of open chromatin via the TN5 enzyme. In the case of nuclei separation via cell sorting, single nuclei are single-cell sorted into 384-well plates containing lysis buffer and barcoded primers. Afterwards, the transposase is released and SDS is quenched to not interfere with the following library amplification via PCR, which induces different barcodes for every single cells' chromatin fragments. Subsequently libraries from different cells can be pooled and sequenced, followed by demultiplexing, which is made possible via the cell-specific barcodes. (Bottom panel) Graphical layout of individual cell states leading to differential chromatin accessibility (left). In the upper cell 1, TF binding is blocked via closed chromatin, whereas in cell 2 the TF can bind to its motif because the chromatin is accessible. The differential chromatin accessibility can be analyzed via ATAC-seq and hypothesis for the cell type can be drawn from information such as TF motif enrichment or gene accessibility. Adapted from [33] with permission under the creative commons license (<http://creativecommons.org/licenses/by/4.0/>). Adapted from [7] with permission under the creative commons license (<https://creativecommons.org/licenses/by-nc-nd/4.0/>). Adapted by permission from Springer Nature Customer Service Centre GmbH: Springer Nature, Nature, Single-cell chromatin accessibility reveals principles of regulatory variation, Jason D. Buenrostro et al. Copyright© 2015 [25].

Recently, more and more analysis tools, especially designed for the analysis of single cell ATAC-seq data and their integration with multiomics data, are developed, augmenting the possibilities to study very complex biological systems via data integration [222]. To conclude, scATAC-seq is the perfect tool to study gene-regulatory mechanisms of heterogeneous CD8<sup>+</sup> TILs.

### 2.3.2 CRISPR/Cas9 based genome editing

CRISPR/Cas9 (Clustered regularly interspaced short palindromic repeats/ CRISPR associated protein 9) based genome editing is a genetic engineering technique, which was first published by Jennifer Doudna and Emmanuelle Charpentier in 2012 [94] and earned them the Nobel Prize in Chemistry in 2020. This groundbreaking technology is, contrary to others, very precisely, can provide complete gene knock-out, can be multiplexed and is cost efficient. Moreover, the system offers great potential to adapt it to further use cases such as gene activation or targeted mutation.

CRISPR/Cas9 is based on parts of the bacterial immune system and allows bacteria to fight viral infections [45]. In more detail, bacteria cleave viral DNA and integrate pieces of it into their own DNA, in the form of CRISPR DNA sequences, where the spacer sequences (protospacer) in between the repeats derive from the viral DNA [18, 157, 132]. Further, the CRISPR sequences contain repetitive regions called protospacer-adjacent motifs (PAMs) [117, 45]. The CRISPR sequences are transcribed and processed to crRNAs (CRISPR RNA) and together with trans-activating RNA (tracrRNA) form complexes with CRISPR associated proteins (such as Cas9 from *Streptococcus pyogenes*) [21, 94]. The crRNA (also named guide RNA) then serves as a guide for the Cas9 to detect sequence-specific viral DNA. Cas9 can then induce double-strand breaks in the target DNA due to its endonuclease activity [45], and thereby stops viral infection.

By manipulation of the guide RNAs' nucleotide sequence, the CRISPR/Cas9 system can be used to induce desired genome modifications in almost every cell type of eukaryotic organisms [38, 41, 42]. Different delivery systems of CRISPR-Cas9 have been developed, among them delivery via plasmid DNA, mRNA (messenger RNA) or as an already preformed ribonucleoprotein complex (RNP). Once in the cell, the Cas9 complex, also referred to as 'genetic scissor', can detect PAM sequences within the genome. When Cas9 could bind to its PAM recognition site it unwinds

## 2. INTRODUCTION

---

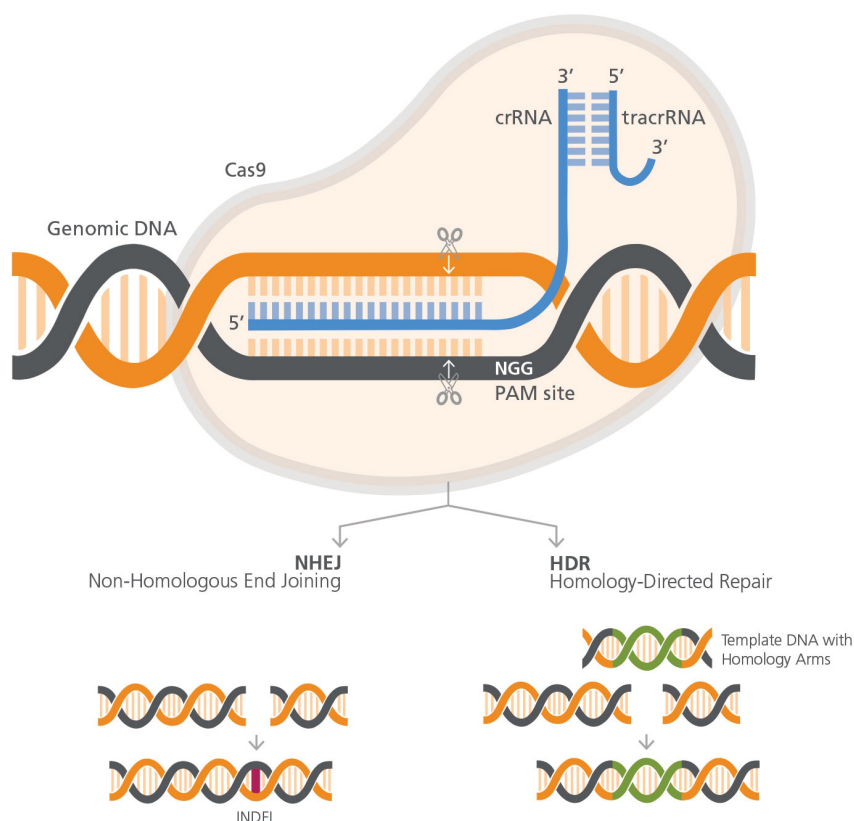


**Figure 2.9: Schematic of genome editing via CRISPR/Cas9**

Schematic of the CRISPR/Cas9 complex, which can facilitate genome editing. The Cas9 protein can induce double strand breaks by its endonuclease activity when the crRNA sequences matches a target sequence. Cellular repair mechanisms either induce gene knock-out via NHEJ (non-homologous end joining) by inducing insertions/deletions (INDELs) or knock-in via HDR (homology-directed repair) if a DNA template with homology arms is included. Taken from [198].

the DNA double helix and when the designed guide RNA aligns to the target DNA sequence Cas9 induces nicks, leading to double strand breaks (Figure 2.9). Eventually, the breaks will be repaired by the non-homologous end joining (NHEJ) if no DNA template is delivered. Since this process is error-prone, insertion or deletions (INDELs) will occur, resulting in the disruption of gene functionality, also called gene knockout (see figure 2.9, [123, 170]). If a knock-in mutation is desired, it is possible to insert a DNA template, which might be used for homology directed repair (HDR, [46]). To date, CRISPR is not only used for research purposes but to treat patients, and the first clinical trials to treat diseases such as sickle cell disease, HIV,

or cancer are already going on. It could be shown that CRISPR/Cas9 can be used to engineer T cells and thus might comprise a powerful tool to optimize adoptive T cell therapeutics such as CAR T cells [86, 109]. As several studies have proven specific genes are essential for immunosuppressive resistance or counteracting exhaustion and fratricide, CRISPR/Cas9 technology is expected to be the solution for constructing the next generation of CAR T cells by gene ablation, gene overexpression, fine-tuned transcriptional regulation or epigenome modulation [91, 191]. Many researchers and clinicians anticipate, that the CRISPR/Cas9 technology and future derivatives will improve potency and safety of CAR T cells as well as enable production of universal allogenic CAR T cells [164, 205, 56, 74, 190]. In fact, the first CRISPR engineered CAR T cells are already used in preclinical and clinical studies and hopefully prove their potential in the future [162, 194]. Furthermore, CRISPR/Cas9 is the perfect tool to study the influence of genes or enhancers likely involved in T cell exhaustion.

### **2.4 Aim of the thesis**

T cells can become dysfunctional during the tumor immune response and terminal dysfunctional TILs cannot be reinvigorated via checkpoint blockade. It has been shown that distinct gene regulatory mechanisms lock T cells in this dysfunctional state. To date, it is not understood whether these gene regulatory mechanisms are the same for TILs of different tumor entities or in which way the specific TME influences these mechanisms differently. Furthermore, it is an ongoing research question how terminally exhausted T cells could be revitalized, how CAR T cell exhaustion could be prevented, and how response to immunotherapy can be improved. Until now, T cell exhaustion is mostly studied in chronic viral infections and mouse models but gene-regulation determining enhancers are mostly species specific and the tumor microenvironment shapes the T cells in a different way than chronic viral infection sites. Besides, mouse models often use artificial TCRs in combination

## 2. INTRODUCTION

---

with tumor cells, which express high levels of antigens. This does not resemble the situation in tumor patients, where different TCR affinities or avidities exist, different amounts of antigens are presented or immune escape occurs.

To circumvent the limitations of mouse models we wanted to study the gene-regulatory landscape of exhausted T cells in the human setting. We therefore aimed to extract CD8<sup>+</sup> TILs from human tumors of different tumor entities and to subject them to single cell chromatin profiling to study their gene-regulatory landscape. To distinguish, which accessible chromatin sites and gene regulator activities are specific for cell states shaped by the TME, we included CD8<sup>+</sup> T cells from adjacent healthy tissue and healthy blood donors as controls. We further integrated public available data of chromatin profiles of relevant CD8<sup>+</sup> T cell states to further increase the power of our analysis.

With extensive bioinformatic analysis we wanted to dissect whether there exist common gene-regulatory programs leading to T cell dysfunction, which are shared between human tumor entities. Further, we aimed to extract genes and gene regulators of this data whose role in establishment, regulation or maintenance of TIL dysfunction is not known yet. Moreover, we intended to establish an *in vitro* exhaustion model using CRISPR/Cas9-based gene disruption to functional validate the selected target genes. In the future, these data could help to combat CAR T cell dysfunction by manipulating exhaustion-related genes, gene regulators or exhaustion-specific enhancers and overall increase knowledge about gene-regulatory mechanisms leading to terminal T cell dysfunction in human malignancies.

## 3 Material and Methods

### 3.1 Material

#### 3.1.1 Laboratory consumables and equipment

**Table 3.1: Laboratory consumables**

<b>Laboratory consumables</b>	<b>Supplier</b>
Cell Culture Plates Cellstar®	Greiner BioOne
96 well Microplate, PS, F-bottom	Greiner BioOne
96 well Microplate, PS, round-bottom	Greiner BioOne
96 well Microplate, PS, V-bottom	Greiner BioOne
CASY Cups	Roche
Cell culture flasks	Greiner BioOne
Cryo vials	Eppendorf, Germany
Falcon tubes (15 mL, 50 mL)	Falcon
G-rex® flasks	Wilson Wolf
GentleMACS C tubes	Miltenyi
LoBind Tubes (1.5 mL)	Eppendorf
MACS Separation columns (LS/MS)	Miltenyi
MACS SmartStrainers (30, 70, 100 µM)	Miltenyi
MicroAmp Optical 384 well reaction plate	Thermo Fisher Scientific
MicroAmp Optical 96 well reaction plate	Thermo Fisher Scientific
PCR tubes (0.2 mL)	Kisker

### 3. MATERIAL AND METHODS

---

Petri Dishes	Greiner Bio-One
Pipette filter tips, lobind	Corning
Pipette filter tips	Sarstedt, ThermoFisher, Greiner Bio One
Polystyrene round bottom tubes	Falcon
Pre-Separation Filters (30 µM)	Miltenyi
Reservoir (10-25 ml), sterile	INTEGRA Bioscience
Safe-lock reaction tubes (1.5, 2 mL)	Sarstedt
Sample tube (5mL), flow cytometry	Sarstedt
Scalpels (no. 10), disposable	Feather
Serological pipettes	Greiner BioOne, Germany
Steriflip® Filter Units	Merck Millipore
Syringe filter units (0.22 µm-pores)	Millipore
Syringes and Needles	BD

---

**Table 3.2: Laboratory equipment**

<b>Laboratory equipment</b>	<b>Supplier</b>
4D-Nucleofector™ Core Unit	Lonza Bioscience
4D-Nucleofector™ X-Unit	Lonza Bioscience
CASY Cell Counter and Analyzer TT	Roche
DNA/RNA UV-cleaner box	Biosan
FACS Aria™ Ilu Cell Sorter	BD Biosciences
FACS Canto™ II	BD Biosciences
FACS Celesta™	BD Biosciences
FACS LSR II	BD Biosciences
FACS Symphony™ A5 SORP	BD Biosciences
GentleMACS™ Octo Dissociator	Miltenyi Biotech
Heracell™ 240i Incubator	Thermo Fisher Scientific
Incucyte ZOOM	Essen BioScience

---

Incucyte/textcopyright SX5 Live-Cell Analysis System	Sartorius
G/R	
Laminar Flow Hood	Thermo Fisher Scientific
Magnetic MACS Separator frame	Miltenyi Biotech
Multipette M4	Eppendorf
Neon™ Transfection System	Thermo Fisher
Neubauer Counting Chamber	Bio-Rad
NextSeq 550	Illumina
PCR machine	Bio-Rad
Pipetman L Multichannel P12x200L	Gilson
Pipettes	Eppendorf, Gilson, ThermoFisher
QuantStudio 5 Real-Time PCR Light Cycler	Thermo Fisher Scientific
Qubit Fluorometer	Thermo Fisher Scientific
Tapestation 2200	Agilent
ThermoCycler	Eppendorf
Vacuum manifold	Qiagen

---

### 3.1.2 Reagents and media

**Table 3.3: Reagents, chemicals and media**

<b>Reagents and media</b>	<b>Supplier</b>
AB serum (heat-inactivated), human	Valley Biomedical
AccuCheck Counting Beads	Thermo Fisher Scientific
ACK Lysis Buffer	Thermo Fisher Scientific
AIM V medium	Thermo Fisher Scientific
Alt-R® Electroporation Enhancer	Integrated DNA Technologies
Alt-R® S.p. HiFi Cas9 Nuclease V3 (62 µM)	Integrated DNA Technologies
Aqua ad iniectabilia	B. Braun
Beta-mercaptoethanol (50 mM)	Gibco
Bovine Serum Albumin (BSA)	Sigma Aldrich

### 3. MATERIAL AND METHODS

---

Buffer PB	Qiagen
Buffer PE	Qiagen
CASY Ton	Roche
Collagenase IA	Sigma
Compensation Beads	Miltenyi Biotec
Digitonin	Promega
Dimethyl Formamide	Sigma
Dimethyl sulfoxide (DMSO)	Sigma Aldrich
DNase I Type IV	Sigma
Dulbecco's Modified Eagle Medium (DMEM)	Gibco
Dulbecco's phosphate-buffered saline (DPBS)	Gibco
EDTA	Invitrogen™
EDTA (1M)	GIBCO
Ethanol	Thermo Fisher Scientific
Ethanol absolute	Sigma Aldrich
FACS Clean	BD
FACS Flow	BD
FACS Rinse	BD
Fetal calf serum (FCS), heat-inactivated	PAN Biotech
Glutamin	Biochrom KG
Ham's F12 Nutrient Mix	Gibco
HBSS with calcium, with magnesium	Sigma Aldrich
HBSS without calcium, without magnesium	Sigma Aldrich
HEPES buffer (1M)	Gibco
IL-15 (human, recombinant)	Peptotech
IL-2 (human, recombinant)	Peptotech
IL-7 (human, recombinant)	Peptotech
Incucyte Caspase-3/7 Green Dye (5mM)	Sartorius
Ingenio© Solution	Mirus Bio LLC
Ionomycin	Calbiochem

### 3. MATERIAL AND METHODS

---

Kiovig	Baxter
L-Glutamin	Gibco
LymphoSpin medium (Density Gradient Centrifugation)	PluriSelect
MEM Vitamin Solution	Sigma
MgCl <sub>2</sub>	Invitrogen™
NP-40 (IGEPAL® CA-630)	Sigma
Nuclease-Free IDTE Buffer	Integrated DNA Technologies
Nuclease-Free Water	Invitrogen™
Penicillin/Streptomycin (PenStrep)	Gibco
Phosphate Buffered Saline (PBS, 10X)	Invitrogen™
Potassium chloride (KCl)	Invitrogen™
Proleukin S (recombinant human IL-2)	Novartis Pharma
Propidium Iodide	Sigma Aldrich
Proteinase K	NEB
Pyruvat	Gibco
Recombinant Golden Nuclease/Benzonase	Speed BioSystems
Roswell Park Memorial Institute 1640 Medium (RPMI 1640)	Gibco
RPMI 1640 (+L-Glutamine)	Gibco
Sodium chloride (NaCl)	Sigma
Sodium dodecyl sulfate (SDS)	Sigma
Streptavidin	AvivaSysBio
SYBR-Green	Thermo Fisher Scientific
Tris-HCl, pH7	Invitrogen™
Tris-HCl, pH8	Invitrogen™
TrueCut™ Cas9 Protein v2	Invitrogen™
Trypan blue solution	Merck Chemicals
Trypsin-EDTA (0.5 %)	Gibco
Tween 20	Sigma Aldrich
X-VIVO 15	Lonza

---

### 3.1.3 Solutions, buffer and media

**Table 3.4: Buffer and media**

<b>Buffer/media</b>	<b>Components</b>	<b>Concentration</b>
FACS-buffer	FCS	2 %
	EDTA	2 mM
	in PBS	
MACS-buffer	FCS	1 %
	EDTA	2 mM
	in PBS	
CLM medium	human AB serum	10 %
	HEPES	1 %
	beta-mercaptoethanol	0.01 %
	PenStrep	1 %
	in RPMI	
CMM medium	FCS	9 %
	Ham's F12 Nutrient Mix	18 % (v/v)
	HEPES	0.01 %
	PenStrep	1 %
	DMEM	54 % (v/v)
	RPMI	18 % (v/v)
TIL209 expansion medium	CLM	50 %
	AIM-V	50 %
TIL209 expansion medium with feeder cells	CLM	50 %
	AIM-V	50 %
	feeder cells	100X TILs
	OKT3	30 ng/mL
	rHuIL-2	3,000 U/mL
TIL209 and primary TILs freezing medium A	AB Serum	60 %
	RPMI	40 %
TIL209 and primary TILs freezing medium B	AB Serum	80 %
	DMSO	20 %

### 3. MATERIAL AND METHODS

T cell medium	FCS	10 %
	beta-mercaptoethanol	1 %
	PenStrep	55 microM
	L-Glutamin	1 %
	IL-2	100 U/mL
in RPMI		
Freezing medium (cell culture cells, PBMCs)	FCS	90 %
	DMSO	10 %
Bulk ATAC sorting buffer	FCS	90 %
	in PBS	
Single-cell ATAC sorting buffer	BSA	0.5 %
	in PBS	

FCS used was heat inactivated (30 min, 56 °C in water bath).

#### 3.1.4 Cell lines

**Table 3.5: Cell lines**

Cell line	Identifier
Jurkat E6.1	CVCL0367
NIH 3T3	CVCL0594, gift from AG Feuerer
TIL209	gift from AG Beckhove
M579-A2	gift from AG Beckhove

#### 3.1.5 Primary human samples for scATAC-seq

**Table 3.6: Primary human samples**

Sample ID	Diagnosis	Sex	Age	Pre-treatment	Viral infections
-----------	-----------	-----	-----	---------------	------------------

### 3. MATERIAL AND METHODS

---

pF380	ccRCCC	male	63	no	-
p254F	ccRCC	male	64	no	-
pAFE1	ccRCC	male	59	no	-
pF60B	ccRCC	female	64	no	-
pC458	HCC	male	73	surgery	no HCV/HBV
p3036	HCC	male	75	no	no HCV/HBV
p1005	HCC	male	78	no	no HCV/HBV
pA388	HCC	male	69	no	no HCV/HBV
p0D3C	HNSCC	male	60	no	no HPV
pB415	HNSCC	male	71	STT and Chemo	no HPV
pBDE5	HNSCC	female	43	no	no HPV
p168C	HNSCC	male	57	no	no HPV
d6E78	healthy blood donor	-	-	-	-
d40A4	healthy blood donor	-	-	-	-
d88D5	healthy blood donor	-	-	-	-
dF9A7	healthy blood donor	-	-	-	-
d5E44	healthy blood donor	-	-	-	-

---

HCC samples were kindly provided by Prof. Jens Werner and Akinbami Rapahel Adenugba (UKR). CcRCC samples and PBMCs were kindly provided by Dr. Peter Siska and Prof. Marina Kreutz. HNSCC samples were kindly provided by Dr. Katrin Singer, Dr. Ines Ugele and Prof. Marina Kreutz.

#### 3.1.6 Antibodies and fluorescent molecules

**Table 3.7: Antibodies**

Target	Fluorochrome	Clone	Dilution	Supplier
CD3	FITC	HIT3a	1:100	Biologend
CD8	PerCp/Cy5.5	SK1	1:100	Biologend
CD45RA	PE/Cy7	HI100	1:100	Biologend

### 3. MATERIAL AND METHODS

CD197 (CCR7)	APC/Cy7	G043H7	1:50	Biologend
CD279 (PD-1)	BV421	NAT105	1:50	Biologend
CD366 (TIM-3)	BV711	F38-2E2	1:50	Biologend
CD223 (LAG-3)	PE	11C3C65	1:50	Biologend
CD137 (4-1BB)	APC	4B4-1	1:100	Biologend
CD28	PE	CD28.2	1:100	Biologend
CD38	BV711/APC	HIT2	1:100	Biologend
TNF $\alpha$	APC	MAb11	1:100	Biologend
IFN $\gamma$	PE	4S.B3	1:100	Biologend
CD8a	BV510	RPA-T8	1:100	Biologend
CD2	APC	TS1/8	1:100	Biologend
CD5	APC/Cy7	L17F12	1:100	Biologend
CD279 (PD1)	PE/Cy7	EH12.2H7	1:50	Biologend
CD279 (PD1)	BV711	EH12.2H7	1:50	Biologend
CD39	BV421	A1	1:100	Biologend
TIM3	BV605	7D3	1:50	BD
CD25	BUV737	2A3	1:100	BD
CD69	PerCP/Cy5.5	FN50	1:100	Biologend
CD69	BV786	FN50	1:100	Biologend
TOX	APC	REA473	1:50	Miltenyi
EOS	PE	W16032A	1:20	Biologend
VDR	-	D2K6W	1:1000	Cell Signaling
BOB-1	-	E5K1D	1:1000	Cell Signaling
GPD2	-	EPR14259	1:310	Abcam
HLA-A2	APC	BB7.2	1:50	BD
HLA,B,C	-	W6/32	0.5 mg/mL	Biologend
anti-rabbit IgG	AF647	-	1:5000	Cell Signaling
Isotypes	*	various	*	Biologend
CD3	-	OKT3	-	eBioscience
CD28	-	4S.B3	-	BD

### 3. MATERIAL AND METHODS

---

CD3	Biotinylated	OKT3	-	Biolegend
-----	--------------	------	---	-----------

---

\*same as antibody we wanted to control for. All antibodies are anti-human specific and monoclonal. Concentrations of FACS antibodies used for 50  $\mu$ l volume and up to  $1 \times 10^6$  cells are listed. Antibodies were diluted as the manufacturers recommendations or were titrated before first use. Isotype controls were from the respective host with the same isotype and labeled with the respective fluorochrome.

**Table 3.8: Fluorescent molecules**

Fluorochrome	Concentration/Dilution	Supplier
7AAD	1:20	Thermo Fisher
Propidium Iodid	0.2 $\mu$ g ml <sup>-1</sup>	Sigma Aldrich
Zombie Violet™	1:500	Biolegend
Zombie Aqua™	1:500	Biolegend
Zombie NIR™	1:500	Biolegend
Fluo-3, AM, Calcium-Indicator	2 $\mu$ M	Thermo Scientific
Fura Red™, AM	2 $\mu$ M	Thermo Scientific

#### 3.1.7 Commercial assays

**Table 3.9: Kits**

Kit	Supplier
Agencourt AMPure XP beads	Beckman Coulter
Anti-human CD45 (TIL) Microbeads	Miltenyi Biotec
Cell Stimulation Cocktail (plus protein transport inhibitors) (500X)	Beckman Coulter
Foxp3/Transcription Factor Staining Buffer Set	eBioscience

High Sensitivity D1000 Reagents	Agilent
High Sensitivity D1000 Screen Tape	Agilent
Illumina Tagment DNA Enzyme and Buffer	Illumina
MinElute PCR Purification Kit	Qiagen
MS columns	Miltenyi Biotec
NEBNext High Fidelity PCR Master mix	NEB
Neon™ Transfection Kit	Thermo Fisher Scientific
NextSeq 500/550 High Output Kit v2.5 (75 Cycles)	Illumina
P3 Primary Cell 4D-Nucleofector™ X Kit S	Lonza
Qubit dsDNA HS Kit	Thermo Fisher Scientific
T Cell TransAct, Human	Miltenyi Biotec
Zymo clean and concentrator-5 kit	Zymo

### 3.1.8 Oligonucleotides

**Table 3.10: Oligonucleotides**

Name	Sequence/target sequence	Supplier
Barcoded primers as published by Corces et. al, 2017 [39]	see publication	Sigma
Alt-R @Cas9 Negative Control (scr)	n.a.	IDT
crRNA CD2.1.AA	GCATCTGAAGACCGATGATC	IDT
crRNA CD2.1.AD	CTGGACATCTATCTCATCAT	IDT
crRNA CD2.1.AE	ATACAAGTCCAGGAGATCTT	IDT
crRNA CD5.1.AA	CGTTCCAACCTCGAAGTGCCA	IDT
crRNA IKZF4.1.AB*	TATTGGACCCAACGTGCTCA	IDT
crRNA IKZF4.1.AC	TCCGGAACACACCCTCCTGA	IDT
crRNA IKZF4.1.AD	GTCACACTTGAGCTTGCCAT	IDT
crRNA IKZF4.1.AH*	AGGCACCACACTGGTTGCAA	IDT
crRNA PDCD1.1.AA*	CGTCTGGGCGGTGCTACAAC	IDT

### 3. MATERIAL AND METHODS

---

crRNA PDCD1.1.AB	CGGAGAGCTTCGTGCTAAAC	IDT
crRNA PDCD1.1.AC	CCCCTTCGGTCACCACGAGC	IDT
crRNA PDCD1.1.AQ* [182]	CGTGTCACACAACTGCCCAA	IDT
crRNA PDCD1.1.SR1* [182]	CTGCAGCTTCTCCAACACAT	IDT
crRNA POU2AF1.1.AB	TACTCGGTGTAAGGTGTCCA	IDT
crRNA POU2AF1.1.AC	CCTGGCGACCTACACCACAG	IDT
crRNA POU2AF1.1.AD*	GGCATAGGTCAACACTGAGG	IDT
crRNA VDR-7* [128]	GAACGTGCCCCGGATCTGTG	IDT
crRNA VDR-8 [128]	GGGGTCGTAGGTCTTATGGT	IDT
crRNA VDR.1.AA	ACTTTGACCGGAACGTGCCC	IDT
crRNA VDR.1.AB	GGACAACCGACGCCACTGCC	IDT
crRNA VDR.1.AC	CCATCATTACACGAACTGG	IDT
crRNA VDR.1.AG	GGTGATACAGTGATCTGAGC	IDT
crRNA VDR.1.AK	ACGTTCCGGTCAAAGTCTCC	IDT
crRNA VDR.1.AO	CCACCATCATTACACGAAC	IDT
tracrRNA	n.a.	IDT
CD2.AA-for	GTCAGGACATCAACTTGGACA	Sigma
CD2.AA-rev	GACATGCATCTGGTTTCCTGT	Sigma
CD2.AD-for	CCTGGGAGTTATGGGGTGAA	Sigma
CD2.AD-rev	CGCTGACTACAACCCTGACA	Sigma
CD2.AE-for	CCCTAACTGACTCCATCCCC	Sigma
CD2.AE-rev	TCGACACTGGATTCCTTGCT	Sigma
GPD2.AA-for	CAGATGAGAGCCTTTTGTGG	Sigma
GPD2.AA-rev	CCCTTAGAAACGAGTATTGCCA	Sigma
GPD2.AB-for	CACAGTGTCTTATTATTGGGATGG	Sigma
GPD2.AB-rev	AGGATTCAGTTGGGCCTTTT	Sigma
GPD2.AC-for	AATTGTGCCCTGTCAAGCTG	Sigma
GPD2.AC-rev	TGACTCTGAAGCGTGGCATA	Sigma
PDCD1.AA-for	ACGTGGATGTGGAGGAAGAG	Sigma
PDCD1.AA-rev	CAGAGAGGAACCCAGGAGTT	Sigma

PDCD1.AAC-for	AGACTTCTCAATGACATTCCAGC	Sigma
PDCD1.AAC-rev	GTAGGTGCCGCTGTCATTG	Sigma
VDR.AA-for	CATCTGGAGCTGAGAGGAGG	Sigma
VDR.AA-rev	GAAACCAGGCAGCTGATTCC	Sigma
VDR.AB-for	CCTCTGACACCAACACACAG	Sigma
VDR.AB-rev	GTAGGAATCGTTTGGTGCCC	Sigma
VDR.AC-for	CTGTTGTGAAGACGCTGCAT	Sigma
VDR.AC-rev	GCCCACCATAAGACCTACGA	Sigma

\*Taken for final experiments. crRNAs were reconstituted to a concentration of 200 microM in Nuclease-Free IDTE Buffer and stored as per the manufacturers instructions.

### 3.1.9 Software and Algorithms

**Table 3.11: Software and algorithms**

Software/Algorithms	Purpose
Affinity Designer (v1.9.3)	Graphs
CASY	Cell Counting
FACS Diva (v8.0.2)	Acquisition and compensation of flow cytometry data
FlowJo (v10.7.2)	Analysis of flow cytometry data
GraphPad Prism (v9)	Figures and statistics
ImageJ	Western Blot measurement
LaTeX TeXstudio (v3.1.2)	Writing of the thesis
Mendeley (v2.59.0)	Managing references
ArchR (v1.0.1)	scATAC-seq data analysis
bcl2fastq	Demultiplexing
bedtools	bam to bigWig file conversion

### 3. MATERIAL AND METHODS

---

Bowtie2 (v2.3.3)	Mapping of reads
chromVAR	Calculation of TF motif accessibility
EnhancedVolcano (v1.4.0)	Creating volcano plots
FastQC (v0.11.5)	QC of sequencing data
Harmony	Batch effect correction
Heatmaply (v1.2.1)	Creating heatmaps
HOMER (v4.10.1)	<i>De novo</i> TF motif enrichment
IDT crRNA selection tool	crRNA design
IGV browser (v2.10.3)	Visual exploration of chromatin accessibility
Incucyte© Base Analysis Software	Analysis of killing assays
Java (v1.8.0)	Programming language
Leiden (v0.3.8)	Clustering
macs2 (v2.2.7.1)	Peak calling
MAGIC	Denoising sparse scATAC-seq data
Mendeley	Literature organization
Microsoft Office 2019	Raw data processing
R (v3.6.3)	Data analysis and plotting
sambamba (v0.7.1)	Data processing
Skewer (v0.2.2)	Trimming ATAC-seq reads
Snappgene	Primer design
snaptools (v1.4.8)	Pre-processing of scATAC-seq data
sambamba (v0.7.1)	Duplicate removal
TIDE	INDEL quantification
UCSC genome browser	crRNA selection, in-silico PCR
vbc score	crRNA design

---

## **3.2 Methods**

### **3.2.1 Ethics**

Primary tumor samples and adjacent healthy tissue from HCC, ccRCC and HNSCC tumor patients were collected solely after signed informed consent of the patients and with approval of the ethics committee (University Regensburg, reference numbers 19-1414-101, 16-355-101, 13-257-101) in accordance with the Helsinki Declaration. Peripheral blood mononuclear cells were isolated from leukocyte reduction chambers derived from healthy thrombocyte donors after their signed informed consent (University Regensburg, reference number 13-101-0240).

### **3.2.2 Cell culture**

Murine NIH 3T3 cells were cultured in DMEM supplemented with 10 % FCS and 1 % PenStrep. Human Jurkat cells were cultured in RPMI containing 10 % FCS and 1 % PenStrep according to the vendors recommendations. M579-A2 cells were kindly provided by the group of Prof. Beckhove (LIT) and were already described in the literature [120, 99]. The original melanoma cells (M579) derived from a melanoma patient and a cell line was established from it at the Sharett Institute of Oncology (Jerusalem, Israel). M579 cells are originally HLA-A2 negative and were therefore stably transfected with the pcDNA3-HLA-A2 plasmid to generate M579-A2 cells. M579-A2 cells were cultured in CMM medium and detached by use of trypsin and subsequently split 1:10 when they reached around 80 % confluency. All cells mentioned here were handled under sterile conditions and incubated at 37 °C, 5 % CO<sub>2</sub> and 95 % humidity. Cell lines were tested for mycoplasma contamination on a regular basis. Living cells were counted using the Neubauer chamber and Trypan blue exclusion.

#### 3.2.3 Sample collection and cell preparation

Collection of tumor-, tissue- and blood samples was carried out under the observance of the Helsinki Declaration (see 3.2.1). Primary HCC tumor samples and adjacent non-tumor liver tissue samples were collected from 4 male patients with an average age of 73.8 years ( $\pm 4$ ; range from 69 to 78) undergoing major liver resection. Primary HNSCC samples from the tumor center and tumor periphery were derived from 3 male and 1 female patients (all HPV negative) with an average age of 57.8 years ( $\pm 14$ ; range from 43 to 71), which underwent oropharyngeal or oral cavity surgery. Primary ccRCC samples from the tumor center and the tumor periphery as well as from adjacent healthy kidney tissue were collected after surgical tumor resection from patients with an average age of 63 years. To isolate immune cells from ccRCC and HNSCC tumor and adjacent-tissue specimen, samples were cut into pieces using scalpels, dissociated in HBSS +Ca/Mg using program h-tumor\_02 of the MACS dissociater and digested for 1 hour at RT using collagenase IA (218 U/mL) and DNase I (435 U/mL) in T cell medium (10 % human AB serum, 2 mM Glutamin, 2 mM Pyruvat, 0,4X MEM Vitamin Solution, 50  $\mu$ M beta-Mercaptoethanol, 0.5 % PenStrep). Subsequently, red blood cell lysis was performed as per the manufacturers instructions and the obtained single cell suspensions from ccRCC samples were cryopreserved in liquid nitrogen using a 1:1 mix of primary TILs freezing medium A and B. HNSCC derived single cell suspensions were further processed without cryopreservation. To isolate immune cells from HCC tumor and adjacent healthy liver tissue, first samples were washed with HBBS followed by dissection into small fragments using scalpels. Digestion of the tissue was performed using collagenase IV and DNase I. This step was followed by removal of hepatocytes via filtration through a 40  $\mu$ m mesh. Immune cell isolation was performed using Ficoll gradient centrifugation. Isolated cells were cryopreserved in freezing medium and stored in liquid nitrogen until further use. PBMCs (peripheral blood mononuclear cells) were isolated using Ficoll gradient centrifugation, followed by red blood cell

lysis and cryopreservation in freezing medium until further use.

All samples were provided by the people mentioned in (3.1.5) and immune cell isolation was performed by technicians in most cases.

### **3.2.4 FACS staining, acquisition and cell sorting for ATAC-seq experiments**

To isolate immune cells from tumor single cell suspensions, in order to subject them to single-cell ATAC-seq, HCC and ccRCC samples were thawed according to 10X protocol for primary/fragile cells (protocol “CG000169”, 10X genomics), whereas HNSCC samples were always freshly provided and did not need to be thawed. Subsequently, CD45 positive enrichment was performed with HCC and ccRCC samples, but not with HNSCC samples, according to the manufacturer’s recommendations. We used PBMC-derived CD8<sup>+</sup> T cells from healthy blood donors as controls. PBMCs were thawed the same way as primary tumor samples and were either subjected directly to cell sorting for subsequent scATAC-seq (“resting”) or activated for 18 hours (“18 hours activated”) or 3 days (“3d activated”), respectively. Activation was performed as follows: 100,000 cells per well were activated using anti-human TransAct (containing  $\alpha$ -CD3 and  $\alpha$ -CD28 antibodies conjugated to a polymeric nanomatrix) diluted 1:100 in T cell medium supplemented with 100 U/mL IL-2 for the contemplated time frame.

Cell staining for FACS sorting or flow cytometry was performed as described in the following section: Cells were stained in 1.5 mL Eppendorf tubes for cell sort or 96-well v-bottom plates for flow cytometry. All centrifugation steps for the following procedure were carried out at 1000 x g for 2 min at 4 °C. Prior to surface staining, cells were washed in PBS followed by blocking unspecific binding sites and Fc-receptors with human Kiovig solution (1:20 in PBS) for 10 minutes at 4 °C. After a centrifugation step, cells were resuspended in 50  $\mu$ l antibody mastermix (FACS buffer mixed with respective antibodies) per million cells and surface staining was

### 3. MATERIAL AND METHODS

---

performed for 20 minutes at 4 °C. The following anti-human antibodies were used for surface staining: CD3 (clone HIT3a), CD8a (SK1), CD45RA (HI100), CD38 (HIT2), 41BB (4B4-1), CD28 (CD28.2), CD197 (G043H7), PD1 (NAT105) LAG3 (11C3C65) and TIM3 (F38-2E2). For dead cell exclusion, cells were stained with fixable viability dye Zombie aqua according to the manufacturer's protocol.

To assess cytokine production capacity of T cells derived from tumors, adjacent healthy tissues and blood, cells were incubated for 5 hours with 1X Cell Stimulation Cocktail containing transport inhibitors, which was diluted in T cell medium. Subsequently, staining of cytokines IFN $\gamma$  and TNF $\alpha$  was performed by use of the Foxp3/Transcription Factor Staining Buffer Set as per the manufacturers recommendations using IFN $\gamma$  (4S.B3) and TNF $\alpha$  (MAb11) antibodies. Directly before acquiring the samples on a FACS LSR II, cell suspensions were passes through a 40  $\mu$ m filter unit. FACS device functionality was validated using BD CS&T beads on a regular basis. Compensation for fluorescence spillover was performed using lymphocytes stained with CD4 (OKT4) antibodies labeled with the respective fluorochromes for cell sorting experiments, and using compensation beads incubated with respective antibodies for flow cytometry experiments, respectively.

Sorting of cells for ATAC-seq experiments was conducted using a FACS Aria™ II cell sorter and was performed by the LIT Cell Sorting Core Unit. Prior to sorting, cell suspensions were filtered using a 30  $\mu$ m pre-separation filter. Whenever possible, post-sort quality controls were conducted. When performing scATAC-seq, target cells were sorted into normal Eppendorf tubes (not low-bind tubes, as this could lead to cell loss when sorting limited cell numbers), which were precoated with 500  $\mu$ l 0.5%BSA-PBS. When performing bulk ATAC-seq, target cells were sorted into DNA LoBind tubes, which were precoated with 500  $\mu$ l 10%FCS-PBS. Flow cytometry data were analyzed using FlowJo and subsequent statistical analysis was performed using GraphPad Prism. The gating was conducted as depicted in figure 3.1.

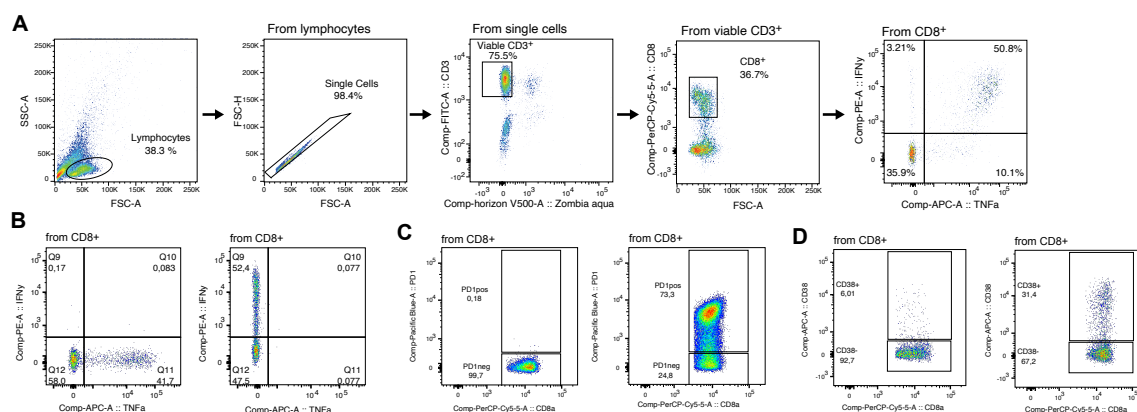


**Figure 3.1: Gating strategy**

(A) Gating strategy to gate lymphocytes<sup>+</sup>single cells<sup>+</sup>dead<sup>-</sup>CD3<sup>+</sup>CD8<sup>+</sup> cells. As an example, gating for IFN $\gamma$  and TNF $\alpha$  is shown. (B) FMO (Fluorescence Minus One) staining controls for adjusting the cytokine gating are shown. (C) Gating strategy for gating PD1<sup>+</sup> and PD1<sup>-</sup> is shown, respectively. PD1 expression of naive CD8<sup>+</sup> T cells derived from blood samples are shown on the left panel, PD1 expression of CD8<sup>+</sup> TILs isolated from a HCC tumor is shown on the right panel. (D) Gating strategy for gating CD38<sup>+</sup> and CD38<sup>-</sup> is shown, respectively. CD38 expression of naive CD8<sup>+</sup> T cells derived from blood samples are shown on the left panel, CD38 expression of CD8<sup>+</sup> TILs isolated from a HCC tumor is shown on the right panel.

### 3.2.5 Establishment of scATAC using a species mixing experiment

A species mixing experiment was performed in order to establish and optimize plate-based single-cell ATAC-seq as published by Chen et al. 2018 [33]. For this purpose, human Jurkat T cell line and murine NIH 3T3 cell line were mixed 1:1, stained with 7-AAD as per the manufacturers instructions and subsequently 50,000 viable cells were FACS sorted by excluding 7-AAD positive cells. Afterwards, cells were pelleted by centrifugation (5 min, 500 x g, 4 °C), followed by a washing step with pre-chilled 1 x PBS. This step was repeated one more time. Subsequently, the supernatant was discarded and cells were either resuspended in 50  $\mu$ l tagmentation mix “Chen et al. 2018” consisting of high salt TD buffer (33 mM Tris-HCl pH 7.8, 66 mM KCl, 10 mM MgCl<sub>2</sub>, 16 % dimethylformamide) supplemented with 0.5  $\mu$ l 1 % Digitonin and 5  $\mu$ l Tn5 in nuclease-free water or in 50  $\mu$ l tagmentation mix “Corces et al. 2017” [39] consisting of 1 x low salt TD buffer (2 x buffer: 20 mM Tris-HCl pH 7.6, 10 mM MgCl<sub>2</sub>, 20 % dimethylformamide) supplemented with 16.5  $\mu$ l PBS, 0.5  $\mu$ l 1 % Digitonin and 5

### 3. MATERIAL AND METHODS

---

$\mu\text{l}$  Tn5, respectively. To allow for the tagmentation reaction through the Tn5 enzyme, the mixes were incubated for 30 min at 37 °C on a shaker set to 800 rpm. Thereafter, 50  $\mu\text{l}$  of ice-cold tagmentation stop buffer (10 mM Tris-HCl pH 8.0, 20 mM EDTA pH 8.0 in nuclease-free water) was added followed by incubation on ice for 10 min in order to stop the reaction. Afterwards, 100-300  $\mu\text{l}$  0.5 % BSA-PBS were added and the mix was transferred to a FACS tube. Herein, nuclei were stained with DNA intercalating fluorescent propidium iodide (PI, 0.2  $\mu\text{g}/\text{mL}$ ) for 15 minutes (4 °C, dark). Subsequently, single nuclei were sorted into 384-well plates, which contained 2  $\mu\text{l}$  2 x reverse crosslinking buffer (RCB) and 2  $\mu\text{l}$  of 10  $\mu\text{M}$  forward and reverse custom Nextera index primer mix [39] per well. Each well contained a different primer mix so that every single cell in the plate was labeled with different barcodes during final amplification via PCR. To compare the performance of several reverse crosslinking buffers, nuclei which were tagmented with “Chen et al. 2018” tagmentation mix were sorted into plates containing different RCB buffers. The following RCB buffers were tested: “hiSDSprotK-TWEEN” (2 x RCB: 100 mM Tris-HCl pH 8, 100 mM NaCl, 40  $\mu\text{g}/\text{mL}$  Proteinase K, 0.4 % SDS in nuclease-free water) and “loSDS-TWEEN” (2 x RCB: 100 mM Tris-HCl pH 8, 100 mM NaCl, 0.04 % SDS in nuclease-free water). The same procedure was carried out with nuclei, which were tagmented with “Corces et al. 2017”. For a fifth condition, parts of the “Corces et al. 2017” nuclei were additionally sorted into plates containing RCB buffer “EDTA-MgCl” (2 x RCB: 50 mM EDTA in nuclease-free water). To perform Tn5 release and proteinase K digestion (where applicable), nuclei were spun down and plates were incubated for 30 min at 65 °C with lid temperature set to 105 °C. To every well containing SDS, 4  $\mu\text{l}$  of 10 % TWEEN-20 were added to quench SDS. To wells containing EDTA, 4  $\mu\text{l}$  of 25 mM  $\text{MgCl}_2$  were added so EDTA could build complexes with it. A quantitative PCR reaction (10  $\mu\text{l}$  2X NEBNext PCR Master Mix, 1 x SYBR green, final volume 20  $\mu\text{l}$ ) was carried out, using 8 nuclei per sample and an appropriate PCR program (72 °C 5 min; 98 °C 30 s; 30 cycles: 98 °C 10 s, 63 °C 30 s, 72 °C 1 min), in order to estimate the optimum number of amplification cycles. The final amplification was performed using

the same settings and the number of cycles set according to the average of the C<sub>q</sub> values of the 8 single nuclei qPCRs. Since all tagmented chromatin fragments per cell contained now oligonucleotide barcodes, libraries could be pooled afterwards. DNA purification was performed using the MinElute Purification Kit and a vacuum manifold. Thereafter, SPRI (solid-phase reversible immobilization) size selection with AmpureXP beads to exclude fragments smaller than 150 bp was carried out (lower cut-off, 1.8 x). Library quantification and quality control was performed using a Qubit fluorometer to assess DNA concentration and an Agilent Bioanalyzer to measure average fragment size and to check for the expected nucleosome pattern. Equimolar amounts of each library were paired-end sequenced (2<sup>x</sup>38 bp, 75 cycles) on a NextSeq 550 instrument using the NextSeq 500/550 High Output Kit v2.5.

#### **3.2.6 Optimized scATAC-seq protocol for primary samples**

T cells derived from human tumors, adjacent healthy tissue and blood were isolated, pre-enriched, stained and sorted as described in subsections 3.2.3 and 3.2.4. To receive an approximate information about the exhaustion level of cells derived from tumors and surrounding tissue on the proteomic level, either Dead<sup>-</sup>CD3<sup>+</sup>CD8<sup>+</sup>PD1<sup>+</sup> or Dead<sup>-</sup>CD3<sup>+</sup>CD8<sup>+</sup>PD1<sup>-</sup> were sorted into Eppendorf tubes, as described in 3.2.4. Either rested or activated Dead<sup>-</sup>CD3<sup>+</sup>CD8<sup>+</sup> cells were sorted from peripheral blood of healthy donors as a control. After sorting of cells was completed, scATAC-seq was performed as described in the section 3.2.5, with minor adaptations. After sorting, washing was omitted. Instead steps from the 10X Genomics protocol (protocol “CG000169”, 10X Genomics) were implemented. The steps included the following: Cells were resuspended and lysed by adding 100 µl of chilled lysis buffer (10 mM Tris-HCl pH 7.4, 10 mM NaCl, 3 mM MgCl<sub>2</sub>, 0.1 % TWEEN-20, 0.1 % NP-40, 0.01 % Digitonin, 1 % BSA in nuclease-free water), pipette mixed and incubated on ice for 3 minutes. Thereafter, 300 µl pre-cooled wash buffer (10 mM Tris-HCl pH 7.4, 10 mM NaCl, 3 mM MgCl<sub>2</sub>, 0.1 % TWEEN-20, 1 % BSA in nuclease-free water)

### 3. MATERIAL AND METHODS

---

was added followed by pipette mixing (5 x). After centrifugation (500 x g, 5 min, 4°C ) nuclei were resuspended in 50 µl tagmentation mix according to Corces et al. 2017 with minor adaptations (1X TD buffer as described previously, 16.5 µl PBS, 0.5 µl 1 % Digitonin, 0.5 µl 10 % TWEEN-20, 2.5 µl Tn5 in nuclease-free water). Tagmentation took place for 30 minutes at 37°C on a shaker set to 800 rpm. After the tagmentation reaction was stopped, single nuclei were stained with PI as described above. Subsequently, single nuclei were sorted into 384-well plates containing 2 µl of the “loSDS” 2X RCB buffer (100 mM Tris-HCl pH 8.0, 100 mM NaCl, 0.04 % SDS) as well as a primer mix of forward and reverse custom Nextera index primers. Afterwards, plates were incubated at 55°C for 30 minutes to perform Tn5 release. This step was followed by SDS quenching by adding 4 µl of 4% TWEEN-20. Final amplification was performed as described in 3.2.5 by adding 8 µl of 2X PCR MM to each well and setting the number of amplification cycles according to the results of the qPCR, which was usually a value around 20. Sequencing of libraries was performed as described in 3.2.5.

#### 3.2.7 Bulk ATAC-seq

Chromatin accessibility mapping in bulk was performed by use of the ATAC-seq method as described by Corces et al. [39], but with minor adaptations. In short, 50,000 viable-sorted cells per condition were pelleted by centrifugation (10 min, 4°C , 500 x g). Thereafter, the pellet was lysed for 3 min on ice by adding 50 µl resuspension buffer with supplements (10 mM Tris-HCl pH 7.4, 10 mM NaCl, 3 mM MgCl<sub>2</sub>, 0.1 % NP-40, 0.1 % Tween-20, 0.01 % Digitonin). Subsequently, 1 mL of ice-cold resuspension buffer supplemented with Tween-20 was added followed by a centrifugation step (10 min, 4°C , 500 x g). After discarding the supernatant, the cell pellet was carefully resuspended in the transposition mastermix (25 µl 2 x TD buffer, 2.5 µl Tn5, 16.5 µl PBS, 5 µl nuclease-free water, 0.5 µl 1 % Digitonin, 0.5 µl 10 % Tween-20) and incubated for 30 min at 37°C on a shaker set to 1000 rpm.

After DNA purification (Clean and Concentrator-5 kit as per the manufacturers instructions) DNA was eluted with 23  $\mu$ l elution buffer. 2  $\mu$ l of the DNA were used in a qPCR reaction (1.25  $\mu$ M forward and reverse custom Nextera primers [39], 1 x SYBR green final concentration, final volume 10  $\mu$ l) to assess the optimal number of amplification cycles using PCR (72°C 5 min; 98°C 30 s; 25 cycles: 98°C 10 s, 63°C 30 s, 72°C 1 min). Final amplification was carried out using custom Nextera primers and the aforementioned PCR program, whereby numbers of cycles were set according to the Cq value of the qPCR. Following amplification, SPRI size selection was performed using AmpureXP beads to exclude fragments larger than 1,200 bp and primer dimers. After measuring DNA concentration by use of the Qubit fluorometer and average fragment size by use of the Agilent Bioanalyzer, libraries were equimolarly pooled and paired-end sequenced using the NextSeq 550 platform (2<sup>\*</sup>38 bp, 75 cycles).

#### 3.2.8 Pre-processing and analysis of bulk ATAC-seq

After sequencing was accomplished, demultiplexing was performed using `bcl2fastq` and the parameters: `--barcode-mismatches 1`. Subsequently, ATAC-seq reads were trimmed with `Skewer` [92] and mapped to the hg19 genome by use of `Bowtie2` [104] utilizing the `'--very-sensitive'` parameter and a maximum fragment length of 2,000 bp. `Sambamba` [197] `'markdup'` command was used to remove duplicate and unpaired reads, whereas reads with mapping quality  $>30$  and successful alignment to the nuclear genome were retained. All pursued downstream analyses were performed by utilizing these filtered reads. To depict the centered transposon binding event, all reads aligning to the + strand were offset by +4 bp, and all reads aligning to the -strand were offset -5 bp as described previously [24]. To be able to visualize chromatin accessibility, for example via the IGV genome browser, bigWig files were produced. This was done as follows: first coverage files were produced using `bedtools` [160] `genomeCoverageBed` with the filtered bam files as input. Each position

### 3. MATERIAL AND METHODS

---

was normalized by division through the total library size as well as multiplication by 106. This step was followed by utilizing the `bedGraphToBigWig` command from the UCSC genome browser tools to convert coverage files to the bigWig format. Dr. Nicholas Strieder and Prof. Dr. Michael Rehli from the LIT NGC Core Team performed demultiplexing. Dr. Christian Schmidl performed bioinformatic analysis.

#### 3.2.9 Pre-processing and analysis of scATAC-seq

Demultiplexing was performed using `bcl2fastq` and the parameters: `--barcode-mismatches 0`. Demultiplexed single-cell sequencing reads deriving from the same sample were combined and all reads were formatted in the following way: starting with "@" + "barcode" + ":" + "read\_name" so that the SnapATAC pipeline [53] could process it. Reads were aligned to the hg19 genome using `bowtie2` with the option "`--maxins 2000`" and duplicates of mapped bamfiles were removed using `sambamba` in order to keep only unique and paired reads with a quality  $\geq 30$ . Within ATAC-seq analysis, peak calling is one of the most essential processes. For scATAC-seq, peaks cannot be called on a single cell basis, since per-cell scATAC-seq data is binary (accessible or not accessible). Therefore, groups of cells were defined, typically in the form of clusters. Furthermore, pseudo-bulk replicates were produced to enable controlling for reproducibility of the called peaks. Integrated data of droplet-based scATAC-seq were already pre-processed with `cellranger`. Filtered .bam files derived from plate-based scATAC-seq as well as the pre-processed droplet-based scATAC-seq data were put into the ArchR R package [70] whereby cell barcodes with minimum 100 fragments per cell and a TSS enrichment score  $\geq 3$  were kept. Thereafter, doublets were identified and filtered (`'addDoubletScores'` and `'filterDoublets'`), followed by quality evaluation of the retained data. Subsequently, further filter steps were applied to retain only cell barcodes with a minimum of 1000 fragments and a TSS enrichment score  $\geq 10$ , followed by dimensionality reduction to be able to filter out non CD8<sup>+</sup> T cells. Dimensionality reduction was performed using the `'addIter-`

ativeLSI' method (iterations = 4, res = 2, maxClusters = 6, varFeatures = 25000, dimsToUse = c(1:24), LSI method: "log(tf-idf)", scaleDims=TRUE). In the following downstream analysis dimensions 1-21 were used, as this was suggested by the explained variances. Next, clustering ('addClusters', res = 1, dimsToUse =c(1:21), scaleDims=TRUE) and UMAP dimensionality reduction (nNeighbors = 30, metric = cosine, minDist = 0.3) were performed. Subsequently, non-CD8<sup>+</sup> clusters were removed from the dataset based on gene-activity scores of CD8A, CD8B, and CD4 loci. Iterative LSI dimensionality reduction was repeated on remaining data (iterations = 3, res = c(0.1, 0.4) , varFeatures = 25000, dimsToUse= c(1:24), LSI method: "log(tf-idf)", scale-Dims=TRUE). Afterwards, dimension 1-11 were chosen for downstream analyses, based on inspection of explained variances. After clustering (addClusters, res = 1, dimsToUse =c(1:11), scaleDims=TRUE), batch effects arising from the scATAC technology (plate vs droplet-based processing) were removed by use of Harmony [102]. In order to visualize data, UMAP dimensionality reduction was performed. ArchR gene activity scores were used to estimate gene activity, which were imputed by MAGIC [208] for visualization purposes. Identification of marker genes was performed utilizing the 'getMarkerFeatures' and 'getMarkers' functions with a foldchange of 1.5 (wilcoxon test, cutOff "FDR <= 0.01 & Log2FC >= 0.58"). In order to be able to perform peak calling with macs2 [229], first pseudobulk replicates were created from scATAC-seq datasets (ArchR functions 'add-GroupCoverages' and 'addReproduciblePeakSet'). For downstream peak-based analysis, marker peaks for each cluster were called using the 'getMarkerFeatures' function on the ArchR peak-matrix (wilcoxon test, cutOff = "FDR <= 0.01 & Log2FC >= 1"). To control for total accessibility and GC content, a background peak set was generated using 'addBgdPeaks'. To calculate enhanced chromatin accessibility at different TF motif sequences within single cells, ChromVAR [176] was used with 'addDeviationsMatrix', and the HOMER motif set [80]. To visualize the derived motif deviations, scores were imputed with MAGIC. The ArchR functions 'get-Footprints' and 'plotFootprints' (flank = 250, flankNorm = 50, normMethod = "subtract", smoothWin-dow = 6") were used

### 3. MATERIAL AND METHODS

---

to calculate and visualize transcription factor footprinting. The same cutoffs ("FDR  $\leq 0.01$  & Log2FC  $\geq 1$ ") were used to compute pairwise comparisons for marker peak detection. The output peak sets were analyzed for *de novo* motif enrichment using HOMER's 'findMotifsGenome.pl' function. Co-accessibility was computed with the ArchR function 'addCoAccessibility'. Dr. Nicholas Strieder and Prof. Dr. Michael Rehli from the LIT NGC Core Team performed demultiplexing. Dr. Christian Schmidl performed bioinformatic analysis.

#### 3.2.9.1 Analysis of core ATAC-seq profiles

For the 'core' analysis as described in chapter 4.5, first the scATAC-seq dataset was refined by removing all PBMC samples and the MAIT cell cluster. Subsequently, the 'addIterativeLSI' method (iterations = 3, res = c(0.1, 0.4), varFeatures = 25000, dimsToUse = c(1:24); LSI method: "log(tf-idf)", scale-Dims=FALSE) was used for dimensionality reduction with the aim to reduce major sample-specific biases. This was done since we sought to generate generalized ATAC-seq signature for universal T cell chromatin landscapes. Since the first dimension correlated with sequencing depth ( $>0.75$ ), this dimension was filtered according to ArchR's standard settings. Dimensions 2-13 were used for downstream analysis, since inspection of explained variances suggested this. Subsequently, data were harmonized for technology (10x droplet based scATAC-seq vs. plate-based approach) and entity, as well as for clustering ('addClusters', res = 0.3), and UMAP dimensionality reduction. Marker gene identification, peak calling, marker peak identification as well as ChromVAR motif deviations were performed as defined in the previous section (3.2.9).

#### 3.2.9.2 Enrichment of published signatures in scATAC-seq clusters

Published signatures (among them already preprocessed signatures [103]) were used to derive the expression of genes in these signatures in single cells by using the 'addModuleScore' function from ArchR. This step was followed by computing the

median module score for each signature in each cluster. This was then plotted by use of the ggheatmap package and normalized by the "percentize" function. This bioinformatic analysis was performed by Dr. Christian Schmidl.

#### **3.2.9.3 Pseudotime trajectory analysis**

To be able to analyze peak accessibility-, transcription factor activity- and gene activity-dynamics along a hypothetical time axis, as identified by progressive changes in chromatin accessibility from the precursor exhausted to the terminally exhausted T cell state, pseudotime analysis was performed. To this end, the harmony-corrected ArchR object from the core analysis was subjected to "addTrajectory". Thereby, a user-defined trajectory was used as a guide, which was as follows: first "Cluster 3", followed by "Cluster 2", ended by "Cluster 1" was used. Next, peak accessibility, ChromVAR deviation scores, and gene activity scores were correlated throughout pseudotime using the 'getTrajectory' and 'plotTrajectoryHeatmap' commands under consideration of standard parameters for gene activities as well as peak accessibility. Further, a "varCutOff = 0.8" for the motif matrix was used. This bioinformatic analysis was performed by Dr. Christian Schmidl.

#### **3.2.10 TIL209 expansion and cell culture**

TIL209 are tumor-infiltrating lymphocytes derived from an inguinal lymph node from a melanoma patient. They are polyclonal CD8<sup>+</sup> T cells specific for typical melanoma antigens such as MART-1 (melanoma antigen recognized by T cells 1) or gp100 (glycoprotein 100). The TIL209 used in this thesis derived from the third round of expansion (counted from after surgical removal from the patient). We expanded the TIL209 using TIL209 expansion medium with feeder cells (mix of PBMCs from three different donors, irradiated with 60 Gray) as described in a published rapid expansion protocol (REP, [93]). TIL209 cells were tested negative for HBV, HCV, HIV and mycoplasma after expansion. Freshly expanded TIL209 were frozen in 1:1 mix

### 3. MATERIAL AND METHODS

---

of TIL209 freezing medium A and B and stored in liquid nitrogen. For thawing TIL209 cells, cryovials were removed from liquid nitrogen and thawed in the water bath at 37 °C for 1 min. Subsequently, cells were transferred to a Falcon tube containing 10 mL of prewarmed 10%FCS-RPMI and benzonase. After centrifugation (300 x g, 5 min, RT) cells were washed one more time and cultured at a density of 1 mio cells per mL in CLM medium supplemented with 3,000 U/mL IL-2, 5 ng/mL IL-7, and 5 ng/mL IL-15 for 48 hours. Afterwards, the IL-2 concentration was reduced to 200 U/mL. Viability and cell numbers were assessed using the CASY cell counter as per the manufacturers instructions. Jasmin Mühlbauer from the Beckhove group and I expanded TIL209 cells in a collaborative effort.

#### 3.2.11 CRISPR/Cas9-based genome editing via electroporation

Human expanded TIL209 cells were transfected with ribonucleoprotein complexes (*S.p.* Cas9:gRNA) via electroporation to induce knockout of specific target genes. Different devices were tested and compared for transfection, namely the Neon™ Transfection System and the 4D-Nucleofector™ System. The Alt-R® CRISPR/Cas9 system from Integrated DNA Technologies was used for genome editing. In general, three to seven crRNAs were tested per target, depending on the outcome of the first crRNA screens. CrRNAs were either pre-designed from IDT according to their proprietary algorithm ([www.idtdna.com/CRISPRPREDESIGN](http://www.idtdna.com/CRISPRPREDESIGN)), designed by use of the VBC score algorithm ([www.vbc-score.org](http://www.vbc-score.org)) or taken from a published paper [182]. The cutting side was chosen to be in the first exons whenever possible. For each target gene, guide RNAs, targeting either different exons or the same exon within a distance of 50-80 bp (which could lead to deletions according to Seki et al. [182]), were selected. Furthermore, preference was given to guides with the highest IDT on-target score ([https:// eu.idtdna.com/site/order/designtool/index/CRISPR\\_SEQUENCE](https://eu.idtdna.com/site/order/designtool/index/CRISPR_SEQUENCE)). All crRNAs (listed in 3.10) were purchased from Integrated DNA Technologies in the modified Alt-R® format.

To prepare TIL209 cells for transfection, cells were thawed and rested for 2 days as described in 3.2.10. On the day of the experiment TIL209 were counted via CASY cell counter. Thereafter, a 24-well or a 48-well flat-bottom plate was prepared with CLM medium without antibiotics (final volume 500  $\mu$ l per 48-well and 1000  $\mu$ l per 24-well, respectively) containing 200 U/mL IL-2, 5 ng/mL IL-7, and 5 ng/mL IL-15 and prewarmed in the incubator. In the meantime, guide RNAs were prepared. Therefore, respective crRNA and tracrRNA were mixed in a 1:1 ratio in PCR tubes and adjusted to a concentration of 88  $\mu$ M by adding IDTE buffer. crRNA:tracrRNA duplexes were produced via incubation for 5 minutes at 95 °C and a cooling phase (RT) afterwards to form functional gRNAs. Thereafter, different gRNAs could be combined in desired ratios if multiple gRNAs were used for gene knockout. gRNAs were stored on ice until usage.

#### **3.2.11.1 Transfection of RNPs using the Neon™**

For RNP transfection using the Neon™, Cas9 was diluted to 36  $\mu$ M in a 0.2 mL PCR tube using Resuspension Buffer T. Furthermore, the Electroporation Enhancer was diluted to a final concentration of 10.8  $\mu$ M in a 0.2 mL PCR tube using Resuspension Buffer T as well. Both were stored on ice until further usage. RNP complexes were prepared by gently mixing pre-assembled gRNA and diluted Cas9 in a 1:1 ratio, followed by incubation for 20 minutes at RT. The respective amount of cells were taken and washed once in 1x PBS (centrifugation at 300 x g, 10 min, RT). Afterwards PBS was entirely removed and cells were resuspended in Resuspension Buffer T at a concentration of 5.5 mio cells per mL. Subsequently, per electroporation 9  $\mu$ l of the cell suspension (containing 500,000 cells), 1  $\mu$ l of the RNP complex as well as 2  $\mu$ l of the Electroporation Enhancer were combined in a PCR tube and directly subjected to electroporation, since the Resuspension Buffer T is toxic to the cells. Neon Transfection was performed as per the manufacturers instructions using 10  $\mu$ l of the final electroporation mix and the Neon® Pipette. Different electroporation set-

### 3. MATERIAL AND METHODS

---

tings were tested as described in 4.7.1, whereas the final settings were 1400 V, 30 ms, 3 pulses. After electroporation, cells were immediately transferred to the plate containing pre-warmed CLM medium including supplements. Afterwards, the plate was left for 15 minutes untouched at RT and thereafter transferred to the incubator. TIL209 cells were incubated for 5 days at a density of 1 mio/mL in order to left time for introducing the gene knockout and letting still present target gene products being degraded.

#### **3.2.11.2 Transfection of RNPs using the Nucleofection™**

TIL209 and cell culture plate preparation as well as gRNA duplex generation was performed as described in 3.2.11. To prepare RNPs for nucleofection, per reaction 3 µl of gRNA were mixed with 1.2 µl of Cas9 enzyme by gently swirling the pipet tip while pipetting and filled up to 12.6 µl with IDTE buffer afterwards. Amount of Cas9 was multiplied by number of gRNAs taken and IDTE buffer reduced as needed in this case. Subsequently, RNPs were incubated for minimum 20 minutes at RT. Respective amount of TIL209 cells needed were transferred to an eppendorf tube and centrifuged (100 x g, 10 min, RT). Afterwards, cell culture media had to be removed entirely and cells were resuspended in Electroporation Buffer P3 (or in Ingenio buffer in some cases) to a concentration of 1 mio cells per 20 µl buffer. Beforehand, Buffer P3 was prepared by adding the Supplement as described by the manufacturer. Per condition 20 µl of the cell suspension and 12.6 µl of the RNP complex were combined in a PCR tube. 30 µl of the RNP/cell suspension mix was transferred to a well of the 16-well Nucleocuvette™ Strip. After closing the strip, transfection was performed by using the settings described in chapter 4.7.1. Thereafter, 70 µl of pre-warmed CLM (without antibiotics, with supplements) were added to each well without resuspension, followed by incubation for 15 minutes at RT. Afterwards, the nucleofected cells were transferred to a prepared plate as described in 3.2.11, adjusted to a cell density of 1 mio cells per mL and incubated for

5 days. Meike Neureither helped me with testing of the Nucleofector electroporation conditions as a Bachelor's student under my supervision.

### **3.2.12 TIDE assay for determination of INDEL mutations after CRISPR/Cas9**

Genomic DNA of WT and genome edited TIL209 was extracted, purified and quantified. Subsequently a PCR was performed to amplify the sequences around the expected Cas9 cutting site. Therefore, NEBNext® High Fidelity 2X PCR Master Mix (NEB) was combined with 10 µM of forward and reverse primer respectively as well as 100 ng of DNA. The PCR was carried out using the following program as recommended by NEB with minor adaptations: initial denaturation at 98°C for 3 min, 98°C denaturation for 15 sec, adjusted annealing temperature for 30 sec, extension at 72°C for 25 sec. Step 2-4 were repeated 34 times followed by final extension at 72°C for 2 min. The annealing temperature was adjusted to the respective primers used. Afterwards, the PCR product was checked via DNA electrophoresis and send to Sanger sequencing. Final INDEL quantification was performed by use of the online TIDE tool (<https://tide.nki.nl>, [19]).

### **3.2.13 Quantification of CRISPR/Cas9 KO efficiency via flow cytometry**

To assess target KO efficiency, 200,000-500,000 TIL209 cells were taken on day five after genome editing and transferred to a 96-well V-bottom plate. Cells were washed with PBS and centrifuged (1000 x g, 2 min, 4°C ). Afterwards, cells were resuspended in 25 µl antibody mastermix per 0.5 mio cells and surface staining was performed in FACS buffer for 20 minutes at 4°C in the dark. The following antibodies were used for surface staining: CD8 (RPA-T8), CD69 (FN50) and PD1 (EH12.2H7). Zombie NIR fixable viability dye was used for dead cell exclusion. Afterwards, intra-

### 3. MATERIAL AND METHODS

---

cellular staining was performed using the Foxp3/Transcription Factor Staining Buffer Set as per the manufacturers instructions together with the following antibodies: VDR (D2K6W) and EOS (W16032A). Secondary staining of VDR was performed by use of anti-rabbit IgG labeled with AF647. Stained cell suspensions were filtered (40  $\mu\text{m}$ ) before acquiring on the FACS Celesta™. Gating was conducted as follows using FlowJo: lymphocytes were selected, doublets and dead cells excluded, and CD8<sup>+</sup> selected. To calculate the KO efficiency, the control (scr) was set as 100 % and the percentage of remaining target positive cells in the KO condition were divided by 1 % of the control condition. Subtracting the remaining % positive from 100 % creates the KO efficiency.

#### 3.2.14 Ca<sup>2+</sup> influx assay

We examined calcium flux in genome edited TIL209 cells, since calcium flux is an essential determining factor in T cell activation [156] and we wanted to determine whether target KO induces changes in calcium flux. We used fluorescent calcium indicators Fluo-3, AM and Fura-Red™, AM for ratiometric measurement of changes in cytosolic calcium levels. The two indicators change their fluorescence emission upon binding to Ca<sup>2+</sup> ions, which can be detected by flow cytometers already starting from Ca<sup>2+</sup> concentrations around 100 nM. 500,000 TIL209 cells were taken from culture on day six after CRISPR/Cas9 and resuspended in XVIVO medium. Subsequently, cells were stained with 2  $\mu\text{M}$  of the aforementioned calcium indicators for 30 min at RT in the dark. Afterwards, cells were washed and incubated with biotinylated anti-CD3 antibodies (OKT3, 10  $\mu\text{g}/\text{mL}$ ) at RT in the dark for another 45 minutes. After incubation cells were washed again, resuspended at a concentration of 0.5 mio/mL and transferred to flow cytometry tubes whereby technical duplicates were created. Afterwards, first the cytosolic Ca<sup>2+</sup> baseline was assessed for 30 seconds on a FACSCanto™ flow cytometer. Subsequently, TCRs were crosslinked via addition of streptavidin (40  $\mu\text{g}/\text{mL}$ ), thereby enabling measurement of quantity and

kinetics of cytosolic  $\text{Ca}^{2+}$  flux upon TCR ligation for another 300 seconds [156]. As a quality control, 1  $\mu\text{l}$  of ionomycin was added to drain the  $\text{Ca}^{2+}$  stores, which was measured for another 90 seconds. Analysis was performed by use of the FlowJo Kinetics Tool. From the raw data, first the ratio of Fluo-3/Fura-Red was calculated with Excel, followed by normalization to the baseline values. Yvonne-Natascha-Susanne Weiss (AG Jantsch, UKR) performed  $\text{Ca}^{2+}$  flux assays and analyzed the raw data.

#### **3.2.15 Image-based killing assay**

To validate the cytotoxic capacity of genome edited TIL209 we performed real-time image-based killing assays using the Incucyte® SX5 Live-Cell Analysis System or the IncuCyte ZOOM system (both incubators with integrated microscope). M579-A2 melanoma cells were taken as target cells and genome edited TIL209 as well as control (scr) TIL209 cells were taken as effector cells. M579-A2 cells alone were taken as control for effects of the CLM medium as well as the Caspase-3/7 Dye (mock). Target cell death was assessed by green fluorescent staining of nuclear DNA via Incucyte® Caspase-3/7 Dye, which intercalates into DNA only after activation via caspase-3/7, which allows quantification of apoptosis over time.

One day before setting up the co-culture, 10,000 M579-A2 cells in 200  $\mu\text{l}$  CMM were seeded per well in a transparent flat-bottom 96-well plate. The plate was incubated overnight to allow adherence of M579-A2 cells overnight, which was visually controlled via microscopy on the next day. On the day of the experiment, TIL209 cells (day five after CRISPR/Cas9-based target KO) were resuspended, counted using the CASY system, washed and resuspended in CLM without any supplements in a concentration of 50,000 cells per 50  $\mu\text{l}$ , to reach a 5:1 effector:target ratio in the end. Subsequently, CMM medium was taken off the seeded M579-A2 cells and the respective target KO TIL209 cells as well as the scr control TIL209 cells were added. Co-cultures were created in triplicates. Next, 50  $\mu\text{l}$  of Incucyte® Caspase-3/7 Dye, diluted 1:1000 in CLM without supplements was added to the co-culture.

### 3. MATERIAL AND METHODS

---

After allowing the TILs to settle down for approximately 30 minutes, the plate was transferred to the Incucyte analyzer, where cells were co-cultured at 37 °C , 5 % CO<sub>2</sub> and 95 % humidity. Pictures of phase contrast as well as green fluorescence were taken hourly (4 pics per 96 well), with a 10X magnification for 48 hours. Killing of target cells was thereby registered via green fluorescence of target cells and was used as a reference value for cytotoxic capacity of TIL209 cells. Therefore, after the measurement was completed, the integrated GCU (green calibrated unit) per image was calculated (GCUx $\mu\text{m}^2/\text{image}$ ) by the Incucyte© Base Analysis Software for each time point. Background fluorescence was subtracted and green fluorescence of TIL209 was rejected via a size mask, taking only melanoma cells into account. Finally, raw data were analyzed and visualized with GraphPad Prism software.

Additionally to the image-based Incucyte measurement, after 48 hours of TIL209:M579-A2 co-culture, remaining M579-A2 cells were counted with the help of Accucheck counting beads using a flow cytometer. As a readout, viability of remaining M579-A2 cells was first calculated in percent as fraction of M579-A2 cells not co-cultured with TIL209. Afterwards, cytotoxicity (%) of TIL209 conditions was calculated as viability (%) subtracted from 100 %=no cytotoxicity.

#### **3.2.16 Target staining in primary TILs**

Primary TILs, samples from adjacent-tumor tissue, and PBMCs were thawed as described in 3.2.4. After a washing step and removal of cell clumps, cells were counted and resuspended at a density of one mio cells per mL in T cell medium containing 100 U/mL IL-2 and 1  $\mu\text{g}/\text{mL}$   $\alpha$ -CD28 antibodies. 200,000 cells per well were seeded in a flat-bottom 96-well plate that has been pre-coated with  $\alpha$ -CD3 antibodies (10  $\mu\text{g}/\text{mL}$  in PBS) overnight. After restimulation for 24 hours cells were stained for flow cytometry analysis as described before.

### **3.2.17 Statistical analysis**

Statistical tests used, parameters used and numbers of biological and technical replicates as well as statistical significance are declared in the figures and figure legends. Confidence level was always set to 95 % and statistical significance is defined as  $P < 0.05$ . Asterisks in the figures represent P values as follows: \*  $p < 0.05$ , \*\*  $p < 0.01$ , \*\*\*  $p < 0.0002$ , \*\*\*\*  $p < 0.0001$ . Statistical tests were performed using the GraphPad Prism software (version 9).



## 4 Results

### 4.1 Establishment of plate based single-cell ATAC sequencing

With ATAC-seq we can study the non-coding genome, which is responsible for epigenetic regulation of gene expression and thereby can explain differentiation and function of specific cell populations [24]. Since few years, this technique can be performed on the single-cell level, which enables to study even heterogeneous and rare cell sub-populations [25].

To perform ATAC sequencing on the single-cell level, it is necessary to separate single nuclei and amplify their tagmented DNA using a unique barcode. To realize this, one possibility is a plate-based version, which was published by Chen et al. in 2018 [33]. When using this protocol, first the cell population of interest is isolated, then lysed and tagmented in bulk, followed by sorting single nuclei into 384 well plates, where indexing is conducted via barcoded primers. After amplification, the libraries can be pooled, purified, size selected and subjected to sequencing. The plate-based protocol has some advantages when comparing it to microfluidics-based methods. First of all, no special equipment like the Fluidigm C1 device [25] or the 10x Genomics Chromium device [173] is necessary. Second, less amount of the Tn5 enzyme is needed, since tagmentation is pursued in bulk, whereas the microfluidic Fluidigm C1 version performs tagmentation on individual cells. Furthermore, it is thought that the plate-based protocol produces less amounts of unwanted mito-

## 4. RESULTS

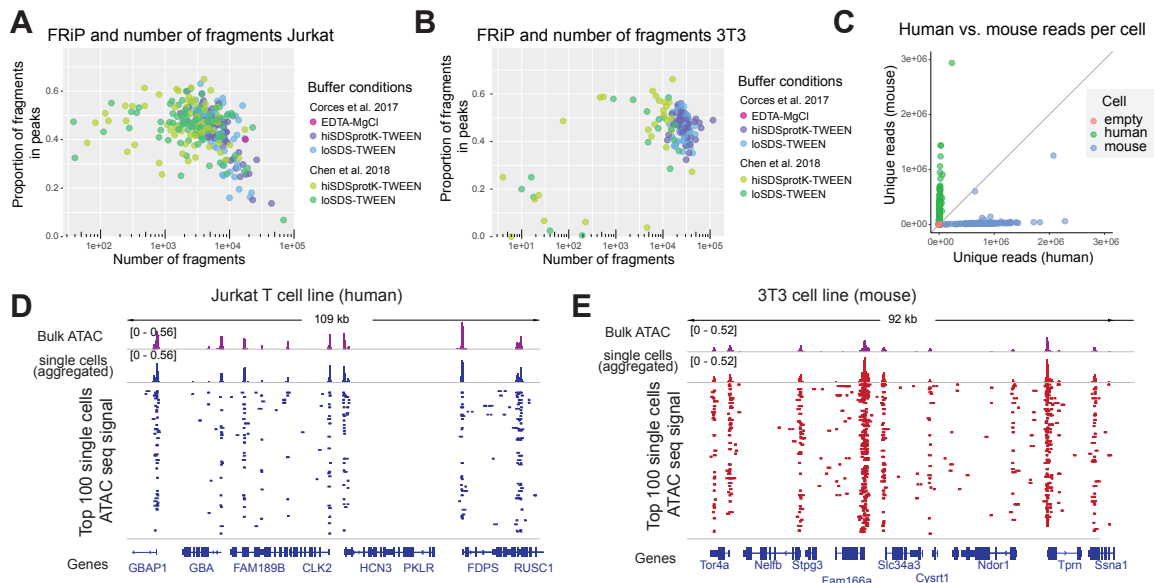


**Figure 4.1: Establishment of plate-based scATAC-seq**

Test of different ATAC-seq lysis buffers and Tn5 release conditions (“EDTA MgCl”, “high SDS and ProteinaseK”, “low SDS without ProteinaseK”) shown as proportion of sequencing fragments in peaks vs number of unique fragments in human Jurkat (A) and murine 3T3 cells (B). (C) Cells mapped to either human or mouse genome according to their sequencing reads. (D-E) Genome browser tracks of bulk ATAC and merged single-cell ATAC signals from 50,000 cells each (top rows) and of 100 single cells (lower rows) at representative gene loci of Jurkat (D) and 3T3 cells (E).

chondrial DNA reads and at the same time a higher fraction of reads in peaks (FRiP) [7]. First, to establish the plate-based single-cell ATAC-seq protocol, the single-cell sorting accuracy needs to be confirmed. For this purpose, we performed a species mixing experiment where equal numbers of human Jurkat and murine 3T3 cells were mixed, assayed, and mapped to the human and mouse genome, respectively. Notably, we could confirm low doublet frequency (Figure 4.1C).

Second, to receive the best possible signal-to-noise ratio, we compared different tagmentation buffers as well as Tn5 release buffers. On the one hand, tagmentation buffers should stabilize the DNA and on the other hand facilitate optimal Tn5 working conditions. After successful tagmentation the Tn5 has to be stripped off the DNA for the subsequent PCR reaction to work properly, hence the need for optimal Tn5 release buffers. The quality control, where FRiP versus fragments per cell are plotted (Figure 4.1A-B), shows that the tagmentation buffer from Corces et al. [39] facilitates

higher numbers of fragments per cell. The "loSDS-TWEEN" Tn5 release condition yielded the highest output regarding sequenced chromatin profiles. Based on this results, we decided to use the Corces tagmentation buffer together with the "loSDS-TWEEN" buffer for all further experiments.

Third, to verify the sequencing quality, we compared bulk ATAC data to single-cell ATAC data derived from the same cell type. We could confirm that aggregated scATAC-seq chromatin profiles match with bulk ATAC-seq profiles, confirming reasonable quality of the plate-based assay (Figure 4.1D-E).

## **4.2 Single-cell open chromatin profiling and functional analysis of human CD8<sup>+</sup> TILs and controls**

To investigate the open chromatin landscape and thereby the gene-regulatory networks of heterogeneous CD8<sup>+</sup> TILs from human tumors, we established the plate-based single-cell ATAC-seq protocol as described in chapter 4.1 in our laboratory. Furthermore, we started collaborations with clinicians to receive human tumor samples from three different cancer types, namely head and neck squamous cell carcinoma (HNSCC), hepatocellular carcinoma (HCC) and clear cell renal cell carcinoma (ccRCC). Besides this, we set up a sorting panel to isolate PD1<sup>+</sup> and PD1<sup>-</sup> CD8 T cells from tumor tissue and adjacent healthy tissue to complement the sequencing data with information about IT relevant immune checkpoint expression on the protein level. In addition, we performed a functional analysis of the samples subjected to scATAC-seq, by measuring cytokine and exhaustion marker expression via flow cytometry. As a control, we applied the same procedure to peripheral blood-derived CD8<sup>+</sup> from healthy donors. The workflow for our study can be seen in Figure 4.2A.

## 4. RESULTS

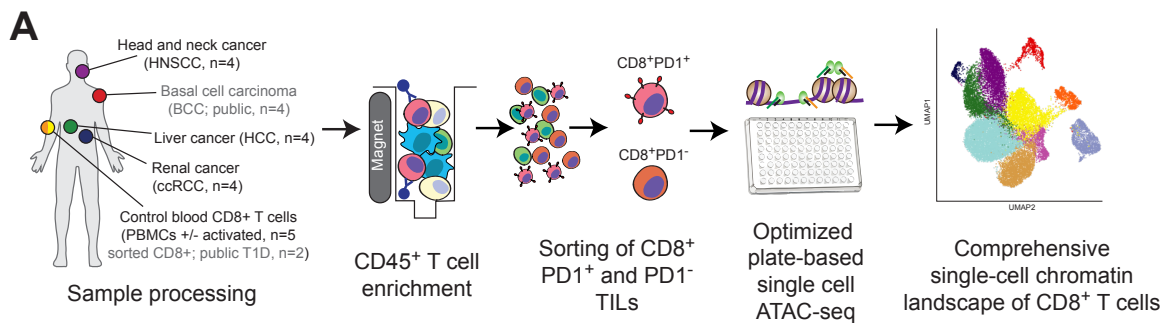


**Figure 4.2: Study setup**

(A) Schematic of sample collection and experimental workflow.

### 4.2.1 Improvement of plate based single-cell ATAC sequencing for primary samples

To receive enough tagmented DNA fragments for sequencing, the DNA has to be amplified via PCR. To avoid over-amplification, which could induce GC bias and PCR duplicates, a qPCR step is recommended to determine the optimal number of amplification cycles. As qPCR as well as PCR only amplify tagmented DNA specifically, the ct (cycle threshold) value is also an estimate of the amount of tagmented DNA. Hence, the quality of the first two runs with primary cells was not as good as anticipated according to tagmented DNA amount, as indicated with significant lower ct values of samples processed with the "Chen et al protocol" (Figure 4.3B). Besides this, the quality of the scATAC-seq data was diminished, since the number of fragments enriched at TSS sites (transcription start site) and the number of unique fragments per samples was lower when compared to samples processed differently (Figure 4.3A, respective samples labeled in pink). To overcome this, few steps from a 10x Genomics protocol (protocol "CG000169", 10x Genomics) for fragile cells and low cell input were adapted (see 3.2.6). These modifications improved the output in regard to tagmented DNA amount (Figure 4.3B) as well as the signal-to-noise ratio (Figure 4.3A).

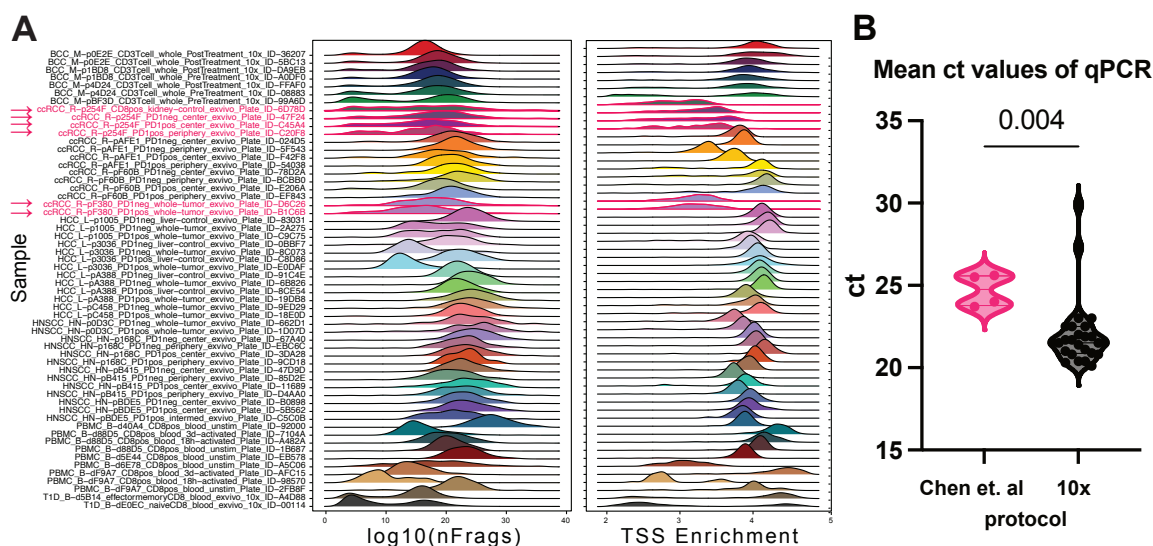


**Figure 4.3: Comparison of scATAC-seq protocols**

(A) Plot of number of fragments (log<sub>10</sub>) for all scATAC-seq samples (left) and transcription start site (TSS) enrichment (right). Pink samples were processed with the "Chen et. al protocol". (B) Violin plot of qPCRs amplifying tagged DNA performed after different scATAC-seq protocols. Each dot indicates the mean ct value of one sample (n=8 cells). Unpaired t-test (Mann-Whitney) was performed to test significance.

#### 4.2.2 Single-cell ATAC sequencing of human CD8<sup>+</sup> TILs and peripheral blood derived CD8<sup>+</sup> T cells worked reliably

After processing 49 samples (PD1<sup>+</sup> and PD1<sup>-</sup> CD8<sup>+</sup> cells sorted from tumor or adjacent non-tumor tissue) from 12 tumor patients (HNSCC, n=4; ccRCC, n=4; HCC, n=4) and 5 healthy blood donors (9 samples in total; +/- *in vitro* activation) we were able to sequence the open chromatin profile from more than 19,000 single cells, and thereby could recover around 80 % of input cells. It is crucial, to verify the quality of the produced scATAC-seq data and filter only high quality profiles before performing downstream analysis. First, the sequenced fragment size distribution of all samples yielded the expected nucleosome occupancy pattern with enrichment of fragments of around 150 bp and 300 bp length, respectively, which corresponds to the DNA length wrapped around one or two nucleosomes, respectively (Figure 4.4A). Second, all samples showed a clear TSS enrichment profile as well as the expected smaller peak downstream of the TSS, where the +1 nucleosome is posi-

## 4. RESULTS

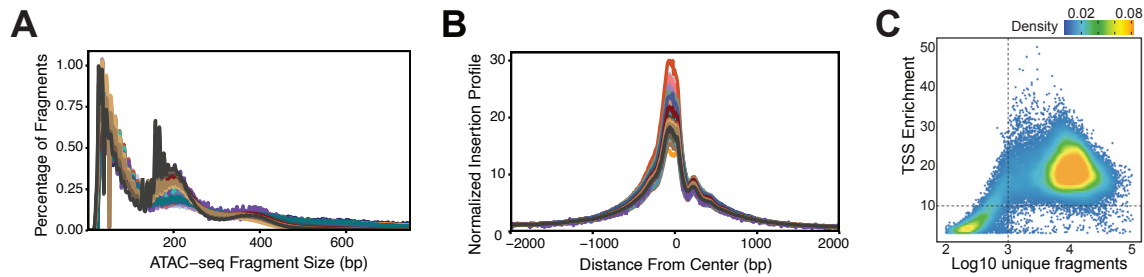


**Figure 4.4: Quality control and filter application of scATAC-seq data**

(A) Sequenced fragment size distribution of all samples. (B) Enrichment of sequencing fragments around TSS sites (-2000 kb to +2000 kb from all annotated TSS). (C) TSS enrichment vs unique fragments of each single cell. Dashed lines indicate filter cut-offs for downstream analysis.

tioned (Figure 4.4B). These observations confirmed the quality of our scATAC-seq data of human CD8<sup>+</sup> TILs and peripheral blood derived CD8<sup>+</sup> T cells. The single-cell data had to reach specific quality scores, in order to be integrated into downstream analysis. The specific cut-offs used are widely accepted [173, 70]. In our analysis, only scATAC-seq profiles with a minimum of 1000 unique fragments and a TSS enrichment score equally or above 10 were included (Figure 4.4C).

### 4.2.3 Implementation of controls and public available data

As described in (4.2.2), we implemented different controls in our study. We aimed to have an additional information on the protein level for every patient-derived CD8<sup>+</sup> cell subjected to scATAC-seq. We therefore decided to use PD1 expression as a marker for the exhaustion level of the cells, as high PD1 expression is often associated with the expression of other exhaustion-related co-inhibitory receptors (such as TIM3 [119]) and is an IT relevant immune checkpoint [203]. To this end, we sorted PD1<sup>+</sup> and PD1<sup>-</sup> CD8<sup>+</sup> TILs, respectively (Figure 4.5A-B). In addition, we wanted to discriminate TIL-specific from peripheral blood-derived chromatin signatures. For this purpose, we subjected unstimulated as well as *in vitro* activated (via anti-CD3/anti-CD28 antibodies) PBMC-derived CD8<sup>+</sup> from healthy donors to scATAC-seq. Furthermore, we included one published scATAC-seq dataset of T cells from patients with basal cell carcinoma (BCC; n=4 patients [173]). The dataset included samples col-

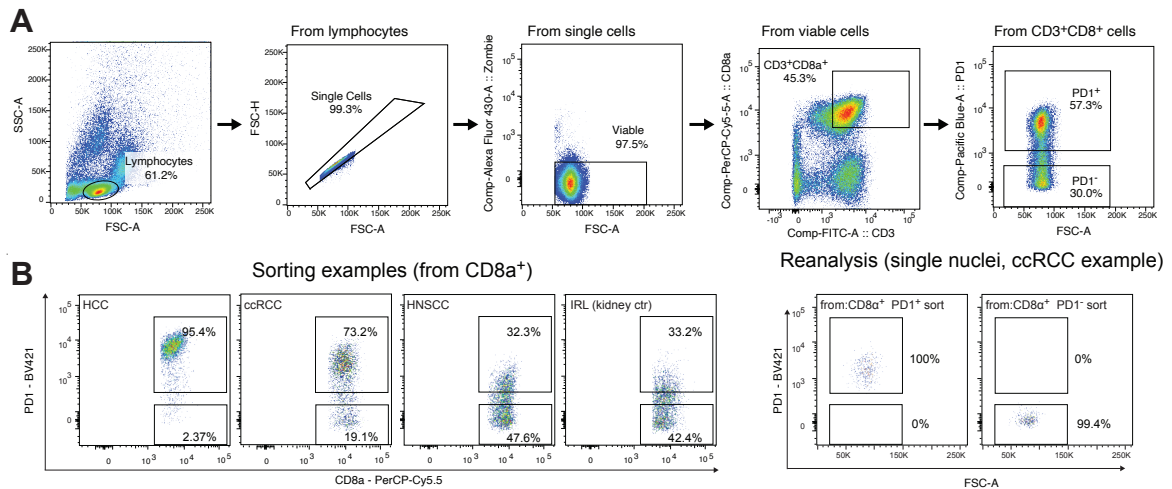


**Figure 4.5: Sorting strategy**

(A) Sorting strategy to sort Dead<sup>-</sup>CD3<sup>+</sup>CD8<sup>+</sup>PD1<sup>+</sup> or Dead<sup>-</sup>CD3<sup>+</sup>CD8<sup>+</sup>PD1<sup>-</sup> cells before subjecting TILs and T cells from tissue control to scATAC-seq. (B) Dot plots showing PD1 expression of exemplary scATAC-seq samples (left) and QC after sorting (right).

lected before and after immunotherapy treatment. We further supported our blood-derived controls by integrating scATAC-seq data from naïve and memory CD8<sup>+</sup> T cells isolated from PBMCs [1]. Since these data were produced with the droplet-based technique from 10x genomics [173], instead of the plate-based technique we used, the difference derived from the technology had to be corrected. For this purpose, we used Harmony, a R-based algorithm, which was developed to perform batch correction (such as for different donors, tissues etc.) of single-cell datasets [102]. To sum up, we were able to include internal controls like sorting markers and IT treated samples as well as biological controls like different blood-derived T cell subsets in our study.

#### 4.2.4 FACS-based phenotypical and functional characterization of TILs

We wanted to investigate the open chromatin landscape and thereby the gene-regulatory mechanisms of heterogeneous CD8<sup>+</sup> T cell states, both functional and dysfunctional, derived from human tumors and peripheral blood of healthy donors.

## 4. RESULTS

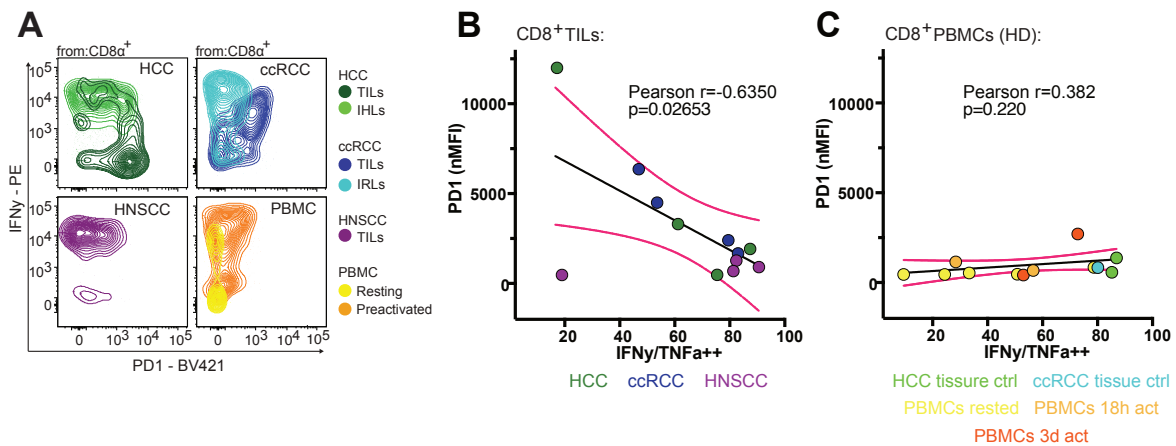


**Figure 4.6: Functional characterization of patient samples**

(A) Exemplary contour plot depicting PD1 vs IFN $\gamma$  expression of the three different entities and healthy donor blood control. (B) Correlation of normalized PD1 expression (MFI of PD1 $^+$  normalized to background (MFI of PD1 $^-$ )) and percentage of IFN $\gamma$ /TNF $\alpha$  double positive cells after 5h incubation with PMA/ionomycin is shown. Each dot is one patient, gated on CD8 $^+$ . Pearson correlation was performed and Pearson  $r$  as well as the  $p$  value of the correlation are shown. (C) Same analysis as for (B) with samples from healthy blood donors and adjacent non-tumor tissue as depicted in the colour code. All data derived from samples subjected to scATAC-seq.

Therefore, we performed FACS-based (Fluorescence-activated Cell Sorting) phenotypical and functional characterization of the sequenced samples (Figure 4.6A). We observed a negative correlation of normalized PD1 expression and IFN $\gamma$ /TNF $\alpha$  double positive cells within CD8 $^+$  T cells isolated from tumors, whereas in CD8 $^+$  T cells derived from adjacent non-tumor tissue and peripheral blood this correlation was slightly positive (Figure 4.6B-C). This indicates that PD1 is a marker for dysfunctional T cell states in TILs but a marker of activation in T cells derived from tissue and blood. In general, cytokine production as well as PD1 expression varied greatly between samples, confirming that we covered different states of functional and dysfunctional TILs here. Besides, all HNSCC TIL samples expressed low amounts of PD1 but almost all were cytokine producers, except one TIL sample. This leads to the impression that HNSCC TILs are rather still functional. This could further be confirmed by the observation that HNSCC TILs barely expressed CD38 (Figure 4.7A), which is an activation but also an exhaustion marker and often found to be co-expressed with PD1 and other co-inhibitory receptors [151, 181, 173]. This was

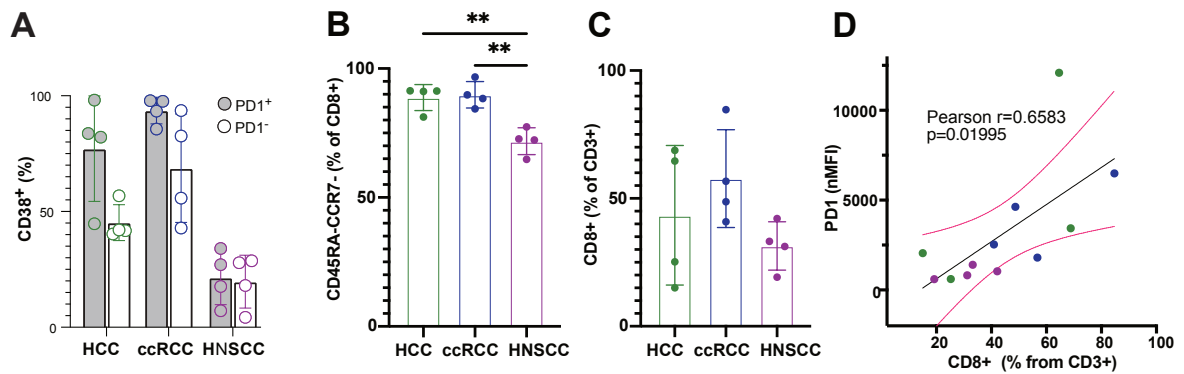


**Figure 4.7: Phenotypical characterization of patient samples**

(A) Bar plot of % CD38 positive expression of PD1<sup>+</sup> vs PD1<sup>-</sup> CD8<sup>+</sup> TILs. Shown is the mean  $\pm$  SD, every point is one patient sample. (B) Bar plot of percentage of effector memory subtype among all CD8<sup>+</sup> in percent. Shown is the mean  $\pm$  SD and individual values. Two-way ANOVA with multiple comparisons was performed. Asterisks depict  $p < 0.01$ . (C) Bar plot depicting percentage of CD8<sup>+</sup> among all T cells. (D) Pearson correlation of normalized PD1 expression and percentage of CD8<sup>+</sup> T cells of every patient. All data derived from samples subjected to scATAC-seq.

indeed the case for HCC and ccRCC TILs, where on average PD1<sup>+</sup> TILs expressed CD38 to a higher extent (Figure 4.7A). Moreover, our FACS analysis showed that percentages of CD8<sup>+</sup> T cells among CD3<sup>+</sup> cells were lower in HNSCC tumors (Figure 4.7C). Besides this, among HNSCC CD8<sup>+</sup> TILs were significantly lower percentages of effector memory (CCR7<sup>-</sup>CD45RA<sup>-</sup>) T cells compared to HCC and ccRCC (Figure 4.7B). All together, we found higher CD8<sup>+</sup> T cell percentages among all TILs to positively correlate with PD1 expression (Figure 4.7C), indicating that T cell inflamed tumors increase T cell dysfunction [64].

All together, we were able to generate single-cell chromatin profiles in high-quality. Within our dataset we covered a broad spectrum of human T cell states, which range from functional to dysfunctional states and derive from different tumor entities, adjacent non-tumor tissue and peripheral blood.

### **4.3 Unbiased analysis reveals heterogeneity and distinct IT relevant cell states among human CD8<sup>+</sup> TILs**

To identify the different cell states within our dataset, data were batch-corrected for the scATAC-seq method (Figure 4.8H) and bioinformatic analysis was performed using ArchR [70] (see 3.2.9). In short, after dimensionality reduction and clustering, Uniform Manifold Approximation and Projection (UMAP) embedding was performed for visualization purposes. With UMAP, the data can be interpreted in a way, that distance between clusters means higher differences between the annotated cell states. Our analysis revealed that 11 distinct clusters were present in our comprehensive dataset (Figure 4.8A), consisting of 26,479 single-cell chromatin profiles from CD8<sup>+</sup> T cells derived from 58 samples (Figure 4.8D), which in turn derived from 4 cancer entities (Figure 4.8B), 16 patients (Figure 4.8C), immune checkpoint treated patients and controls from healthy peripheral blood donors (Figure 4.8E-F). The 11 distinct clusters we detected assured that we covered a variety of primary human T cell states. Furthermore, we identified 8,453 unique marker genes within the dataset, confirming the differential chromatin landscapes underlying the different T cell states (Figure 4.8G).

#### **4.3.1 Different cell states can be identified by gene activity of marker genes**

To perform cell state annotation, ArchR offers the possibility to predict gene expression by computing distance-weighted chromatin accessibility, called gene activity. We plotted gene activity of cluster-specific marker genes as well as known T cell subset marker genes onto the UMAP projection (Figure 4.9A). We could identify mucosa associated invariant T cells (MAIT cells) by high gene activity of *ZBTB16*

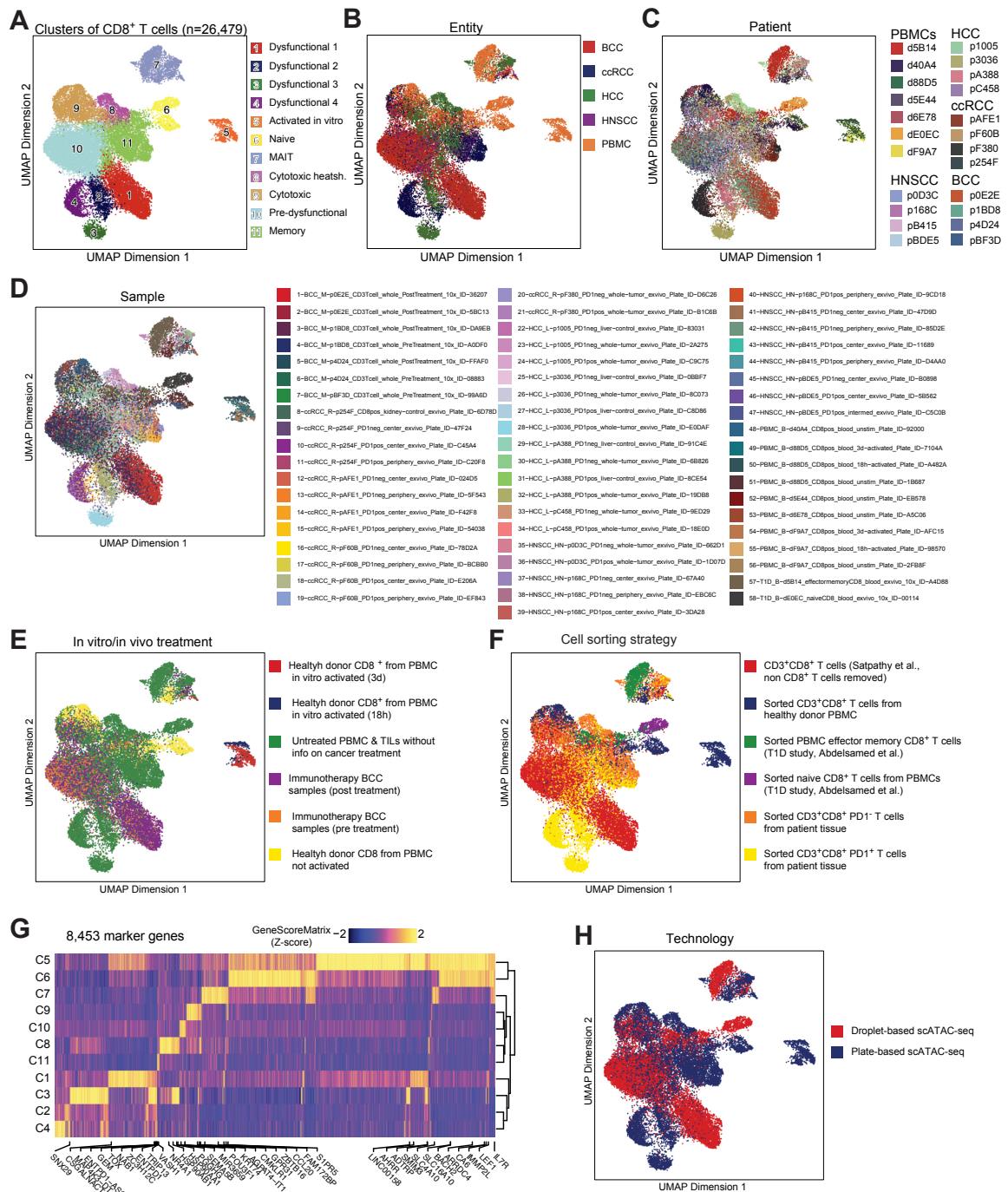


**Figure 4.8: Clustering and UMAP embedding of all single-cell chromatin profiles** (A-F, H) UMAP projection of all CD8<sup>+</sup> T cells. Every dot represents one cell. Cells are either colored by cluster affiliation (A), origin (B), patient/donor (C), sample origin (D), *in vitro/in vivo* treatment (D), cell sorting strategy (F) or single-cell ATAC-seq technology (H). (G) Z-scored heatmap of marker genes across all clusters. Representative genes are depicted.

## 4. RESULTS

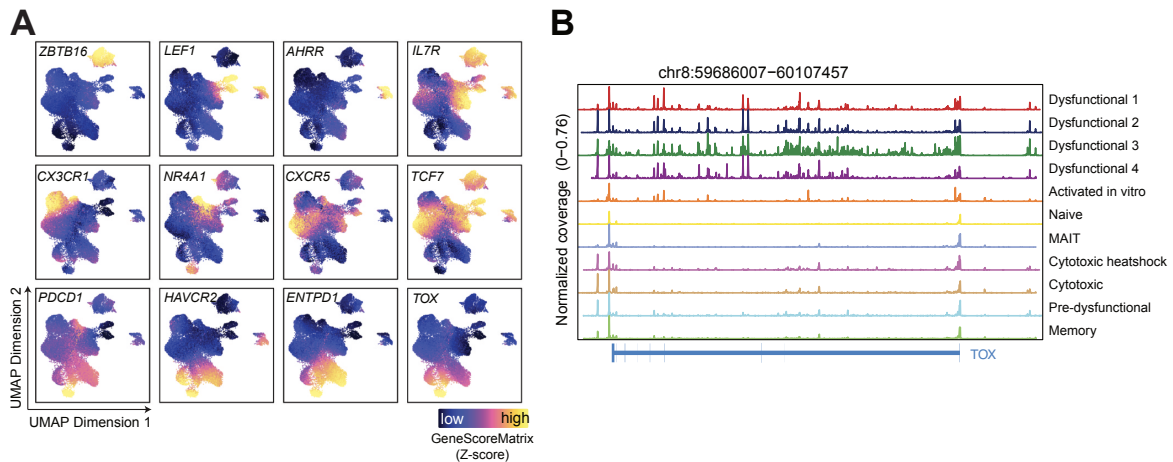


**Figure 4.9: Cluster identification via gene activity of marker genes**

(A) Z-scored per-cell gene activity of selected genes projected on the UMAP embedding. (B) Genome browser track of the TOX locus with merged single-cell signals for every cluster.

(encoding MAIT cell specific transcription factor PLZF in cluster 7. Cluster 6 showed high gene activity of *LEF1* and was populated by naïve CD8<sup>+</sup> T cells isolated from peripheral blood (Figure 4.8E-F). Cluster 5 displays *in vitro* activated cells, since all *in vitro* activated CD8<sup>+</sup> T cells are located within this cluster (Figure 4.8E). Cluster 11 showed increased gene activity of *IL7R* and comprised cells from all entities and from peripheral blood (Figure 4.8B), suggesting a memory-like population. Cluster 9 and a part of cluster 8 were characterized by high gene activity of *CX3CR1*, which is a marker for differentiated cytotoxic T cells [221]. Surprisingly, we found that *NR4A1* (encoding Nur77) as well as heat shock protein (*HSP90AA1*; *HSP90AB1*) gene activity was increased in cluster 8 and 3. These genes are considered to be involved in cellular stress response, for example oxidative stress, which could arise from hypoxia in the tumor microenvironment [8, 149, 2]. Cluster 10 was characterized by high gene activity of marker genes for "precursor exhausted T cells" (T<sub>PEX</sub>, [96]) like *CXCR5* and *TCF7*, which fits to the observation that most of the BCC derived pre-treatment CD8<sup>+</sup> TILs can be found in this cluster (Figure S3A). Finally, clusters 1-4 showed elevated gene activity of co-inhibitory receptors PD1 (*PDCD1*) and TIM3 (*HAVCR2*) as well as of T cell dysfunction markers CD39 (*ENTPD1*), and TOX. TOX is known as a key driver of T cell dysfunction [4, 98, 181]. We found the chromatin

to be intensively remodeled over the whole *TOX* locus in as dysfunctional classified clusters 1-4 (Figure 4.9B). Overall we could identify 11 different cell states by use of the gene activity of known marker genes.

### 4.3.2 CD8<sup>+</sup> TIL states can be annotated by projection of public T cell signatures

We aimed to validate our annotation of the T cell states by projecting published CD8<sup>+</sup> T cell gene-expression signatures onto our scATAC-seq clusters (Figure 4.10A-B). MAIT cell as well as naïve T cell states could be confirmed in cluster 7 and 6 respectively (Figure 4.10A-B), [196, 224]. Furthermore, enrichment of a cytotoxic T cell signature confirmed the assumed identity of cells in cluster 9 [110, 224]. Interestingly, genes associated with an interferon response signature [196] were over-represented in cluster 8 and 3, which could indicate a recent inflammatory response. This observation would fit to the hypothesized cellular stress response 4.3.1, as IFN is suggested to have a proapoptotic effect and decreases metabolic fitness of CD8<sup>+</sup> T cells [23]. Within cluster 11, genes expressed in CD8<sup>+</sup> TILs of checkpoint therapy responders were enriched [172]. Two gene signatures associated with dysfunctional T cells were observed in cluster 1-4. One of them even combined chromatin and transcriptomic data from published studies and validated the findings by Mass-Cytometry of human lung cancer TILs [14]. In addition, a signature found in CD8<sup>+</sup> TILs of checkpoint therapy non-responders was enriched in the as dysfunctional assigned clusters 1-4 [172], which reassured our manual cell state assignment. The fact that, unlike HCC and RCC TILs, TILs from HNSCC patients were enriched in pre-dysfunctional cluster 10, but barely populated dysfunctional clusters 1-4 (Figure 4.10C-D) matches with results from our FACS analysis (chapter 4.2.2), which showed that HNSCC TILs differ from HCC and RCC TILs also on the phenotypical and functional level. All together, we were able to produce a large dataset of chromatin profiles from different T cell states, ranging from functional and presumably IT

## 4. RESULTS

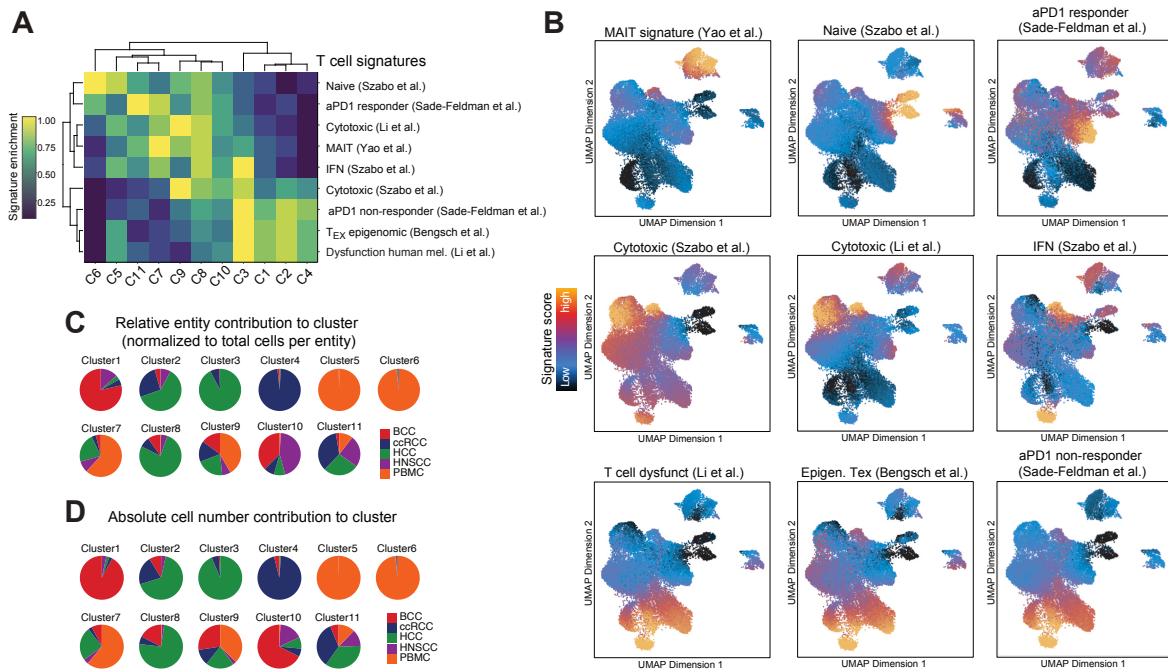


**Figure 4.10: Cluster identification via projection of published signatures**

(A) Heatmap of enrichment of published T cell signatures in all clusters. (B) Signature enrichment on a per-cell basis projected onto UMAP embedding. (C-D) Pie charts of entity contribution to clusters either normalized to total cell number per entity (C) or as absolute cell number per cluster (D).

relevant cell states to dysfunctional states deriving from different tumor entities.

### 4.4 Dissection of gene-regulatory cues, differential gene regulation and the tissues' influence on human CD8<sup>+</sup> TILs

Next, we wanted to dissect the underlying gene-regulatory mechanisms and identify key regulators of the cell states we found in our broad dataset of chromatin landscapes of human TILs. Analyzing, which TF motif sequences are enriched in the open chromatin regions or if TF occupancy at the predicted binding sites is changing can tell us, which transcription factors might regulate gene transcription in a specific cell state. To this end, peaks (accessible chromatin regions) have to be

called and marker peaks for each cluster have to be identified. Furthermore, the deviation of accessibility of transcription factor motif sequences from the HOMER motif set [80] are predicted using chromVAR [176]. This motif deviation can be interpreted as transcription factor activity and is computed on the single-cell level. In addition, TF footprint analysis can be performed to predict TF occupancy. This can be done, since the Tn5 transposase cleaves only unoccupied chromatin, meaning where nucleosomes or DNA binding proteins like transcription factors are binding, Tn5 cannot cut. This results in missing sequenced fragments around occupied TF binding motifs, which is referred to as "footprint". The deeper the valley of the footprint and the higher the accessibility of the chromatin around it, the higher is the probability that the TF was actually binding. All together, we identified 200,015 unique peaks in distal, exonic, intronic and promoter regions within our dataset (Figure 4.11A), from which 56,894 represented marker peaks (Figure 4.11A). On average, dysfunctional clusters 1-4 possess less open chromatin regions, which could indicate their terminally differentiated character (Figure 4.11A). Among the top 100 most variable motifs we found binding sites of TFs, which are well known for T cell activation, differentiation and exhaustion such as AP-1, BATF, NF $\kappa$ B, RUNX, T-bet, Nur77 (NR4A1), TCF, and NFAT (Figure 4.11C). In summary, the chromatin accessibility at gene-regulatory elements and TF binding sites differs between distinct CD8<sup>+</sup> cell states and thus could explain differences in phenotype and function.

#### **4.4.1 CD8<sup>+</sup> TIL states are driven by differential gene-regulatory mechanisms**

We next looked at motif deviations on the cluster (Figure 4.12A, presented as heatmap) as well as on the single-cell level (Figure 4.12B, presented as UMAP). To confirm that motif activity accounted for true TF occupancy we analyzed the TF footprints (Figure 4.12C). To begin with, in PBMC-derived naive T cells, we found increased activity of several stem-cell associated TCF transcription factors (Figure 4.12A). Fur-

## 4. RESULTS

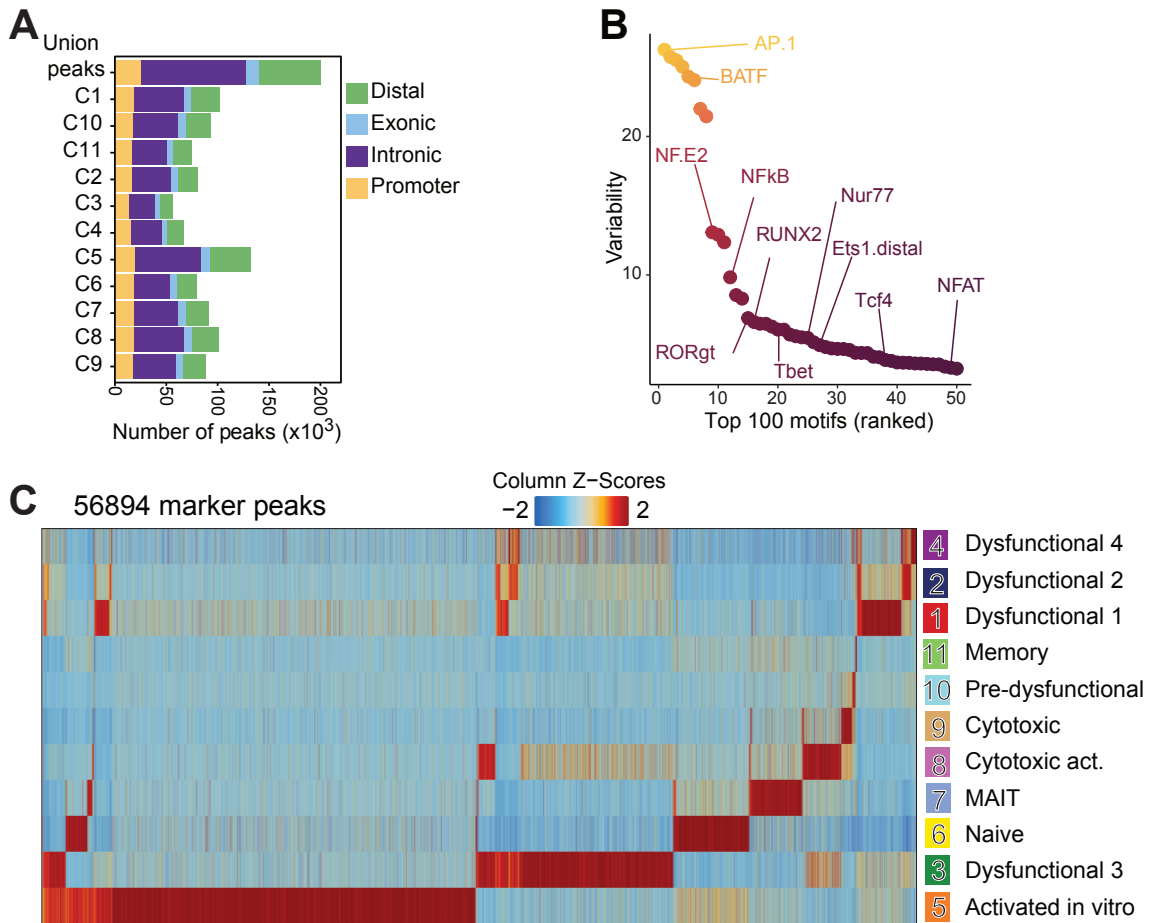


**Figure 4.11: Variability of chromatin accessibility among T cell states**

(A) Bar chart showing proportion of peaks with different genomic regions. (B) Top 100 variable motifs among the whole dataset as computed by chromVAR. (C) Heatmap illustrating marker peaks within the scATAC-seq clusters. Chromatin accessibility is z-score normalized.

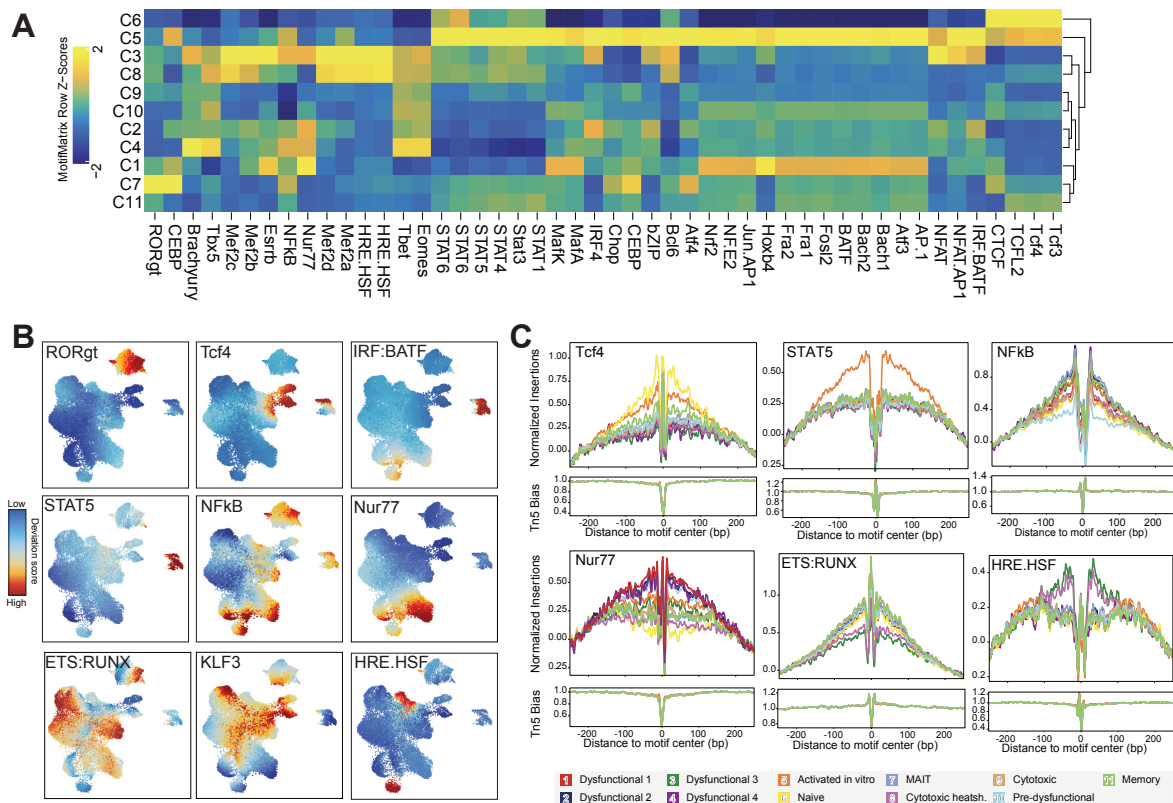


**Figure 4.12: Differential TF motif accessibility between T cell states**

(A) Heatmap showing motif deviations across all cells as predicted by chromVAR. Motifs with an FDR  $\leq 0.001$  (Wilcoxon test) and a mean difference of  $\geq 0.07$  are shown. (B) Overlay of z-scored TF motif deviations on the UMAP embedding. (C) Transcription factor footprint analysis of specific motifs. Motif containing ATAC-seq signals for each cluster are normalized for Tn5 insertion sequence bias.

ther, TCF4 activity could only be observed in memory and short *in vitro* activated T cells (Figure 4.12B). STAT5 activity was solely found in *in vitro* activated T cells, confirming recent IL-2 signaling (Figure 4.12B). Besides this, several other STAT factors as well as TCR pathway TFs crucial for T cell activation, such as NFAT, AP-1, BATF, and IRF4, seem to be active and occupy their binding sites (Figure 4.12A-B). As expected, MAIT cells showed TF activity of MAIT transcription factor ROR $\gamma$ t (Figure 4.12B). Interestingly, HCC-populated clusters 3 and 8 show enhanced activity of factors that regulate heat shock (HSF; heat shock factor) and hypoxia response (HRE.HSF motif activity, Figure 4.12B-C), which fits to the observation in chapter 4.3.1, stating gene activity of heat shock proteins. Furthermore, almost all tumor

## 4. RESULTS

---

tissue derived cells except memory T cells and dysfunctional T cells from cluster 1 (populated by BBC-derived TILs) showed activity of T cell function and differentiation TFs Eomesodermin (Eomes) and T-bet (*Tbx21*) (Figure 4.12A). Pre-dysfunctional and cytotoxic TILs (cluster 10 and 9, respectively) were the only cell types besides PBMC-derived naive T cells, which did not display NF $\kappa$ B activity (Figure 4.12B-C). Of note, functional cell states, namely memory (and presumably checkpoint blockade responders (chapter 4.3)) and cytotoxic T cells both possess enhanced activity of KLF3 and ETS:RUNX complexes, whereby in dysfunctional T cells both of their activity decreases (Figure 4.12B). In more detail, pre-dysfunctional cells and dysfunctional cells are the only ones, which do not exhibit KLF3 motif activity (Figure 4.12B). In line with findings from Liu et al. and others, we observed enhanced TF activity of known exhaustion drivers NF $\kappa$ B and Nur77 (*NR4A1*) in dysfunctional cells (cluster 1-4) [131, 113, 173]. Interestingly, besides Nur77 activity, motif activity of another nuclear receptor Esrbb was increased (Figure 4.12A). Dysfunctional cells also exhibited a certain level of IRF:BATF composite motif activity (Figure 4.12B), which fits to the observations from Satpathy et al. who found that IRF4 and BATF motifs were enriched in scATAC-seq data from BCC-derived exhausted TILs [173]. However, it is challenging to identify the specific TF accounting for a observed TF activity as often TFs of one family share very similar binding motifs. Thus, often it can rather be referred to the TF family.

### 4.4.2 The specific tumor tissue might influence the chromatin landscape of CD8<sup>+</sup> TILs

We further noted that the clusters 1, 2 and 4, which resemble dysfunctional cells, are relatively homogeneous regarding gene activity of dysfunction markers (Figure 4.9A) and show comparative enrichment of exhaustion signatures (Figure 4.10B), but still separate on UMAP dimension 1 (Figure 4.13A). This gave us the idea to look for differences in the gene-regulatory elements (GREs), since it was already

described by researchers, that the tissue can influence the gene regulatory landscape of immune cells [44, 108]. To this end, we first excluded dysfunctional cluster 3, since here the dysfunction is very intense compared to the other clusters and it displays the special heat-shock signature (Figure 4.10B).

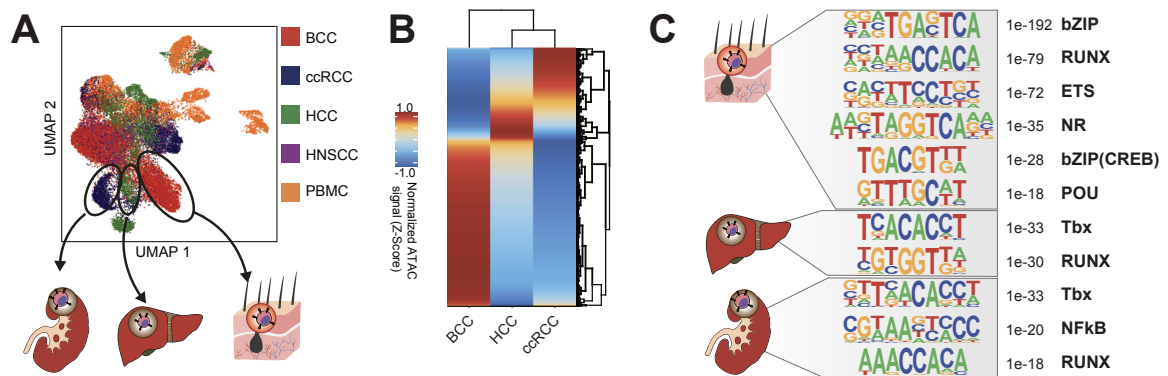


**Figure 4.13: Detection of tissue-specific TF motifs**

(A) Scheme depicting analysis of renal, liver and skin-specific influence on chromatin landscapes of dysfunctional TILs. (B) Heatmap showing z-score normalized chromatin accessibility of tissue-specific peaks of clusters indicated in (A). (C) De novo motif discovery in cluster/tissue-specific peaks. p-value and most related known motif or motif family is shown.

Next, marker peaks were identified for each tissue-specific dysfunctional cluster (cluster 1 BCC; cluster 2 HCC; cluster 4 ccRCC, Figure 4.10C-D) by performing pairwise testing between each cluster and the two remaining clusters. An additional filter step was applied, which rejected all peaks that only occurred once, resulting in 6,332 peaks that are unique to one of the three tissue-specific clusters (Figure 4.13B). Next, we performed *de novo* motif discovery in cluster-specific peaks (Figure 4.13C). The RUNX motif was enriched in open regions of all three clusters, whereas T-box (Tbx) motifs were accumulated only in HCC- and RCC-specific GREs. Besides this, the RCC-specific peaks were characterized by NF $\kappa$ B motif enrichment (Figure 4.13C). Basic Zipper (bZIP), ETS, nuclear receptor (NR) and octamer (POU) motifs were found to be specific for BCC peaks. Interestingly, the octamer TF family is known for their role in B cells [71] but not yet described in the context of T cell dysfunction in humans. Of note, one TF belonging to the octamer factor fam-

## 4. RESULTS

---

ily, namely BOB1, was found to be enriched on the mRNA level in as exhausted classified OT I TILs from a melanoma mouse model [131]. Moreover, the *de novo* motif of the nuclear receptor family (NR) was solely enriched in BCC specific peaks (Figure 4.13C). The motif found resembles the hexameric consensus sequence of the DNA-binding domain of the NR factor VDR (vitamin D receptor) [28], which regulates gene expression upon binding to vitamin D. It could be hypothesized, that VDR might be active here, since in the skin the precursor of vitamin D is synthesized and keratinocytes can metabolize it into the active form of vitamin D (1,25(OH)<sub>2</sub>D or calcitriol) [57, 16]. The clusters resembling functional T cell states and their regulatory programs (cluster 9, 10, and 11; cytotoxic, memory and pre-dysfunctional T cells, respectively) contain TILs from from all entities. This indicates influence of the tissue onto TIL chromatin landscapes is increasing along the trajectory towards dysfunction. All together, our data show evidence that the tumor tissue or microenvironment could shape the chromatin landscape of TILs.

### **4.5 Identification of an entity-shared trajectory to terminal dysfunction of human TILs**

Since we recognized a putative effect of the tumor tissue onto the chromatin landscape of human TILs, we next aimed to identify an entity-shared pathway to terminal dysfunction. To this end, we used exclusively conventional CD8<sup>+</sup> T cells isolated from human tumor samples and adjacent non-tumor tissue and rejected T cells derived from peripheral blood as well as MAIT cells, which resemble a very different cell type. In the following analysis 47 samples from 16 patients were retained and Harmony for batch-correction of the tissue effect as well as clustering and 2D visualization using UMAP was performed. As a result, we identified 6 clusters including 2488 marker genes (Figure 4.14A-B). As described in chapter 4.3 we used marker genes and published gene signatures to understand the identity of the different T cell

states. First, we assessed the activity of known T cell state marker genes and identified marker genes (Figure 4.14B-C). In cluster 1 and 2 we observed the highest gene activity of exhaustion markers *PDCD1*, *HAVCR2*, *TOX*, *LAYN*, *CTLA4* and *ENTPD1*, identifying these cells as exhausted (Figure 4.14C). Since the gene activities of the aforementioned genes were lower in cluster 2 and we further detected high gene activity of proliferation marker *MKI67* here, we therefore refer to cells in cluster 1 as terminal exhausted ( $T_{EX}^{term}$ ) and to cells in cluster 2 as exhausted proliferating cells ( $T_{EX}^{prolif}$ ), respectively (Figure 4.14A-C). Further, we identified cluster 3 as representing precursor exhausted cells ( $T_{PEX}$ ), since gene activity of precursor exhausted marker genes *TCF7* (encoding TCF1) and *CXCR5* [88, 96] was the highest here. Cluster 4 showed high gene activity of memory markers *IL7R* and *LEF1* and cluster 6 displayed high gene activity of cytotoxic molecules *PRF1*, *GZMB* and cytotoxicity markers *CX3CR1* and *FGFBP2*. Therefore we associate cluster 4 with memory T cells and cluster 6 with cytotoxic T cells, respectively. In cluster 5, over 10 heat shock genes are identified as marker genes as well several further chaperons (e.g. *DNAJB1*, Figure 4.14C). When analyzing marker genes of cluster 5, enrichr [31] detects the genes in pathways such as “HSF1-activation”, “cellular response to heat stress” or “hypoxia” (Figure 4.14E-F). Furthermore, we find marker genes indicating TCR activation (*NR4A1*) in this cluster (Figure 4.14C). To sum up, we identified the cells in this cluster as activated and responding to cellular stress like heat and/or hypoxia.

Second, we validated our cluster annotation by projecting published CD8<sup>+</sup> T cell gene-expression signatures [14, 110, 159, 172, 196, 103, 130], onto our unified TIL analysis (Figure 4.14D). In particular, in cluster 1 several exhaustion and aPD1 non-responder signatures were enriched, whereas in cluster 2 one exhaustion signature including *MKI67* expression confirmed representation of exhausted proliferating cells. Consistently with gene activity results, two progenitor exhausted signatures were found to match genes of cluster 3, which supports  $T_{PEX}$  potential. Cluster 4 matched with aPD1 responder and to some extent with memory-effector signatures.

## 4. RESULTS

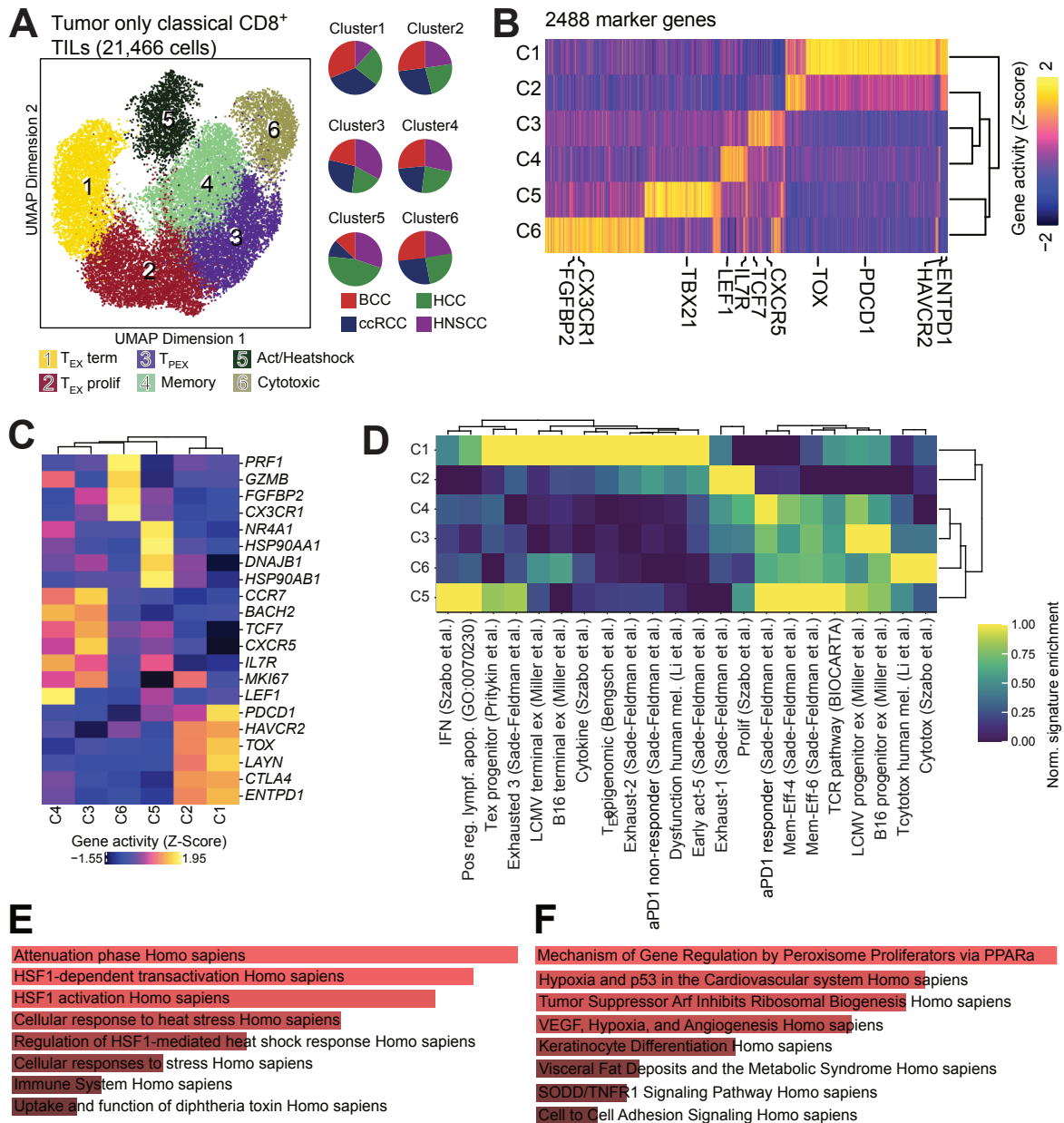


**Figure 4.14: Entity-harmonized analysis of the TIL chromatin landscape**

(A) UMAP of tissue derived conventional CD8<sup>+</sup> T cells coloured by clusters and pie charts of relative entity distribution (normalized to whole cell number of respective entity) within clusters. (B) Heatmap of z-score normalized gene activity of marker genes. Selected marker genes are shown. (C) Heatmap showing z-score normalized gene activity of selected genes. (D) Heatmap of enrichment of published T cell signatures in all clusters. Data was normalized using Empirical Percentile Transformation. (E-F) Enrichr analysis of top 50 marker genes of cluster 5 with the lowest FDR.

Further, in cluster 6 we found cytotoxic T cell signatures to be enriched. Association of cluster 5 with an activated/heat shock T cell state fits to enrichment of published signatures such as an IFN signature, TCR pathway (BIOCARTA) and positive regulation of lymphocyte apoptosis (GO:0070230) since the heat shock response is also a cell stress response, which can be associated with cell death. Furthermore, we see that cluster 3, 2 and 1 are close to each other on the UMAP embedding indicating close relationship of these clusters (Figure 4.14A). In addition, gene activity leads from precursor-exhaustion marker *TCF7* activity in T<sub>PEX</sub> cells towards exhaustion marker *HAVCR2* (encoding TIM3) activity in exhausted cells and projection of signatures support this notion from progenitor exhausted towards terminal exhausted cells from cluster 3 towards cluster 2 and 1 (Figure 4.14C-D). This indication is supported by several observations. First, when we plot the PD1 protein expression status of every single cell (from sorting of PD1<sup>+</sup> and PD1<sup>-</sup> CD8<sup>+</sup> TILs for scATAC-seq, see chapter 4.2.3) onto the UMAP we observe an increase of PD1<sup>+</sup> cells from cluster 6 and 5 over cluster 3 and 4 leading to primarily PD1<sup>+</sup> cells in exhausted clusters 1 and 2 (Figure 4.15A). Second, when we plot the distribution of T cells deriving from non-tumor tissue controls (in total 6 samples from adjacent non-tumor kidney and liver tissue) on the UMAP embedding, we detect the cells mainly in clusters 3-6 and almost none in terminally exhausted cluster 1 (Figure 4.15B). Although we have no information about antigen-specificity of the TILs, this observation could indicate that the tumor tissue and long-lasting TCR stimulation *via* tumor antigens promotes the process of terminal exhaustion. Third, as it can be seen in the entity distribution over the clusters, HNSCC TILs were underrepresented in the T<sub>EX</sub>term cluster 1 (Figure 4.14A). We observed this difference to TILs from the other entities already in the main chromatin landscape analysis before (4.3) and within our expression-based analysis via FACS (4.2.4). Again, this supports the trajectory towards terminal exhaustion. Fourth, we analyzed the influence of anti-PD1 blockade on cluster identity of BCC TILs (Figure 4.15C). As can be seen, the fraction of terminally exhausted TILs is increasing, whereas the fraction of T<sub>PEX</sub> cells is decreasing

## 4. RESULTS

post-treatment.

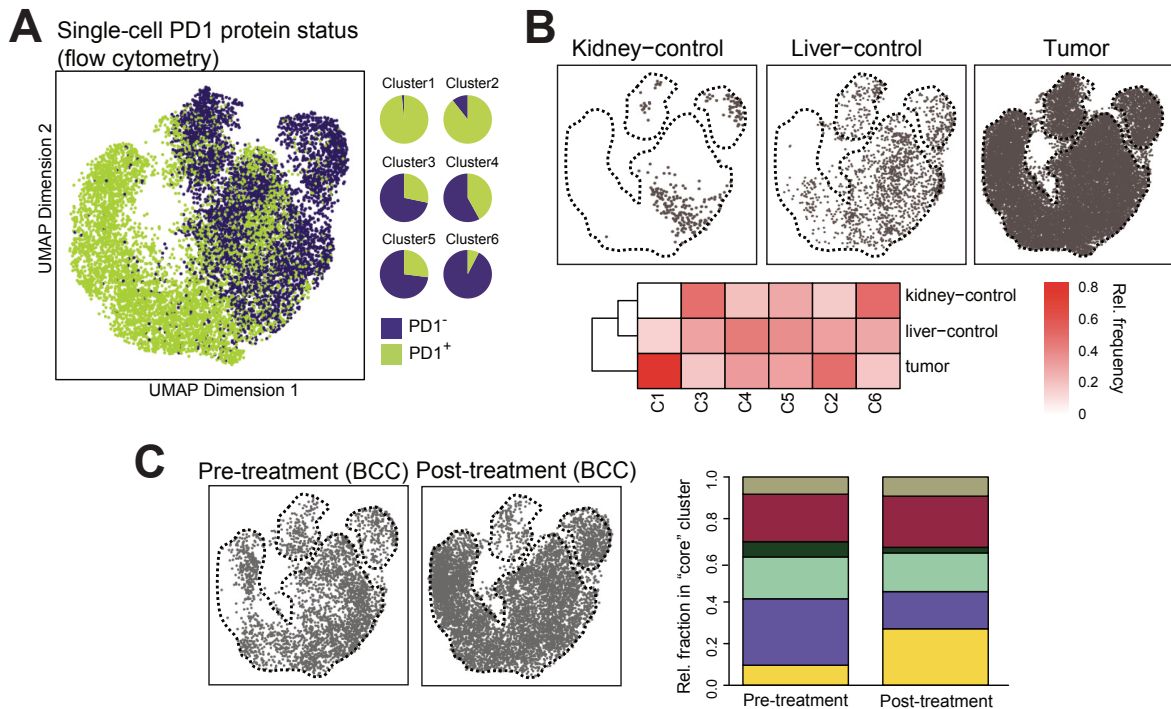


**Figure 4.15: Evaluation of developmental relationship between cell states**

(A) PD1 expression status of single cells projected on the UMAP embedding and pie charts of absolute contribution of PD1<sup>+</sup> and PD1<sup>-</sup> cells to each cluster. (B) Projection of cell origin (adjacent non-tumor tissue of the kidney or of the liver vs from intratumoral tissue (all entities)) on the UMAP embedding and heatmap showing relative cell frequencies on cluster basis. Cell frequencies are normalized to total number of cells from each cell origin (all clusters). (C) Distribution of BCC TILs among clusters. Comparison from samples taken before (pre-treatment) and after (post-treatment) aPD1 therapy.

As other researchers found that checkpoint blockade leads to expansion of terminally differentiated cells [189, 226] this observation further supports the “core” trajectory towards dysfunction.

Therefore, we next aimed at identifying a “core” pathway to CD8<sup>+</sup> T cell dysfunction based on entity-shared chromatin accessibility profiles. To this end, we performed pseudotime analysis from cluster 3 over cluster 2 to cluster 1 using ArchR (Figure 4.16A). Next, changes in peak accessibility, motif deviations and gene activity scores along pseudotime were analyzed (Figure 4.16C-E). In agreement with the hypothesized trajectory from T<sub>PEX</sub> towards T<sub>EX</sub> term we observed a gradual decrease in gene activity of precursor-exhausted marker *TCF7* (TCF1) whereas we

detect a steadily increase in exhaustion marker *HAVCR2* (TIM3) (Figure 4.16B). This „core“ dysfunction trajectory facilitates an overview of chromatin accessibility dynamics along the developmental pathway of T cell exhaustion. Thereby enabling identification of transcription factor activity and gene activities along this process (Figure 4.16D-E). In general, our “core” trajectory analysis, revealed transcriptional regulators that seem to account for the development towards terminal dysfunction. On the one hand, within T<sub>PEX</sub> cells, primarily ETS, zinc finger, and Tbox TF family members are active. On the other hand, within terminal T<sub>EX</sub> cells, TFs containing a bZIP domain (Basic Leucine Zipper Domain), such as BATF, AP-1 or Bach2 show high activity as well as TFs belonging to the nuclear receptor family, such as VDR, which is also a marker gene in T<sub>EX</sub>term cells. Further NR family members, such as VDR binding partner RXR, estrogen related receptor beta (*Esrrb*) and Nur77 show high activity as well (Figure 4.16D). In more detail, at the beginning of the „core“ dysfunction trajectory we could detect KLF motif activity and *KLF3* gene activity, which gets lost during the transition towards T<sub>EX</sub>term (Figure 4.16D-E). This observation is in accordance to our observation in chapter 4.4.1, where we found KLF3 motif activity in functional but not in dysfunctional T cell states. We further noted a gradual loss in gene activity of several genes within T<sub>PEX</sub> cells (Figure 4.16E), such as *FOXP1* (found in aPD1 responder signature from Sade-Feldman et al.), *SOCS2*, (*SOCS1* found in T<sub>EX</sub> progenitor from Pritykin et al.), *TGFBR3* (also found in gene signatures of cytotox. hum. melanoma [110] and IFN signaling [196]), indicating functionality of T<sub>PEX</sub>. Interestingly, we detected enhanced *IL2* gene activity in T<sub>PEX</sub> cells, which got lost in T<sub>EX</sub> cells. IL-2 is known as a cytokine needed for adequate T cell activation and survival. It was recently described that IL-2 can also act as an inducer of T cell exhaustion [115]. Whether autocrine/paracrine IL-2 signaling in T<sub>PEX</sub> cells is advantageous for their survival or is an indicator of their future differentiation into terminal T<sub>EX</sub> cells stays a question of interest. Furthermore, gene activities of unfamiliar factors such as *BRDT* (bromo domain), *SETD7* (histon lysine methyltransferase), *SNAI2* (zinc finger), all involved in epigenetic and transcriptional reg-

## 4. RESULTS

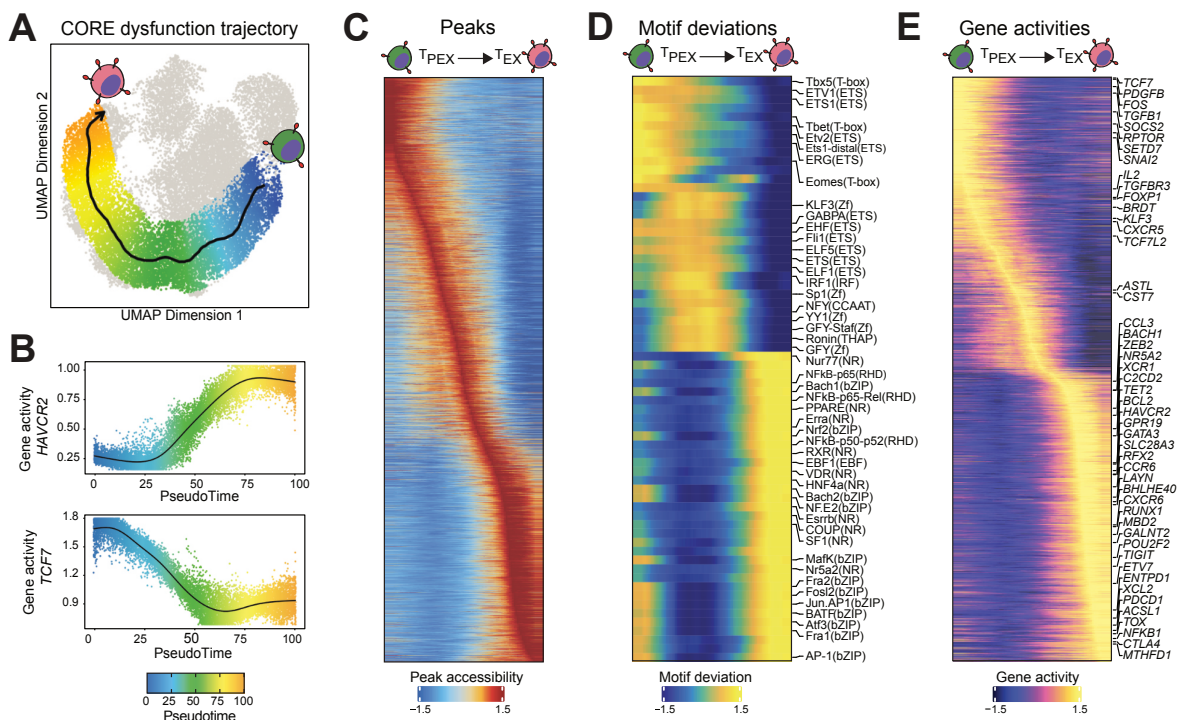


**Figure 4.16: Entity-shared core trajectory to terminal CD8<sup>+</sup> TIL dysfunction**

(A) "Core" dysfunction trajectory as computed with entity-shared chromatin accessibility profiles from  $T_{PEX}$  towards  $T_{EX}^{term}$ . (B) Gene activity of *HAVCR2* (TIM3) and *TCF7* (TCF1) along pseudotime of the "core" dysfunction pathway depicted in (A). (C-E) Heatmap of peak accessibility (C), motif deviations (D) and gene activities (E) along the core dysfunction trajectory.

ulation, were detected on the beginning of the trajectory (Figure 4.16E). Within the entity-shared progression towards terminal dysfunction, in addition to genes associated with T cell dysfunction, such as *TOX*, *ENTPD1*, *LAYN*, and *HAVCR2*, we observed gene activity of genes that are barely described in this regard (Figure 4.16E). Amongst others, this included epigenetic modifiers (*MBD2*, *TET2*), transcription factors (*POU2F2*, *ETV7*, *BACH1*, *ASCL1*, *RFX2*), metabolism related genes (*MTHFD1* (found in aPD1 non-responder signature from Sade-Feldman et al.), *SLC28A3*), and molecules involved in intra/intercellular signaling (*CXCR6*, *CCR6*, *GPRR19*, *XCL2*, *XCR1*) (Figure 4.16E). In summary, our analysis identified an entity-shared single-cell chromatin accessibility-based “core” dysfunction trajectory from functional towards terminal dysfunctional human tumor-infiltrating T cell states.

## 4.6 Selection of novel, entity-shared target genes that might influence T cell (dys)function

Next, we aimed to identify potential target genes, which might play a (positive or negative) role in the establishment or maintenance of T cell dysfunction and are shared by multiple entities. We selected target genes from marker genes within the  $T_{EX}$  term clusters of the core analysis (4.5) and, which were largely unknown for their role in  $CD8^+$  T cells (Figure 4.17). The selection criteria included amongst others: increased chromatin accessibility in published bulk ATAC-seq of PD1 high TILs from human melanoma [151], increased chromatin accessibility in expanded TIL209 from human melanoma (4.7; 3.2.10), presence of mouse homologs and ideally increased chromatin accessibility in mouse model of T cell exhaustion [131], not being extensively investigated in T cell dysfunction related studies, no clinical trial ongoing involving the putative target gene in the context of immunotherapy, no patent pending. Among the top eight putative targets were transcription factors, metabolic enzymes, and proteins involved in cellular signaling processes (Figure 4.18). As

## 4. RESULTS

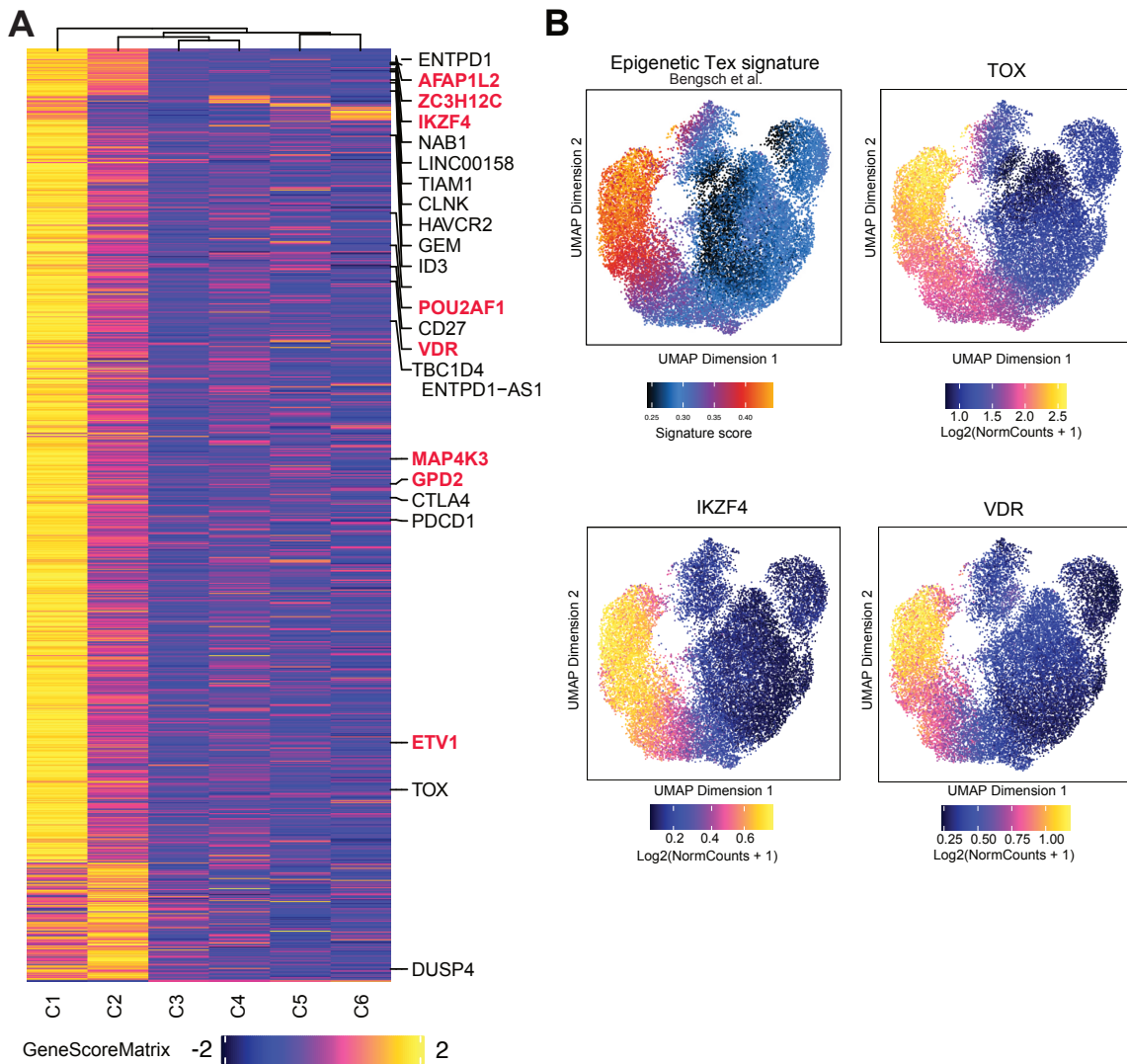


**Figure 4.17: Selection of putative target genes**

(A) Heatmap showing gene scores of selected genes, which are most active in core-exhaustion clusters 1 and 2. Pink genes were selected as putative target genes. (B) UMAP of entity-shared analysis. Signature scores (published epigenetic exhaustion signature from Bengsch et al.) or gene scores (TOX, IKZF4, VDR) are projected onto UMAP embeddings.

gene name	gene type	log2FC (C1 vs background)	chromatin accessibility in:		
			human PD1 hi TIL from melanoma (Philip et al., 2017)	TIL209 (our data)	exhausted OT I TILs (Mognol et al., 2016)
ZC3H12C	RNAse	1.72	3	3	3
POU2AF1	Octamer TF	1.67	2	2	2
IKZF4	Zinc finger TF	1.53	2	2	2
AFAP1L2	Cytoskeletal signaling	1.42	3	3	2
VDR	Hormone receptor	1.34	3	3	0
ETV1	ETS TF	1.19	1	3	0
GPD2	Oxidoreductase	0.96	3	3	3
MAP4K3	Kinase	0.90	3	1	2

**Figure 4.18: Table of putative target genes**

List of putative target genes found in T<sub>EX</sub>term cluster 1 of the core analysis (4.5). Sorted after decreasing log<sub>2</sub>FC value. Color code and numbers indicate chromatin accessibility (0=none; 3=high) in published human PD1 high sorted TILs from melanoma patients [151], in as exhausted classified OT I TILs from a B16-OVA tumor mouse model [131], and in our own bulk ATAC-seq data of TIL209.

the top eight putative targets we selected *ZC3H12C* (an RNAse), *POU2AF1* (a octamer TF), *IKZF4* (a zinc finger TF), *AFAP1L2* (involved in cytoskeletal signaling), *VDR* (a hormone receptor), *ETV1* (an ETS TF), *GPD2* (an oxidoreductase) and *MAP4K3* (a kinase). Following target selection, we aimed to perform a functional validation of the selected genes via an *in vitro* approach, to get first hints before moving forward to using an *in vivo* mouse model in the future. For this purpose, we wanted to knock-out the targets via CRISPR/Cas9 in expanded exhausted TILs from a melanoma patient and challenge the genome edited TILs in functional assays to detect a possible influence of the target gene. We sought to use PD1 KO as a positive control in the following, since it is an established immune checkpoint molecule and its impact on T cell function in the tumor context is well known (2.1.2). In the first validation phase we focused primarily on target genes *VDR* and *IKZF4*. *VDR* encodes the hormon receptor for vitamin D3, VDR (vitamin D receptor), and belongs to the nuclear receptor family of TFs. Upon binding of calcitriol, the active form of vitamin D, VDR forms a heterodimer with retinoid-X-receptor RXR. This complex can then enter the nucleus and bind to vitamin D responsive elements (VDRE), thereby activating or repressing gene transcription [100]. For a long time known primarily as involved in bone mineralization and calcium homeostasis, the role of VDR as an

#### 4. RESULTS

---

immunomodulator comes recently more into focus. For example, several COVID-19 studies showed a favourable effect of vitamin D treatment on COVID-19 outcome, suggesting a role of VDR here [138, 3]. On the one hand, VDR is transcribed upon TCR signaling, thereby inducing PLC- $\gamma$  1 transcription, which increases intracellular Ca<sup>2+</sup> levels. On the other hand, VDR outcompetes binding of NFAT1 to the IL-2 promoter and represses IFN $\gamma$ , thereby balancing T cell activation [100]. Further, one study found that vitamin D supplementation improved CD8<sup>+</sup> T cell infiltration in breast cancer [97], but this effect could also be explained by the influence of other immune cells in the TME. A recent study reported that gene loci of exhaustion markers *CTLA4* and *CD38* were acetylated at H3K27 after vitamin D treatment of helper T cells, whereas the *IFNG* locus was deacetylated [29]. All together, VDR is needed for T cell activation [100] but on the other hand seems to dampen overshooting immune responses by repressing Th1 programs during viral infections such as SARS-CoV-2 infections [29], illustrating a bilateral function of VDR. *IKZF4* belongs to the Ikaros family of transcription factors and encodes the zinc finger TF EOS. IKZF family members, due to their structure, are known to regulate gene expression via chromatin remodeling, interacting with RNA Pol II complexes and mediating chromosome conformational changes [158]. EOS is required for the suppressive activity of regulatory T cells (Tregs) [144, 68], but not much is known about its role in CD8<sup>+</sup> T cells. EOS is involved in IL-2 expression and can induce Blimp-1 expression via the IL-2/STAT5 axis [158, 144]. Blimp-1 is known for upregulating inhibitory receptor expression and was reported to be involved in T cell exhaustion during chronic viral infection [158, 188].

To summarize, we selected target genes, which we found to have a high, entity-shared gene activity in dysfunctional TILs to study their role in CD8<sup>+</sup> T cell functionality, especially in the context of T cell dysfunction in the tumor.

## 4.7 Establishment of CRISPR/Cas9 based genome editing in TIL209 cells

CRISPR/Cas9 based genome editing is a powerful tool to genetically manipulate cells. We aimed to employ this method to validate a possible influence of our selected target genes on T cell dysfunction. For this purpose, we used *in vitro* expanded human polyclonal CD8<sup>+</sup> TIL209 cells, which were isolated from a melanoma patient [49] and resemble exhausted T cells on the epigenetic level. We kindly received the cells from Prof. Beckhove's group (LIT). Open chromatin profiling of TIL209 revealed epigenetic similarity to exhausted TILs as found in our scATAC-seq data (Figure 4.19A-B). The gene loci of known exhaustion markers are highly accessible (Figure 4.19A) and we could verify expression of the same markers via flow cytometry (Figure 4.19B). Contrary, TIL209 do not express KLF3 (data not shown),

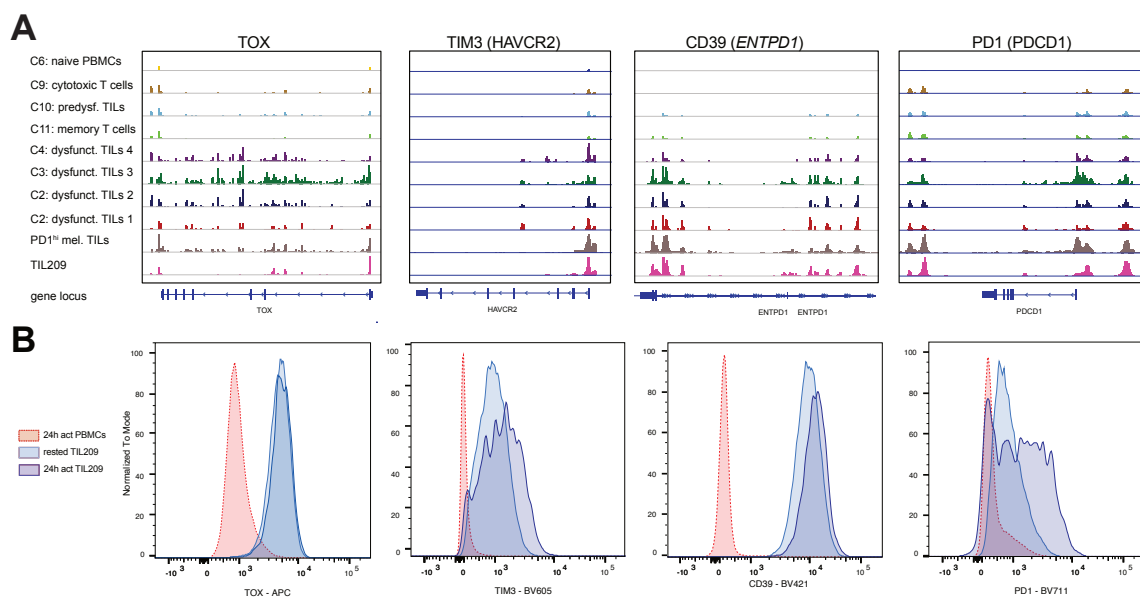


**Figure 4.19: Chromatin accessibility and expression of exhaustion markers**

(A) Genome browser plots of exhaustion markers *TOX*, *HAVCR2*, *ENTPD1* and *PDCD1*. Shown are merged scATAC-seq signals (8 upper rows) of analysis shown in chapter 4.3 and bulk ATAC-seq signals from PD1<sup>hi</sup> melanoma TILs [177] and TIL209. (B) FACS histograms of exhaustion marker *TOX*, *TIM3*, *CD39* and *PD1* expression. Shown is the expression level of 24h aCD3/aCD28 activated blood-derived CD8<sup>+</sup> T cells (red, dotted line), rested TIL209 (light blue) and 24h aCD3/aCD28 restimulated TIL209 (dark blue).

## 4. RESULTS

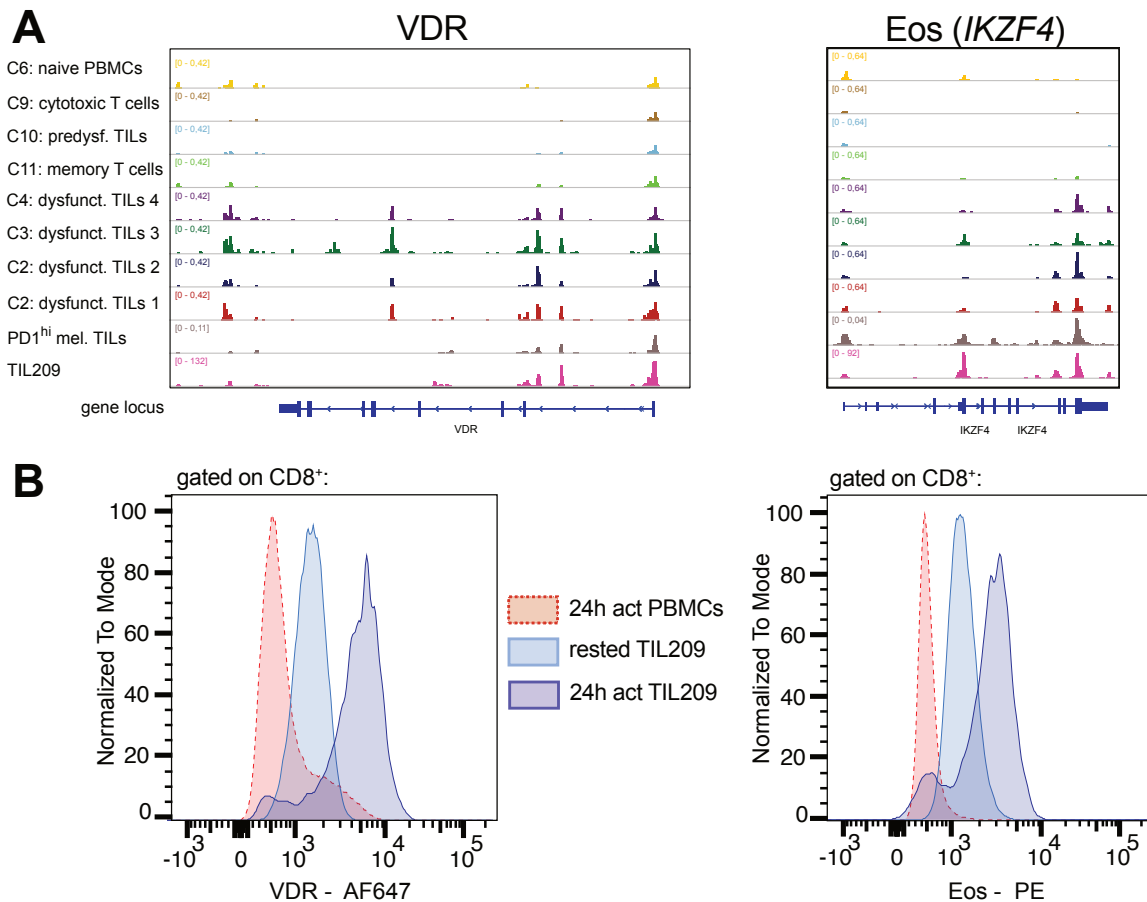


**Figure 4.20: Chromatin accessibility at target loci and expression of targets VDR and EOS**

(A) Genome browser plots of target loci *VDR* and *IKZF4*. Shown are merged scATAC-seq signals (8 upper rows) of analysis shown in chapter 4.3 as well as bulk ATAC-seq signals from PD1<sup>hi</sup> melanoma TILs [177] and TIL209. (B) FACS histograms of VDR and EOS expression. Shown is the expression level of 24h aCD3/aCD28 activated blood-derived CD8<sup>+</sup> T cells (red, dotted line), rested TIL209 (light blue) and 24h aCD3/aCD28 restimulated TIL209 (dark blue).

a TF, which we found to lose its motif activity in T<sub>EX</sub> clusters and could therefore be necessary for preservation of effector function and survival. We could further confirm chromatin remodeling at gene loci as well as expression of our top targets in TIL209 cells (Figure 4.20A-B). TIL209 cells became highly activated during the *in vitro* expansion process and still produce effector cytokines and cytotoxic molecules, unlike *ex vivo* terminal exhausted TILs (Figure 4.6B). This observation is shared by Thommen et al., who noticed that *in vitro* expanded PD1 high TILs from NSCLC patients showed restored cytokine production and enhanced tumor reactivity [201]. Nonetheless, TIL209 cells seem to be at the end of their differentiation since they do not survive long-lasting TCR restimulation, probably because of activation induced cell death (AICD).

#### **4.7.1 Comparison of knock-out efficiency using different electroporation devices and programs**

First, CRISPR/Cas9 had to be established and optimized for TIL209 cells (Figure 4.21). Since a couple of years, CRISPR via transfection of a Cas9 ribonucleoprotein (RNP) complex, consisting of CRISPR-Cas9 guide RNA (crRNA:tracrRNA duplex) and Cas9 nuclease, is the most commonly applied CRISPR method for gene disruption and has been shown to work well in primary cells [180, 86]. Most RNP transfection techniques are electroporation-based. The Amaxa™ 4D-Nucleofector™ (Lonza Bioscience) and the Neon™ Transfection System (Invitrogen) are well established for RNP delivery and probably the most used devices [180, 86]. Nucleofection® is said to be especially suitable for primary cells and advantageous over viral delivery, regarding safety issues [6]. Nonetheless, protocol optimization is critical and often not straightforward, since pitfalls like insufficient KO and cell death can occur, the latter often due to toxicity of the electroporation buffer [187].

## 4. RESULTS

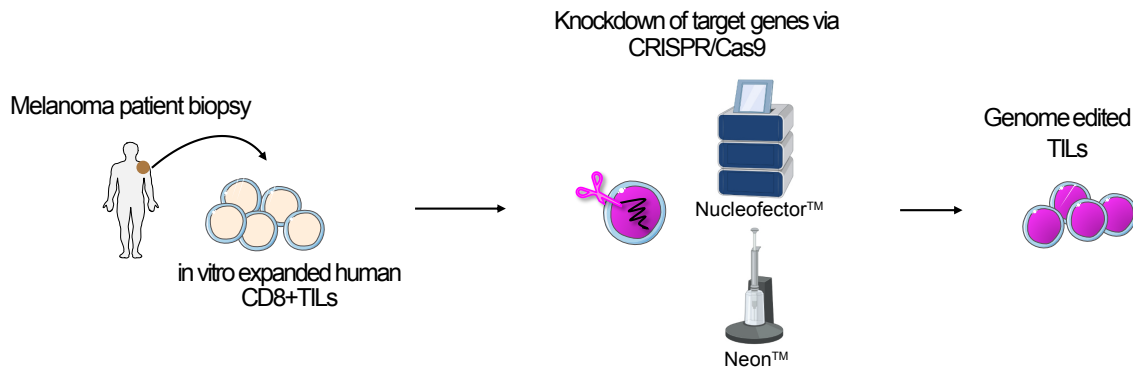


**Figure 4.21: Workflow of CRISPR/Cas9 in TIL209 using the Neon™ or the Nucleofector™**

Workflow for electroporation-based CRISPR/Cas9 in TIL209. Adapted from Servier Medical Art ([smart.servier.com](https://smart.servier.com)) and BioRender ([biorender.com](https://biorender.com)) with permission under the creative commons license (<https://creativecommons.org/licenses/by/3.0/>).

The success of CRISPR/Cas9 depends on many factors. One of them is the transfection efficiency, which refers to the percentage of cells receiving the RNP molecule. This can depend on pulse intensity, pulse duration, and number of pulses as well as on RNP concentration, electroporation buffer, cell type and cell stimulation [182]. Transfection efficiency is often contrary to viability of the electroporated cells. Another factor is KO efficiency, which is defined as the percentage of cells that do not express the target gene anymore. If transfection efficiency is satisfying, KO efficiency depends mainly on gRNA performance but can also depend on the Cas9 enzyme used [182].

First, we tested different CRISPR conditions using the Neon™ Transfection System. We found, that restimulation of TIL209 prior to electroporation led to very low cell viability, which is not acceptable when further functional assays are planned (Figure 4.22A). Although KO efficiency was reduced around 75 % when TIL209 were not restimulated, viability was much better (Figure 4.22A). This goes in line with the findings of Seki et al., who reported that KO efficiency was worse in non-stimulated T cells but could be enhanced by using optimal electroporation programs [182]. Therefore, we next aimed to test different Neon™ electroporation programs, namely one recommended for Jurkats ("IDT"), one recommended for primary T cells ("Stem-

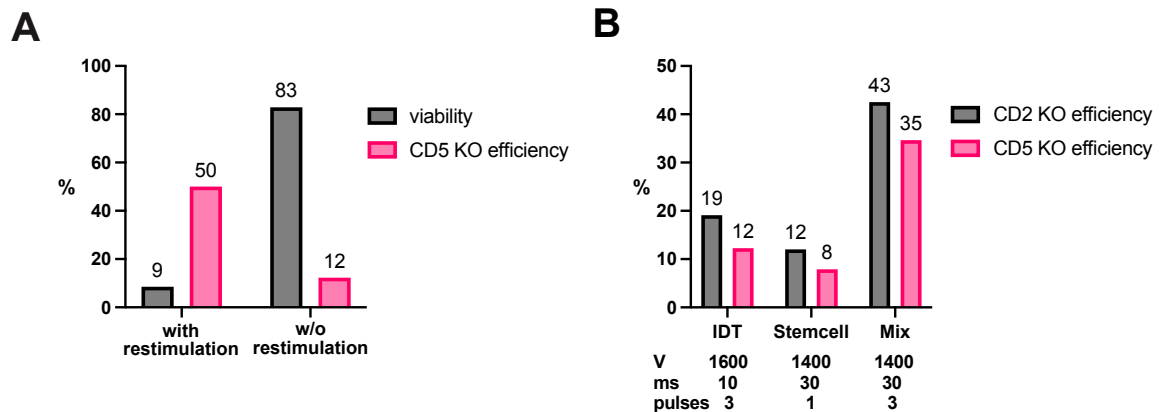


**Figure 4.22: Test of CRISPR conditions using the Neon™**

(A) CRISPR performance with vs w/o restimulation of TIL209. Shown is the viability and the CD5 KO efficiency in percent, 3 days after electroporation. (B) Test of different electroporation programs using the Neon™. Shown is the CD2 and CD5 KO efficiency of rested TIL209 in percent, 3 days after electroporation.

cell”), and as a third option we tried a mix of both (“Mix”) (Figure 4.22B). The mix of both programs - reduced voltage with higher pulse duration in combination with several pulses - gave the best results and increased KO efficiency about two-fold to three-fold, depending on the target. Finally, acceptable KO efficiencies could be received using the Neon™ (Figure 4.23) as described in (4.7.2).

Second, we tested different CRISPR conditions using the 4D-Nucleofector™, since the improved electroporation technology of this device is recommended for primary cells and enables delivery of RNPs directly into the nucleus [6, 182]. We used the P3 Primary Cell 4D-Nucleofector™ Kit, as this kit was successfully used for primary CD8<sup>+</sup> T cells in our laboratory. We compared two different nucleases, which were reported to be used with nucleofection®, namely Alt-R® S.p. HiFi Cas9 Nuclease V3 from IDT and TrueCut™ Cas9 Protein v2 from Invitrogen, the latter of which was also used by Seki et al. [182]. Furthermore, we compared different nucleofection® programs. Program EH 100 is recommended for resting human T cells [182], program EH 115 is more powerful and recommended for stimulated T cells [86], whereas CA 137 is said to work well for sensitive cells. As a result, we could see that the Alt-R® S.p. HiFi Cas9 Nuclease V3 worked much better regarding KO efficiency

## 4. RESULTS

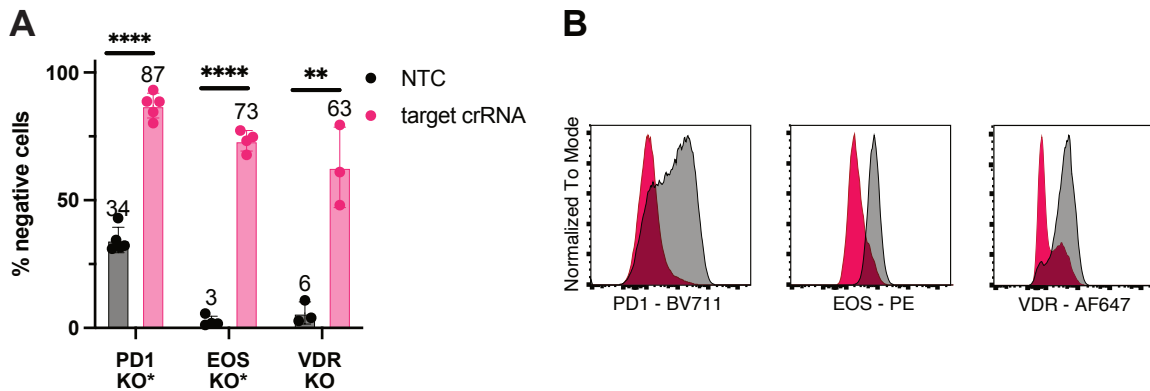


**Figure 4.23: Target KO using the Neon™**

(A) Target KO 5 days after transfection shown as percentage of negative cells. Shown is the mean (as bar and in numbers)  $\pm$  SD from 3 to 5 independent experiments. Unpaired t-test was performed. Asterisks above bars depict \*\*  $p < 0.01$ , \*\*\*  $p < 0.0002$ , \*\*\*\*  $p < 0.0001$ . Asterisks at KO condition label indicates that several crRNA were used for KO. (B) Exemplary histograms of target KOs. NTC control is depicted in grey and KO condition in pink.

(Figure 4.24A left panel). This could be due to the Alt-R® S.p. HiFi Cas9 Nuclease V3 being designed to be compatible with the Alt-R CRISPR-Cas9 guide RNA from IDT. Interestingly, the viability was reduced when using this nuclease (Figure 4.24A right panel). In summary, program EH 100 gave the best results regarding trade off between KO efficiency and viability (Figure 4.24A).

Comparison of viability and KO efficiency between Neon™ and the 4D-Nucleofector™ (Figure 4.24B) showed a significant reduction of TIL209 viability with nucleofection®. This can probably be explained by use of the electroporation buffer P3, which might be more toxic to the cells than the buffer used with the Neon™. This is supported by our observation, that the Mirus buffer (Ingenio) was better for viability (but worse for KO efficiency; data not shown). Furthermore, the specific nucleofection® program seems to reduce the viability, since the use of program CA 137 led to increased viability, but could not be used because the KO efficiency was not acceptable (Figure 4.24A). Interestingly, even though the 4D-Nucleofector™ is said to be the best option for primary cell transfection, we could not achieve a better KO efficiency of TFs EOS and VDR (Figure 4.24B). Only KO of PD1 worked better with nucleofection® when compared to Neon™ electroporation. All together, it is crucial to estab-

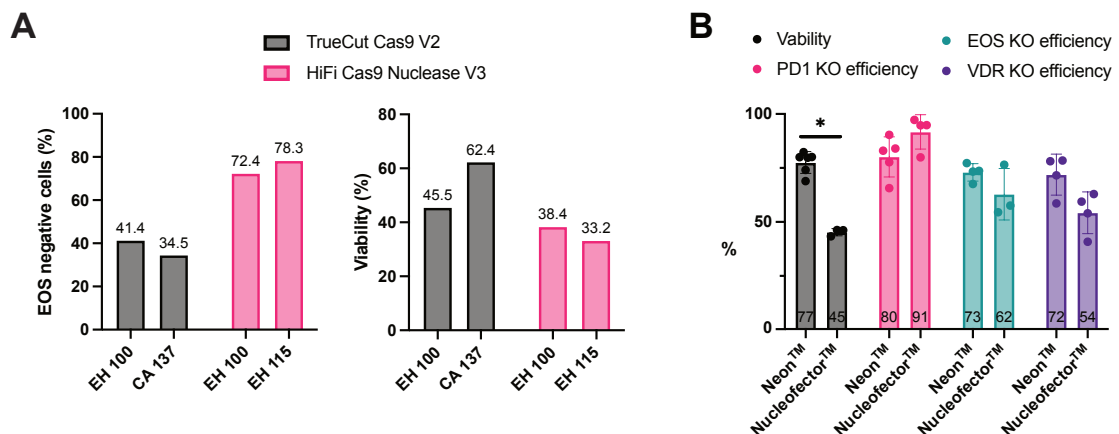


**Figure 4.24: Test of 4D-Nucleofector™ conditions and comparison with Neon™**

(A) KO efficiency of EOS (left panel) and cell viability (right panel) of TIL209 5 days after nucleofection. Shown are the different programs and nucleases in comparison. (B) Comparison of cell viability and target KO efficiency between 4D-Nucleofector™ and Neon™. Shown is the mean  $\pm$  SD of 3 to 5 independent experiments. Statistical significance was calculated using unpaired Mann-Whitney test. Asterisk depicts \*  $p < 0.05$ . Meike Neureither contributed to experiments involving the Nucleofector™ as a Bachelor's student under my supervision.

lish CRISPR/Cas9 for every cell type in order to receive acceptable results. In this regard, comparison of cell treatment, electroporation devices, nucleases, electroporation buffers and electroporation settings might be adjustment screws worth to use. Here, the Neon™ device seems to be the best option for TIL209 cells, mainly due to viability reasons.

#### 4.7.2 gRNA screening is necessary to receive adequate knock-out efficiency

To further improve CRISPR KOs besides testing different transfection programs, choosing the best crRNAs is a promising way to improve KO efficiency. For gRNA design it is advised to target the exogenic sequence right after the start codon if possible [86]. For some targets like VDR it is hard to find crRNA sequences in the first exons. In this case, the advice to test several crRNAs might especially apply. A not to be missed side note in this regard is that the on-target score of crRNAs is

## 4. RESULTS

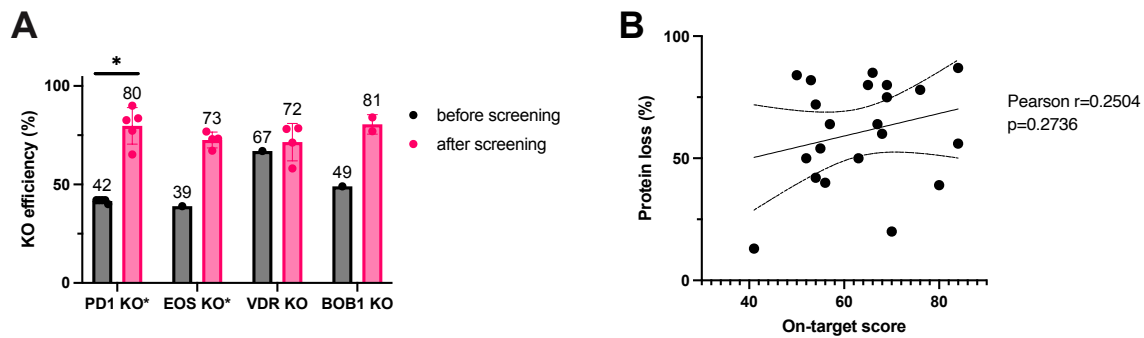


### Figure 4.25: Evaluation of gRNA performance

(A) KO efficiency of targets before and after crRNA screening. Shown is the mean  $\pm$  SD of 1 to 5 independent experiments. Unpaired t-test with Welch correction was performed. Asterisk depicts \*  $p < 0.05$ . (B) Correlation of protein loss and on-target score of single crRNAs tested. Each dot is one crRNA. Pearson correlation was performed and Pearson  $r$  as well as the  $p$  value of the correlation are shown.

only slightly correlating with protein KO efficiency, thus this score should rather not be considered for prediction of crRNA performance (Figure 4.25B). Ideally, already published crRNAs should be used, as in our case the two PD1 crRNAs from Seki et al. produced the best PD1 KO (data not shown) [182]. In concordance with the observations of Seki et al. that several crRNAs per target should be screened and combinations thereof tested, we could improve KO efficiency about 38 % depending on the target (Figure 4.25A). Surprisingly, we found that KO efficiency of some targets was decreased when using several crRNAs (data not shown). In this special cases one crRNA's performance was outstanding, whereas the others performed worse. In this regard, it seems that if one good crRNA is mixed with others, it's performance is outcompeted. This could especially apply to Neon™ transfection, since the amount of RNP complex per reaction cannot be increased, thus a good crRNA gets diluted when mixed with others. In summary, it is worth to invest in crRNA screening as this lead to improved KO efficiencies in most of our cases (Figure 4.25A).

### 4.7.3 Genome editing does not reflect target protein degradation

To calculate KO efficiency, many recommend to determine indel formation around the cut site, e.g. via Sanger sequencing of PCR amplifications over the cut site. Webtools like TIDE can then perform decomposition analysis and present percentage of indels as output [19]. We aimed to use TIDE for the same purpose, since we could not verify the KO efficiency on the protein level in the beginning, due to lack of good antibodies. Surprisingly, we were not able to confirm successful genome editing via TIDE assay (Figure 4.25B). Most of the gene perturbations yielded a very low percentage of indels and these results did not correlate with KO efficiency on the protein level (Figure 4.25A). In general, residual protein expression after successful genome editing can occur via different molecular mechanisms. Exon skipping (in this case skipping the exon with the frameshift mutation) can result in alternative isoform expression, translation can be reinitiated at alternative start codons, mutations can occur in-frame, or mutations at the terminus can enable still functional protein expression [193]. The lack of correlation of genome editing and protein KO in our regard could be due to differences in the ability of RNPs to produce loss-of-function mutations or introduce stop codons, which usually leads to nonsense-mediated decay of the mRNA. To conclude, it is advised to check the residual protein expression rather than relying on genome editing events only, to ensure that the KO was successful and the KO is the reason for a changing phenotype. In frame mutation when terminus is mutated still functional protein In summary, we were able to establish and optimize CRISPR KO of our targets in TIL209, using either the Amaxa™ 4D-Nucleofector™ or the Neon™ Transfection System, whereupon the Neon™ Transfection System is preferable due to better viability outcomes. On the one hand, it is not straightforward to perform CRISPR KO in sensitive cells like the expanded human melanoma TIL209 due to viability problems. On the other hand, it is critical to screen for optimal crRNA performance, especially for the KO of transcription factors and validate the KO via protein-based methods.

## 4. RESULTS

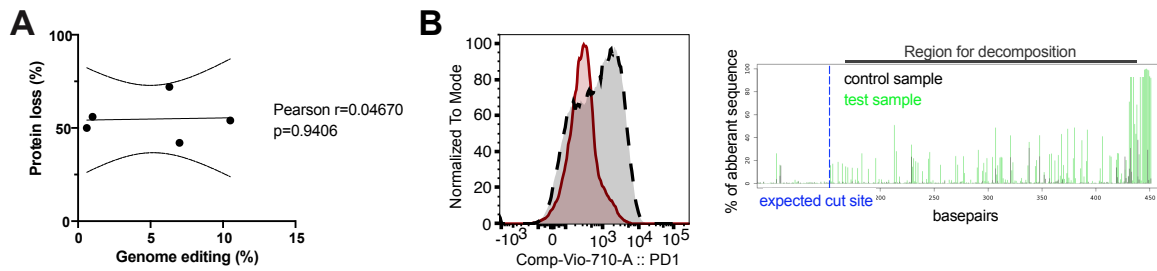


**Figure 4.26: Methods of KO evaluation**

(A) Correlation of genome editing (TIDE assay) and protein loss (FACS). Each dot represents one gene KO with one crRNA. Pearson correlation was performed and Pearson  $r$  as well as the  $p$  value of the correlation are shown. (B) Example for protein loss of PD1 after CRISPR/Cas9 (around 70-80% KO efficiency) with crRNA PD1.AA (red) compared to control (black) as assessed by FACS (left panel) and percentage of INDELs (around 12% genome editing) at the expected Cas9 cut site, as computed by TIDE [19] (right panel).

## 4.8 Target validation in TIL209 cells and primary TILs

After having established CRISPR KO of feasible targets VDR and EOS, we sought to investigate the influence of the KOs onto TIL functionality. Therefore, we planned and started several functional assays, such as killing assays, proliferation assays and transcriptome analysis via RNA-seq. Unfortunately, we recognized that our chosen *in vitro* system had its limitations, since we observed major viability decrease upon restimulation of TIL209 cells, restricting the options for functional assays. As a result, proliferation assays were not feasible since major cell death counteracted an adequate readout. Furthermore, RNA-seq after 3 hours of restimulation gave no evidence of differential gene transcription after target KO (data not shown), which might indicate that it takes longer to observe an effect of the KO on the transcriptome level. Nonetheless, with the TIL209 cells longer restimulation was not possible, as too many cells were dying and thus, together with cell loss during cell sorting, cell numbers and quality needed for RNA-seq were not sufficient. In addition, FACS-based analysis of expression of exhaustion markers TOX, PD1, TIM3 and CD39 and activation marker CD25 did not reveal changes in expression of those markers after 24 hours of restimulation (data not shown), which might indicate that it takes longer to detect changes on the expression level or that changes induced by the

target KOs influence other genes.

One assay, which worked with TIL209, since the restimulation was short, was a  $\text{Ca}^{2+}$  influx assay. Moreover, we used a co-culture system with matching melanoma cells to detect differences in killing capacity of target KO TILs. Furthermore, we aimed to validate expression of VDR and EOS in primary TILs on the proteomic level via flow cytometry, since we only investigated chromatin accessibility but not expression of our targets before.

#### **4.8.1 VDR and EOS knock-out decrease $\text{Ca}^{2+}$ flux in TIL209 cells**

Specific intracellular  $\text{Ca}^{2+}$  levels orchestrate multiple effector functions such as proliferation, differentiation, cytokine secretion and metabolism in T cells [204]. After TCR stimulation, downstream signaling leads to activation of inositol trisphosphate receptor, which acts as a  $\text{Ca}^{2+}$  channel and releases  $\text{Ca}^{2+}$  from intracellular storage sites, mainly from the endoplasmic reticulum (ER). The  $\text{Ca}^{2+}$  flux assay we employed here (in collaboration with AG Jantsch from the UKR) measures intracellular  $\text{Ca}^{2+}$  flux in response to TCR ligation using flow cytometry (see 3.2.14) [156]. This enables analysis of changes in quantity and kinetics of  $\text{Ca}^{2+}$  influx.

We applied this method onto our genome edited TILs (see chapter 4.7), where we knocked-out our target genes VDR and EOS. As a result, VDR and EOS knock-out in TIL209 induced an altered immediate response downstream of TCR signaling resulting in significantly decreased calcium mobilization levels (Figure 4.27). Interestingly,  $\text{Ca}^{2+}$  flux occurred faster in PD1 KO and EOS KO cells (Figure 4.27C). First, it seems that VDR KO decreases TCR response (4.27B), possibly due reduced PLC- $\gamma$ 1 expression, since VDR induces PLC- $\gamma$ 1 expression and PLC- $\gamma$ 1 is involved in inositol trisphosphate receptor activation, which releases  $\text{Ca}^{2+}$  from the ER, as mentioned before. Second, when EOS expression is reduced in TIL209, the cells show a tendency towards a faster but diminished TCR response (Figure 4.27B-C).

## 4. RESULTS

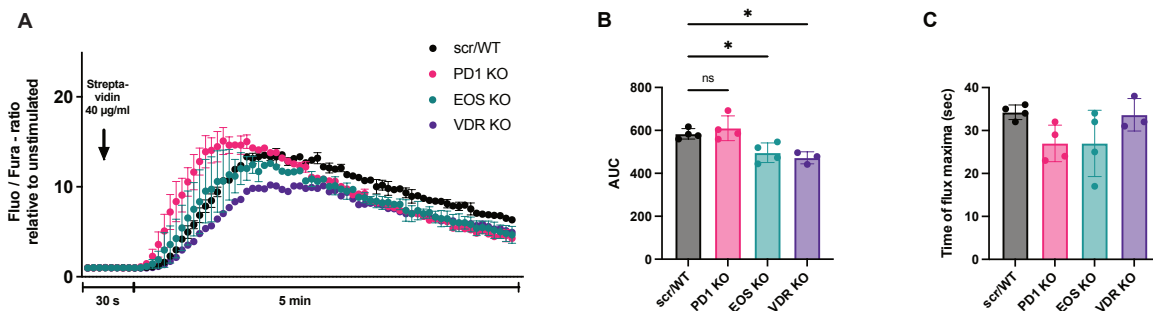


**Figure 4.27: Ca<sup>2+</sup> flux measurement in genome edited TIL209**

(A) Representative Ca<sup>2+</sup> flux curve with baseline (30 s) and Ca<sup>2+</sup> flux after TCR crosslinking via a-CD3-streptavidin (5min). Shown is the Fluo/Fura-ratio relative to the baseline as the mean  $\pm$  SD of technical replicates. (B) Area under the curve of Ca<sup>2+</sup> flux as shown in (A). Shown is the mean  $\pm$  SD of 3-4 biological replicates measured in independent experiments. One-way-Anova with Dunnett's multiple comparison was applied. Asterisks depict \*  $p < 0.05$ . (C) Time of Ca<sup>2+</sup> flux maxima in seconds as estimate for TCR response speed. Shown is the mean  $\pm$  SD of 3-4 biological replicates measured in independent experiments. One-way-Anova with Dunnett's multiple comparison gave no evidence for statistical significance. Yvonne-Natascha-Susanne Weiss from AG Jantsch, UKR performed Ca<sup>2+</sup> flux measurements and analysis of raw data. I performed statistical analysis and created graphs.

Finally, our positive control, the PD1 KO, seems to induce a faster and increased TCR response, although the effect is not significant (Figure 4.27B-C). Usually, upon binding of PD1 ligands to PD1, the ITIM (immunoreceptor tyrosine-based inhibitory motif) and ITSM (immunoreceptor tyrosine-based switch motif) motifs become phosphorylated, which enables activation of the tyrosine phosphatases SHP-1 and SHP-2. SHP-1 and SHP-2 then inhibit TCR signaling and thus also Ca<sup>2+</sup> signaling [140]. Recently, researchers found evidence for a PD1-mediated tonic signaling [55]. Further, Beane et al. reported improved effector function of PD1 knockout TILs, even without the ligands being present [12]. Thus, although PD1 was not engaged by its ligands in our case, the change in Ca<sup>2+</sup> flux could be explained by a decreased tonic PD1-mediated inhibitory signaling due to PD1 knockout in TIL209.

Since we look only on artificial TCR stimulation in a very short time frame here, further experiments should aim to explore the roles of VDR and EOS in functional assays.

### **4.8.2 Target knock-out might change killing capacity of TIL209 cells**

To assess possible changes in the killing capacity of our target KO TIL209 cells, we established a cytotoxicity assay. For this purpose, we chose the Incucyte® SX5 Live-Cell Analysis System that enables measurement of target cell killing in real-time. Being able to quantify cell death over time was an advantage for us as we did not know at which time point differences between TIL209 conditions could be detected. First, we confirmed that TIL209 cells kill M579-A2 melanoma cells (see 3.2.15) in an antigen-dependent manner. To this end, M579-A2 cells were treated with an MHC-I blocking antibody, which should prevent binding of the TCR of TIL209 to MHC-I on the melanoma cells. As a control we left MHC-I unblocked and added melanoma cells alone, without TIL209. As a result, we observed increasing apoptosis of M579-A2 cells, as detected via a caspase-activated DNA dye in the MHC-I unblocked condition, whereas MHC-I blockade inhibited TIL209 mediated killing (Figure 4.28E). Second, we assessed whether target KO has an effect on the killing capacity of TIL209. As a control, to estimate, which effects we could expect, we used TIL209 where we knocked out PD1. As M579-A2 melanoma cells express PD1 ligand PD-L1 (as assessed by Tillmann Michels, former PhD student of the Beckhove lab), we expected that inhibitory signals via PD1 engagement should be abrogated and thus killing capacity of PD1 KO TIL209 should be enhanced to some extent. We observed slightly increased melanoma cell death over the course of co-culture with PD1 KO TIL209 when compared to the scr TIL209 condition (Figure 4.28A-B). This was also true for EOS KO TIL209, although the picture was not as clear, especially in the second run (Figure 4.28B). Pipetting or cell counting errors could be responsible for the high variability between the technical replicates. Further, also VDR KO seems to enhance killing capacity of TIL209 slightly (Figure 4.28C). To confirm our imaging-based results, we counted the remaining M579-A2 cells after 48 hours of co-culture with the target KO TILs via counting beads (Figure 4.28D), and calculated

## 4. RESULTS

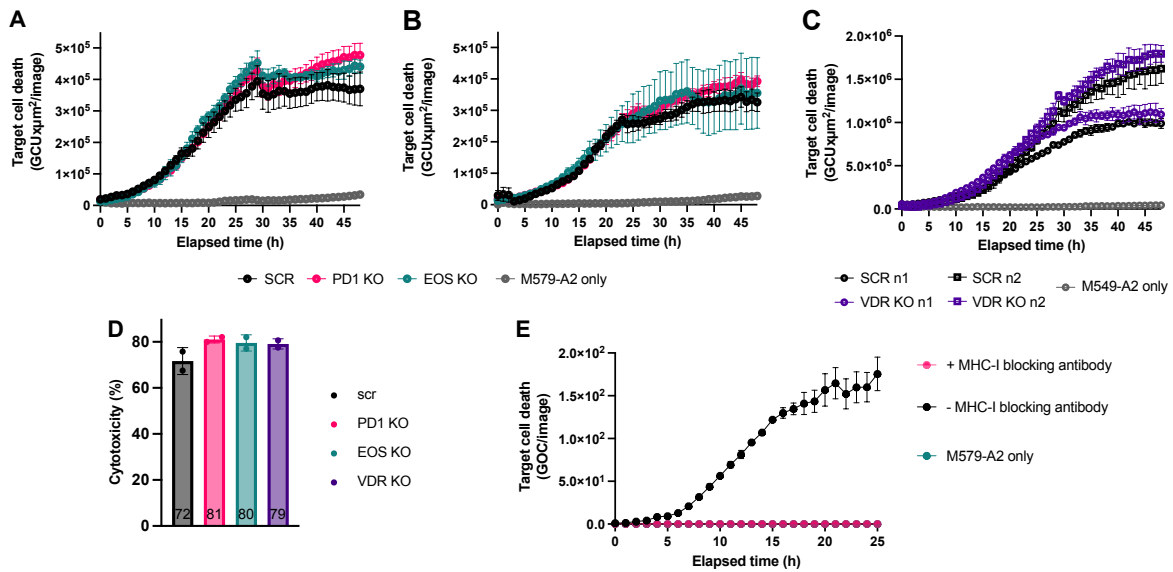


**Figure 4.28: Realtime cytotoxicity assay to analyze killing capacity of genome edited TIL209**

(A,B) Real-time cytotoxicity assay (Incucyte® ZOOM system) of genome edited TIL209 (conditions in the legend) co-cultured with matching melanoma cells M579-A2 for 48 hours in an E:T ratio of 5:1. Apoptosis of melanoma cells was tracked via green fluorescence of a caspase-3/7 activated DNA dye. Target cell death is shown as integrated GCU (green calibrated unit) per image over the 48 hour time-course. Mean  $\pm$  SD of triplicates is shown for two independent experiments (A,B), respectively. (C) Real-time cytotoxicity assay (Incucyte® SX5 system) as described in (A,B). Shown are two independent experiments (n1=round symbols, n2=square symbols). (D) FACS-based measurement of TIL209 cytotoxicity as calculated from M579-A2 cell count after 48 hours of co-culture with TIL209. Shown is the mean  $\pm$  SD of two independent experiments, run in triplicates. (E) Real-time cytotoxicity assay (Incucyte® ZOOM system) to show antigen specific killing of M579-A2 cells by WT TIL209. WT TIL209 were co-cultured with M579-A2 for 25 hours either in the presence or absence of MHC-I blocking antibody. Apoptosis of M579-A2 cells was tracked via the caspase-3/7 activated DNA dye and analyzed as GOC (green object count) per image. Depicted is the mean of technical triplicates  $\pm$  SD.

the cytotoxicity of TIL209 (% cytotoxicity =  $(100 \times (\text{M579-A2 only} - \text{co-culture condition with TIL209}))$ ). Again we could detect a slight increase in cytotoxicity when comparing the KOs with the scr condition. In summary, EOS and VDR might have an effect on effector functions of TILs but TIL209 seem to be a less suitable *in vitro* model to study their role and primary CD8<sup>+</sup> T cells, CAR T cells or *in vivo* mouse models should be enforced in the future.

### **4.8.3 VDR and EOS are co-expressed with TOX in primary TILs**

We wanted to validate the expression of targets EOS and VDR on the proteomic level in primary TILs. Therefore, we collected TILs from tumors and adjacent tumor tissue from RCC and HCC patients and restimulated them for 24 hours with anti-CD3 and anti-CD28 antibodies. As a control we used CD8<sup>+</sup> T cells isolated from PB from healthy donors, which were subjected to the same stimulation.

We found that VDR is expressed in all cell types, CD8<sup>+</sup> T cells isolated from blood, CD8<sup>+</sup> T cells isolated from adjacent non-tumor tissue as well as CD8<sup>+</sup> T cells isolated from one RCC and one HCC patient (Figure 4.29A). VDR expression varied greatly between CD8<sup>+</sup> T cells from blood, which we could confirm in further healthy blood donors (data not shown). Intratumoral TILs partly co-expressed TOX and VDR. Almost the same expression pattern was observed for EOS (Figure 4.29B), where we found EOS only being co-expressed with exhaustion marker TOX in intratumoral TILs, although only to a small extent in RCC TILs. Since this expression analysis was only performed with TILs from two patients, further TIL samples should be investigated. To correlate expression of targets better with other factors or whole transcriptome expression, CyTOF (Cytometry by time of flight) or CITE-seq (Cellular Indexing of Transcriptomes and Epitopes by Sequencing) should be preferred in the future.

## 4. RESULTS

---

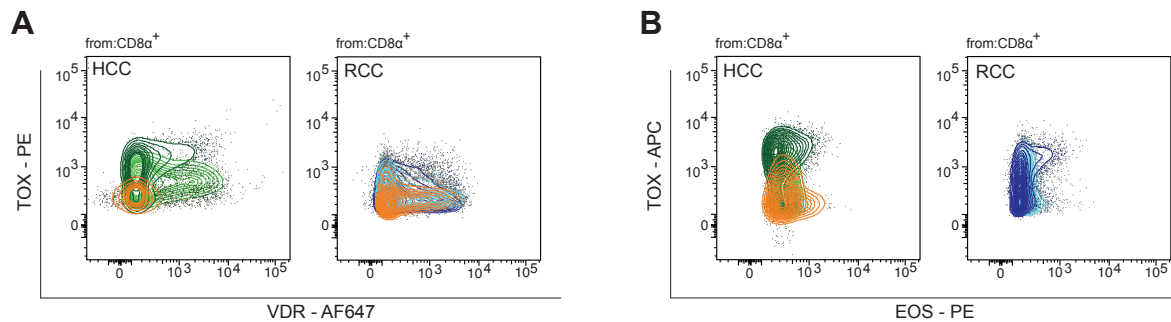


**Figure 4.29: VDR and EOS staining in primary TILs from HCC and RCC patients**

(A) Contour graphs of VDR and TOX expression in HCC TILs (left panel) and RCC TILs (right panel) after 24h restimulation. Gated on CD<sup>+</sup> T cells: from blood (orange), from adjacent non-tumor tissue (brighter color) and from tumor (darker color). (B) Contour graphs of EOS and TOX expression in HCC TILs (left panel) and RCC TILs (right panel) after 24h restimulation. Gated on CD<sup>+</sup> T cells: from blood (orange), from adjacent non-tumor tissue (brighter color) and from tumor (darker color). Blood control for RCC is missing.

## 5 Discussion

In most solid cancers heterogeneous T cell states exist, among others a cell state, which is referred to as dysfunctional, exhausted or hyporesponsive, and characterized by high expression of co-inhibitory receptors, reduced effector function and a specific chromatin landscape, which is influenced by recently identified exhaustion driver TOX [150]. Studies have shown that these T cells cannot be reinvigorated via checkpoint blockade but a population of TCF1 expressing, so called precursor exhausted TILs, expands upon checkpoint therapy [151, 172]. Nonetheless, a majority of patients do not respond or become resistant to IT. Thus, it is of fundamental interest to improve the knowledge about ways to reinvigorate exhausted TILs and promote immunotherapy responsive cell states.

Identifying and manipulating epigenetically regulated TIL genes could increase knowledge of T cell dysfunction and might be a way to improve immunotherapeutic approaches in the future. One attempt could be to eliminate epigenetic traits that cause cells to become dysfunctional in order to prevail cell function of cell-therapeutic products such as CAR T cells.

So far, T cell dysfunction has mainly been studied in mouse models and on the transcriptome level. Merely two studies have investigated the epigenetic regulation of human TILs on the single-cell level, namely in BCC [173] and in TNBC (Triple Negative Breast Cancer, [230]). We therefore aimed to create a generalized description of human T cell states and their underlying gene-regulatory mechanisms in human cancer.

To this end, we performed single-cell ATAC-seq of TILs from several patients and

cancer entities to study the chromatin landscape of heterogeneous TILs in an unbiased way. We included non-tumor tissue controls, healthy PBMC controls, integrated data from already published BCC TILs [173] and validated the functionality of the TILs via flow cytometry. We dissected central gene-regulatory patterns of functional and dysfunctional human T cell states despite tissue-specific chromatin remodeling, defined an epigenetic "core" trajectory to terminal T cell dysfunction in human tumors and identified undescribed putative exhaustion drivers, which we started to validate via state-of-the-art CRISPR approaches.

This thesis provides a broad collection of single-cell chromatin landscapes of human TIL states from four different cancer entities. As a perspective, our data set represents a rich resource of future target gene investigations and enhancer modulations, which might be relevant for the success of immunotherapy.

### **5.1 Heat or hypoxia as well as the tumor tissue could influence chromatin remodeling of TILs**

T cell differentiation and function is influenced by signals from their environment, which render the chromatin landscape [83, 178]. To date, it is still not fully understood, which factors drive TIL fates in the tumor microenvironment. Interestingly, marker genes, enrichment of published signatures, TF activity and pathway analysis, in the extended as well as in the core analysis, suggest that the chromatin landscape of TILs might be influenced by hypoxia, heat and/or oxidative and metabolic stress.

Hypoxia induces HSF1 und HSP expression and HIF1a mediated transcription [186, 8]. The inflammation caused by the anti-tumor immune response can lead to oxidative stress, since immune cells like macrophages produce free radicals. The oxidative stress can further increase necrosis, not only apoptosis, in the tumor tissue, which will even more enhance inflammation. Together with the enhanced

oxygen turnover of the expanding tumor cells, this situation eventually leads to hypoxia, which further drives oxidative cell stress. Hence, heat shock proteins become activated to combat the caused protein structural damage [87, 90]. Moreover, tumor and immune cells switch to glycolysis under hypoxic conditions [165], which leads to elevated lactate concentrations, both intracellular and intercellular. Several studies have shown that glycolysis, lactate uptake and ROS (reactive oxygen species) influence T cell function negatively and impair anti-tumor immune response [62, 126, 166]. It has been shown, that inhibiting those influences, such as restricting glycolysis, inhibiting lactate uptake or terminating ROS with antioxidants, can preserve or reverse T cell effector function [166, 209].

All of this could explain the heat shock response we observed in specific TIL clusters. On the one hand, especially in HCC cases, necrosis and fibrosis occur, which induces hypoxia and oxidative stress by ROS, which in turn promotes fibrosis further [58, 27]. This could be the reason why we observe this HS signature mainly in HCC TILs. On the other hand, we found heat shock proteins and co-chaperons to be expressed in cluster- and entity-matching scRNA-seq data, which derived not only from HCC, but also from BCC, RCC and HNSCC TILs ([36, 196, 226, 227] data not shown, public available data analyzed by Malte Simon, DKFZ). Furthermore, two other studies observed a heat shock signature in as exhausted classified TILs from melanoma as well as from colorectal carcinoma, which expanded in the case of aPD1-blockade non-responsive melanoma patients [172, 147]. This is in accordance with our observation, that the most severely exhausted TILs exhibited the heat shock signature. All together, it might be the case that a heat shock signature is more common in TILs, but not yet studied in more detail.

Data of impact of hypoxia on success of immunotherapy are still missing in humans. However, a study in a B16 melanoma mouse model confirmed that reducing hypoxia decreased T cell exhaustion and improved IT response [175]. Furthermore, it has been reported that hypoxic conditions lead to reduced killing capacity of T cells [78] and hypoxia induced TF HIF1alpha expression was found to correlate with higher

abundance of exhausted T cells in glioma [115]. Regarding the influence of heat on TILs, O’Sullivan et al. observed enhanced tumor control of T cells exposed to heat [143] and others reported that tumor treatment with hyperthermia has an advantageous effect on treatment outcome since it induces immunogenicity, thereby enhances the immune response and sensitizes tumors to further therapies like radiotherapy [43].

Besides the potential influence of heat and hypoxia it seems that the specific tumor tissue or entity has an increasing influence with progression of T cell dysfunction. In our dataset we observed tissue-specific chromatin remodeling in TILs. On the one hand, over 6000 differentially accessible chromatin regions were either specific for ccRCC, HCC or BCC TILs. On the other hand, several TF motifs were differentially enriched in the tissue specific chromatin regions. In contrast, we could not observe many terminal exhausted TILs in HPV (Human papillomavirus) negative HNSCC. These notions are in line with Zheng et al. who reported a clear influence of TME and cancer type, respectively on immune cell composition [232]. Others reported a tissue specific effect on the transcriptional and epigenetic profile of T cells, especially in the case of tissue-resident memory T cells in airways, lung and skin [79, 37, 121]. Altogether, our observations of tissue and microenvironmental influences on TILs, especially dysfunctional TILs, should be further investigated to unwind the gene-regulatory cues, which lead to chromatin remodeling and thereby potential change in functionality of TILs.

## **5.2 A core trajectory to terminal T cell dysfunction can be defined exclusively by profiling multiple entities**

When we want to study gene regulation of T cell exhaustion in humans, we actually have to account for many individual influences, such as the tumor stage, TCR

affinity, the local immune environment, patient specific conditions and many more. These are factors, which can be accounted for in mouse experiments but are hard to deal with in *ex vivo* experiments with human material. Until now, there is only one published study, which profiled the chromatin of TILs of one entity on the single-cell level [173] but we asked whether there is a main epigenetic program of T cell exhaustion, which is shared between tumor entities. To account for tissue and patient specific factors, multiple entities and multiple patients need to be investigated. Therefore, we examined the open chromatin landscape of heterogeneous CD8<sup>+</sup> T cell states of three different tumor entities (ccRCC, HCC, HNSCC) and included the already published dataset (BCC, [173]) as a fourth entity.

In fact, we were able to create a “core” analysis of chromatin states in TILs, which was corrected for the tissue influence (see chapter 4.5). We could show, that functional (cytotoxic, memory, activated) T cell states as well as dysfunctional T cell states (terminal exhausted, exhausted-proliferating, precursor exhausted) existed in all the four entities. The only exception was for HNSCC TILs, which mainly were found to be in functional or precursor exhausted states but barely in terminal exhausted states. This is in accordance with the phenotypical and functional examination via flow cytometry, where we observed that all four HNSCC specimen expressed exhaustion markers PD1 and CD38 on a very low level but on average had the highest percentage of polycytokine-producing cells (IFN $\gamma$ <sup>+</sup>/TNF $\alpha$ <sup>+</sup>) compared to RCC and HCC TILs. Furthermore, fraction of CD8<sup>+</sup> T cells and fraction of CD45RA<sup>-</sup>CCR7<sup>-</sup> CD8<sup>+</sup> T cells were lower than in specimens of the other two entities examined by us. Our observations fit to the fact, that all HNSCC samples were HPV (Human papillomavirus) negative and HPV<sup>-</sup> HNSCC is typically associated with lower levels of CD8<sup>+</sup> T cell infiltration and often found to be immunological “cold” tumors [215, 64]. Moreover, HPV<sup>-</sup> HNSCC TILs were found to express lower levels of multiple exhaustion markers when compared to HPV<sup>+</sup> HNSCC TILs [215, 64]. All together, this shows us that major differences seem to exist between HNSCC TILs and the other entity TILs on the epigenetic, phenotypical and functional level, which would have biased

our analysis if we would have investigated only one additional entity next to HNSCC. Besides this, we observed an influence of the tissue/entity on the chromatin landscape, especially in dysfunctional TILs, as discussed in the previous chapter (5.1), which is in accordance with a recent publication, which described differences between abundance of T cell states when comparing different entities [232].

To conclude, a “core” analysis of a general epigenetic program of T cell exhaustion would not have been reasonable when we would not have studied several specimens of several entities.

### **5.3 Chromatin profiling of human TILs creates a resource of potential immunotherapeutically relevant targets**

T cell exhaustion is controlled by epigenetic mechanisms [151, 177], yet it is unknown, which are the main mechanisms shared by TILs influenced from different tumor microenvironments. The novel exhaustion driver TOX was studied mainly via transcriptomics and in murine tumor models [4, 98, 181]. Thus, we hypothesized that we will find further exhaustion related genes in the human system, by studying the chromatin landscape of human TILs on the single-cell level and that by manipulation of these genes we could increase knowledge of T cell dysfunction and improve immunotherapeutic approaches. Therefore, we profiled the chromatin of heterogeneous TILs of several tumor entities and specimens on the single-cell level to create a resource for future target investigations.

As a result, we were able to produce a large dataset of chromatin profiles from human TILs derived from different tumor entities. The dataset comprised different T cell states, which range from functional and presumably IT relevant to dysfunctional cell states. In addition, we could create an entity-shared trajectory analysis of the progression from functional towards terminal dysfunctional TIL states based

on our plenty single-cell chromatin states. This “core” trajectory is supported by the PD1 expression status, the absence of tissue derived cells and HNSCC TILs in the terminal exhausted clusters, the expansion of exhausted BCC TILs post PD1 blockade therapy and the progression from *TCF7* towards *HAVCR2* (TIM3) activity. Moreover, we found evidence that our entity-shared “core” trajectory towards dysfunction consists of tumor-reactive T cells and not bystander T cells, which tells us that our dataset is meaningful for future target investigations. First, TOX expression is induced by TCR stimulation [181] and we found TOX to be a marker gene for the exhausted clusters, second public signatures of antigen-specific T cells derived from infection and cancer models are enriched in T<sub>PEX</sub> and T<sub>EX</sub> clusters and third proliferation marker *MKI67* (Ki-67) is a marker gene for one of the T<sub>EX</sub> clusters and T cells cycle exclusively upon TCR signaling [72]. Within our “core” trajectory analysis of entity-shared progression towards terminal dysfunction we discovered that different TF families seem to be involved in T<sub>PEX</sub> vs T<sub>EX</sub> cell states. For example, we observed an increase of NR family member activity but a loss of KLF and ETS:RUNX activity in T<sub>EX</sub>, which was not described in other studies so far. Furthermore, we found gene activity of unfamiliar factors, especially epigenetic and transcriptional modifiers, to be associated either with T<sub>PEX</sub> or T<sub>EX</sub>. Thus, our dataset provides a rich resource to identify candidate genes which might play a role in gene-regulation of T<sub>PEX</sub> or T<sub>EX</sub> cell states.

As a perspective, our dataset provides the basis to extract targets, such as genes or enhancers, for therapeutic implementations in the future. As an example, over-expressing or deleting genes, which are either favorable or unfavorable for T cells in the tumor could be a way to improve T cell-based therapies. One of the most promising strategies to fight cancer is the usage of CAR T cells [95]. Nonetheless, exhaustion of CAR T cells was observed, especially in the case of solid tumors [217, 155]. Therefore, engineering CAR T cells, for example via ablation of unfavorable exhaustion drivers, might be a way to overcome this. However, studies have shown that specific expression levels might be important for distinct cell fates and

## 5. DISCUSSION

---

functions and total ablation might not be the most promising way to tune T cell products. For instance, knockout of exhaustion driver TOX did not improve T cell function *in vivo* but rather was found to be necessary for T cell persistence in the tumor [98, 181]. Appropriately, only partial knockdown improved killing capacity and cytokine production [184, 181]. Another example of disadvantageous total ablation of a factor is PD1 KO in CAR T cells, which provoked the dangerous cytokine release syndrome in patients [125]. In contrast, targeting enhancers can decrease instead of eradicate expression as shown by Gennert et al. who reduced PD1 expression in CAR T cells by deleting a distal enhancer of the *PDCD1* gene [66]. Thus, perturbing enhancer activity, for example via CRISPR activation or interference (CRISPR a/i) [191, 199], could be a way to improve cancer immunotherapy in the future. For instance, by integration of our single-cell chromatin data with entity matching single-cell transcriptome data, enhancer-promoter interactions could be predicted and by super enhancer analysis prioritized. The newly discovered, cell state-specific enhancers are currently under validation in our laboratory but preliminary data seem to confirm that with scATAC-seq and computational approaches we can predict enhancers specific for therapeutically relevant targets. In that way, T cell products could be improved in the future.

To date, it is still a matter of debate, which TIL state is the best to become reprogrammed by therapies and how to best design those therapies. Since there is a lot of evidence that dysfunctional TILs are in an epigenetically fixed state and cannot be reinvigorated via immune checkpoint therapy [151, 146], it should be considered to find other ways to reinvigorate them or prevent development to terminally dysfunction, for example via approaches, which target the gene-regulatory landscape. One strategy could be to target TFs, which play a role during chronic antigen stimulation, which has been shown to work successfully in adoptive T cell settings [35, 113, 118]. Therefore, we used our “core” analysis of entity-shared chromatin landscapes to select target genes, which might play a role in the establishment or maintenance of T cell dysfunction. We selected several TFs, among them VDR and EOS, which we

started to investigate further.

First, we confirmed the expression of VDR and EOS in primary TILs via flow cytometry. Second, we employed a CRISPR KO-based *in vitro* approach to study the role of the targets in exhaustion-like melanoma TILs. Third, we started to investigate the influence of the KOs onto the TILs by applying functional assays. We observed a decrease of  $\text{Ca}^{2+}$  influx and a slight increase of killing capacity in VDR and EOS KO TILs.

The question arises whether a decreased  $\text{Ca}^{2+}$  influx is favorable or not for exhausted TILs. Huang et al. found cytotoxic effector T lymphocytes (CTLs) from breast and lung cancer patients being the immune cell subset most sensitive to intrinsic activation-induced cell death (AICD) and confirmed that this was TCR signaling dependent and due to downstream signaling of increased  $\text{Ca}^{2+}$  influx after TCR engagement [85]. Hence, one could hypothesize that decreased  $\text{Ca}^{2+}$  influx as observed in VDR and EOS KO TILs could be favorable and improve T cell survival upon challenges like antigen encounter in the tumor, which might also explain the observed increase in killing capacity of VDR and EOS KO TILs. In contrast, an immunomodulatory compound screening showed that VDR agonists could restore cytokine production in exhausted T cells from chronic LCMV (Lymphocytic choriomeningitis virus) infection [124].

Interestingly, other researchers found evidence that VDR and EOS indeed might play a role in T cell dysfunction. Yang et al. observed RNA expression of VDR to be the highest and the VDR binding motif to be enriched in  $\text{CD103}^+\text{CD39}^+$  exhausted TILs from CRC (Colorectal Cancer) patients. In addition, they reported a strong positive correlation of TOX and VDR expression in the same cell type [223]. Notably, VDR was almost 2-fold higher expressed in PD1-high vs PD1-negative TILs from NSCLC patients [201]. Furthermore, the VDR binding motif was found to be higher accessible in  $\text{CD8}^+\text{CXCL13}^+$  TILs from triple positive breast cancer patients after treatment with combination therapy of anti-PD1 blockade and chemotherapy compared to pre-treatment [230]. For EOS, it has been reported that *IKZF4* expression

## 5. DISCUSSION

---

was decreased in non-treated vs anti-PD-L1 treated exhausted TILs in mice [146]. In addition, a transcriptome-based pan cancer study found VDR and EOS to be among the most universally expressed TFs in exhausted TILs [232]. Unexpectedly, the same study reported that Treg TF FOXP3 was expressed in T<sub>EX</sub> of half of the cancer types profiled [232], and VDR as well as EOS was found to be overexpressed in tumor specific suppressive Tregs of breast cancer patients [220], suggesting similarities between T<sub>EX</sub> and Treg programs.

Nonetheless, the exact mechanism of VDR- and EOS-mediated gene regulation in human TILs and their role in the establishment or maintenance of T cell dysfunction should be further explored, since we and others found evidence that these factors could be involved in these processes.

Another cell population of interest are TCF1 expressing precursor exhausted T cells, which were already described to exist among the heterogeneous exhausted T cells in tumors and chronic viral infection [172, 89, 35]. They exhibit memory characteristics as well as hallmarks of exhaustion, show self-renewal capacity, and sustain the anti-tumor T cell response [172, 189, 206, 88, 89, 103]. Precursor exhausted T cells are associated with anti-PD1 therapy success and accumulate in responsive patients via both local expansion and enrichment from peripheral T cells [111]. Furthermore, studies observed that T<sub>PEX</sub> cells are responsible for the proliferative burst of TILs after anti-PD1 checkpoint therapy [189, 130]. In accordance, we observed accumulation of T<sub>EX</sub> cells together with simultaneous decrease of T<sub>PEX</sub> cells within BCC TILs post therapy, suggesting expansion of terminally T<sub>EX</sub> from T<sub>PEX</sub> cells. Since it is thought that dysfunctional TILs can still maintain tumor control on a homeostatic level but not reject tumors, we need to understand how tumor-specific precursor exhausted T cells can be recruited to the tumor side and how their function and persistence could be supported by IT.

In our data we detected TILs that resemble T<sub>PEX</sub> cells. In more detail, in the entity-corrected core analysis one cluster was enriched for several published T<sub>PEX</sub> signatures and possessed gene activity of T<sub>PEX</sub> markers *TCF7* as well as *CXCR5*. How-

ever, the origin of these cells is unknown to us and we cannot provide final proof that these cells are actually precursor exhausted TILs, as we do not have functional data from the same single cells. Furthermore, we cannot provide data regarding clonal relationship as we did not examine TCR sequences. Nonetheless, we detected motif as well as gene activity of TF KLF3 in T<sub>PEX</sub> cells, which disappeared in the epigenetic landscape of terminal T<sub>EX</sub>. The transcription factor was not described yet in regard to gene regulation of TILs, but was also found in T<sub>PEX</sub> cells of B16 melanoma [130]. Moreover, Chen et al. reported that KLF3 showed a high regulon activity in effector T cells of chronic LCMV infection and proposed that KLF3 together with other family members regulate emigration of effector T cells from lymphoid organs [34]. In this regard, it remains a challenge to elucidate the mechanisms that control the differentiation and maintenance of precursor exhausted TILs in order to improve immunotherapeutic applications. Thus, the influence of genes such as KLF3, which we think to have a regulatory role in T<sub>PEX</sub>, should be investigated further.

To sum up, we were able to define a “core” analysis of the gene-regulatory mechanisms underlying T cell dysfunction. We found promising candidate genes and our first validation results as well as the evidence found in the literature suggests that it is worth to study their role in T cell dysfunction and in general in CD8<sup>+</sup> T cells further. Altogether, our dataset of chromatin profiles from human TILs provides a rich resource of potential immunotherapeutically relevant targets. In more detail, new unknown enhancers or immunotherapeutically relevant genes could be extracted and implemented via CRISPR i/a in cell therapeutic products such as CAR T cells in the future.

## 5.4 Challenges and pitfalls of a CRISPR/Cas9 based target screening using *in vitro* expanded TILs

CRISPR/Cas9 is a well established gene editing technique, widely used in basic research to study the role of target genes. Nonetheless, it depends on the cell type and the genes of interest whether gene knockout via CRISPR/Cas9 is easily to be implemented. We chose CD8<sup>+</sup> TIL209 for our target screening as these cells have been expanded and cell numbers were sufficient to perform experiments with, which is not the case for freshly isolated TILs from human tumor specimen. Nonetheless, establishment of CRISPR/Cas9 via electroporation was not a straightforward process. First, restimulation before electroporation, which usually enhances KO efficiency, was not feasible due to decreased cell viability. Second, cells with successful target KO could not be enriched for following assays as we were targeting intracellular proteins. Besides, we noticed that several features have to be considered, tested and the best solution thereof to be found to receive adequate target KO and at the same time acceptable cell viability. Notably, Cas9 enzymes, electroporation buffers, electroporation settings, gRNAs and their combinations, and KO determination should be considered as adjusting screws in the process of establishing successful CRISPR/Cas9 based genome editing of genes of interest in the desired cell type, especially if CRISPR/Cas9 should be implemented in sensitive cells.

Furthermore, we noticed that the TIL209 cells do not represent the optimal *in vitro* model to assess functional changes upon target KO. On the one hand, they have shown a preserved or regained high killing capacity (see 4.8.2), which is hard to enhance further via target KO and does not resemble functionality of terminal exhausted TILs (see 4.2.4). On the other hand, they do not survive long-term TCR restimulation, which precludes other assays such as proliferation assays or RNA-seq, which both require restimulation of the cells to assess differences between KO conditions.

Nonetheless, we were able to establish CRISPR/Cas9 based KO of several selected target genes in TIL209 and could start to validate their role in TILs via functional assays, such as  $\text{Ca}^{2+}$  flux assays and killing assays. In fact, we observed decreased calcium mobilization levels and slightly increased killing capacity when VDR or EOS expression was reduced around 60-70 %, respectively (see 4.8.1 and 4.8.2). Therefore, it seems promising to study the role of VDR and EOS as well as of the other prioritized target genes (see table 4.18) in more relevant settings, such as in CAR T cells (investigations started in collaboration with the groups from Prof. Abken and Prof. Poeck at our institute) and in *in vivo* mouse models (knockout mouse lines for several targets are now available in our lab) in the future, in order to observe whether ablation of our target genes might improve immunotherapy.

## 5.5 Limitations of the study

The results, as presented in this thesis, have some limitations, which should be discussed. First, as we analyzed only four tumor entities, we are missing information of other tumor microenvironments, which might be highly relevant as we discovered differences in the gene-regulatory landscape of TILs derived from different TMEs as discussed in 5.1. Hence, our generalized gene-regulatory landscape of  $T_{EX}$  might not necessarily match gene-regulatory landscapes of  $T_{EX}$  of all possible entities. Second, our results lack information about the influence of immunotherapies on different T cell states, as we were only able to include data of pre/post IT BCC TILs [173] and did not had the chance to receive further samples of patients treated with IT. Furthermore, samples of IT responders vs non-responders could help to identify genes, which are beneficial for a succesful anti-tumor immune response. Third, we could not track clonal relationship of the investigated cells, which would have helped to distinguish bystander from tumor-reactive TILs and follow differentiation trajectories of distinct T cell clones. Although we found evidence that our clusters of precursor and terminally dysfunctional TILs are populated by tumor-reactive TILs

as discussed in chapter 5.3, clonal relationships should be addressed in the future. Methodological solutions to study this are either multi-omics approaches, which allow simultaneous profiling of TCR sequence and open chromatin from the same cell, or mitochondrial DNA sequencing in combination with chromatin profiling, as mitochondrial DNA mutations enable inference of clonal relationships as well [106]. Fourth, information on spatial interaction with other immune and tumor cells, shortly information about the tumor microenvironment, is missing here due to technical limitations. However, this should be studied using spatial transcriptomic technologies or single-cell laser microdissection in the future. Further, no final conclusions regarding the role of our targets in T cell dysfunction can be drawn from our results, as no mouse models were available yet to infer this in *in vivo* settings. Nonetheless, our group has knockout mouse lines available now (such as KO mouse cited here [212]) and it is planned to investigate the targets' influence on T cell dysfunction in mouse tumor models in the future. Furthermore, the impact of our targets on CAR T cell function could be inferred by studying their persistence and performance in 3D tumor organoids.

## 5.6 Conclusion and Outlook

We aimed to create a generalized description of human T cell states and their underlying gene-regulatory mechanisms in human cancer. Therefore, we performed unbiased single-cell analysis of the open chromatin landscapes of several thousands of CD8<sup>+</sup> TILs derived from 16 patients with different types of solid malignancies. Indeed, we could identify a 'core' gene-regulatory trajectory to terminal T cell dysfunction, which was shared between three out of four tumor entities. Despite this, we also observed tissue-specific influences on chromatin remodeling of TILs. Furthermore, our data suggest that the chromatin landscape of TILs is influenced by hypoxia and/or heat stress.

We identified known but also unknown putative exhaustion drivers within our open

chromatin data of terminal exhausted T cells, which are shared between tumor entities. We started to validate their role in T cell exhaustion by using CRISPR/Cas9-based gene perturbation to knockout selected candidate genes in expanded TILs from melanoma patients. In fact, we observed slight differences in  $\text{Ca}^{2+}$  flux as well as in killing capacity of TILs which lacked candidate factors VDR or EOS. Their specific role in gene regulation of human TILs, especially in the process of establishment and maintenance of T cell exhaustion, should be explored in the future.

To conclude, our broad dataset provides a framework to understand gene regulation of relevant TIL states in human malignancies. As a perspective, our data represent a resource of potential immunotherapeutically relevant target genes and enhancers, which might be useful to tune T cell function in immunotherapeutic approaches such as CAR T cells. As an outlook, our group started collaborations within the institute, to study putative exhaustion drivers selected from our dataset via CRISPR/Cas9-based KO in CAR T cell therapy. Further, a PhD student of our group started to examine TIL state specific enhancers extracted from our dataset, which potentially regulate immunotherapeutically relevant genes, via enhancer perturbations (CRISPR a/i). Furthermore, our group aims to study the role of our target genes in *in vivo* mouse tumor models in the future. Moreover, we started to establish ChIP-seq in the expanded melanoma-derived TIL209 cells to study gene regulation driven by target TFs.



## 6 REFERENCES

- [1] H. A. Abdelsamed, C. C. Zebley, H. Nguyen, R. L. Rutishauser, Y. Fan, H. E. Ghoneim, J. C. Crawford, F. Alfei, S. Alli, S. P. Ribeiro, A. H. Castellaw, M. A. McGargill, H. Jin, S. K. Boi, C. Speake, E. Serti, L. A. Turka, M. E. Busch, M. Stone, S. G. Deeks, R. P. Sekaly, D. Zehn, E. A. James, G. T. Nepom, and B. Youngblood. Beta cell-specific cd8+ t cells maintain stem cell memory-associated epigenetic programs during type 1 diabetes. *Nature Immunology*, 21:578–587, 5 2020. ISSN 15292916. doi: 10.1038/s41590-020-0633-5.
- [2] R. AbouKhouzam, K. Brodaczewska, A. Filipiak, N. A. Zeinelabdin, S. Buart, C. Szczylik, C. Kieda, and S. Chouaib. Tumor hypoxia regulates immune escape/invasion: Influence on angiogenesis and potential impact of hypoxic biomarkers on cancer therapies, 1 2021. ISSN 16643224.
- [3] M. R. Akbar, A. Wibowo, R. Pranata, and B. Setiabudiawan. Low serum 25-hydroxyvitamin d (vitamin d) level is associated with susceptibility to covid-19, severity, and mortality: A systematic review and meta-analysis, 3 2021. ISSN 2296861X.
- [4] F. Alfei, K. Kanev, M. Hofmann, M. Wu, H. E. Ghoneim, P. Roelli, D. T. Utzschneider, M. von Hoesslin, J. G. Cullen, Y. Fan, V. Eisenberg, D. Wohlleber, K. Steiger, D. Merkler, M. Delorenzi, P. A. Knolle, C. J. Cohen, R. Thimme, B. Youngblood, and D. Zehn. Tox reinforces the phenotype and longevity of exhausted t cells in chronic viral infection. *Nature*, 571:265–269, 7 2019. ISSN 14764687. doi: 10.1038/s41586-019-1326-9.
- [5] C. D. Allis and T. Jenuwein. The molecular hallmarks of epigenetic control. *Nature Reviews Genetics*, 17:487–500, 2016. ISSN 14710064. doi: 10.1038/nrg.2016.59. URL <http://dx.doi.org/10.1038/nrg.2016.59>.
- [6] M. Aluigi, M. Fogli, A. Curti, A. Isidori, E. Gruppioni, C. Chiodoni, M. P. Colombo,

## 6 REFERENCES

---

- P. Versura, A. D'Errico-Grigioni, E. Ferri, M. Baccarani, and R. M. Lemoli. Nucleofection is an efficient nonviral transfection technique for human bone marrow-derived mesenchymal stem cells. *Stem Cells*, 24:454–461, 2 2006. ISSN 10665099. doi: 10.1634/stemcells.2005-0198.
- [7] S. Baek and I. Lee. Single-cell atac sequencing analysis: From data preprocessing to hypothesis generation, 1 2020. ISSN 20010370.
- [8] N. A. Baird, D. W. Turnbull, and E. A. Johnson. Induction of the heat shock pathway during hypoxia requires regulation of heat shock factor by hypoxia-inducible factor-1. *Journal of Biological Chemistry*, 281:38675–38681, 12 2006. ISSN 00219258. doi: 10.1074/jbc.M608013200.
- [9] L. Baitsch, P. Baumgaertner, E. Devêvre, S. K. Raghav, A. Legat, L. Barba, S. Wieckowski, H. Bouzourene, B. Deplancke, P. Romero, N. Rufer, and D. E. Speiser. Exhaustion of tumor-specific cd8+ t cells in metastases from melanoma patients. *Journal of Clinical Investigation*, 121:2350–2360, 6 2011. ISSN 00219738. doi: 10.1172/JCI46102.
- [10] J. Banerji, S. Rusconi, and W. Schaffner. Expression of a betaglobin gene is enhanced by remote sv40 dna sequences, 1981.
- [11] S. H. Baumeister, G. J. Freeman, G. Dranoff, and A. H. Sharpe. Coinhibitory pathways in immunotherapy for cancer, 5 2016. ISSN 15453278.
- [12] J. D. Beane, G. Lee, Z. Zheng, M. Mendel, D. Abate-Daga, M. Bharathan, M. Black, N. Gandhi, Z. Yu, S. Chandran, M. Giedlin, D. Ando, J. Miller, D. Paschon, D. Guschin, E. J. Rebar, A. Reik, M. C. Holmes, P. D. Gregory, N. P. Restifo, S. A. Rosenberg, R. A. Morgan, and S. A. Feldman. Clinical scale zinc finger nuclease-mediated gene editing of pd-1 in tumor infiltrating lymphocytes for the treatment of metastatic melanoma. *Molecular Therapy*, 23:1380–1390, 8 2015. ISSN 15250024. doi: 10.1038/mt.2015.71.
- [13] O. Bell, V. K. Tiwari, N. H. Thomä, and D. Schübeler. Determinants and dynamics of genome accessibility, 8 2011. ISSN 14710056.
- [14] B. Bengsch, T. Ohtani, O. Khan, M. Setty, S. Manne, S. O'Brien, P. F. Gherardini, R. S. Herati, A. C. Huang, K. M. Chang, E. W. Newell, N. Bovenschen, D. Pe'er, S. M. Albelda, and E. J. Wherry. Epigenomic-guided mass cytometry

- profiling reveals disease-specific features of exhausted cd8 t cells. *Immunity*, 48: 1029–1045.e5, 2018. ISSN 10974180. doi: 10.1016/j.immuni.2018.04.026. URL <https://doi.org/10.1016/j.immuni.2018.04.026>.
- [15] S. L. Berger, T. Kouzarides, R. Shiekhattar, and A. Shilatifard. An operational definition of epigenetics. *Genes and Development*, 23:781–783, 4 2009. ISSN 08909369. doi: 10.1101/gad.1787609.
- [16] D. D. Bikle. Vitamin d and the skin: Physiology and pathophysiology, 3 2012. ISSN 13899155.
- [17] M. Binnewies, E. W. Roberts, K. Kersten, V. Chan, D. F. Fearon, M. Merad, L. M. Coussens, D. I. Gabrilovich, S. Ostrand-Rosenberg, C. C. Hedrick, R. H. Vonderheide, M. J. Pittet, R. K. Jain, W. Zou, T. K. Howcroft, E. C. Woodhouse, R. A. Weinberg, and M. F. Krummel. Understanding the tumor immune microenvironment (time) for effective therapy. *Nature Medicine*, 24:541–550, 5 2018. ISSN 1546170X. doi: 10.1038/s41591-018-0014-x.
- [18] A. Bolotin, B. Quinquis, A. Sorokin, and S. D. Ehrlich. Clustered regularly interspaced short palindrome repeats (crisprs) have spacers of extrachromosomal origin. *Microbiology*, 151:2551–2561, 8 2005. ISSN 13500872. doi: 10.1099/mic.0.28048-0.
- [19] E. K. Brinkman, T. Chen, M. Amendola, and B. V. Steensel. Easy quantitative assessment of genome editing by sequence trace decomposition. *Nucleic Acids Research*, 42, 12 2014. ISSN 13624962. doi: 10.1093/nar/gku936.
- [20] F. Broere, S. G. Apasov, M. V. Sitkovsky, and W. van Eden. A2 t cell subsets and t cell-mediated immunity, 2011.
- [21] S. J. Brouns, M. M. Jore, M. Lundgren, E. R. Westra, R. J. Slijkhuis, A. P. Snijders, M. J. Dickman, K. S. Makarova, E. V. Koonin, and J. V. D. Oost. Small crispr rnas guide antiviral defense in prokaryotes. *Science*, 321:960–964, 8 2008. ISSN 00368075. doi: 10.1126/science.1159689.
- [22] S. W. Brubaker, K. S. Bonham, I. Zanoni, and J. C. Kagan. Innate immune pattern recognition: A cell biological perspective, 3 2015. ISSN 15453278.
- [23] N. Buang, L. Tapeng, V. Gray, A. Sardini, C. Whilding, L. Lightstone, T. D. Cairns, M. C. Pickering, J. Behmoaras, G. S. Ling, and M. Botto. Type i interferons affect the metabolic fitness of cd8+ t cells from patients with systemic lupus erythematosus.

## 6 REFERENCES

---

- Nature Communications*, 12, 12 2021. ISSN 20411723. doi: 10.1038/s41467-021-22312-y.
- [24] J. D. Buenrostro, P. G. Giresi, L. C. Zaba, H. Y. Chang, and W. J. Greenleaf. Transposition of native chromatin for fast and sensitive epigenomic profiling of open chromatin, dna-binding proteins and nucleosome position. *Nature Methods*, 10:1213–1218, 12 2013. ISSN 15487091. doi: 10.1038/nmeth.2688.
- [25] J. D. Buenrostro, B. Wu, U. M. Litzénburger, D. Ruff, M. L. Gonzales, M. P. Snyder, H. Y. Chang, and W. J. Greenleaf. Single-cell chromatin accessibility reveals principles of regulatory variation. *Nature*, 523:486–490, 7 2015. ISSN 14764687. doi: 10.1038/nature14590.
- [26] M. Burnet. Cancer—a biological approach iii. viruses associated with neoplastic conditions. *British Medical Journal*, 1:841–847, 1957.
- [27] X. Y. Cai, Q. Gao, S. J. Qiu, S. L. Ye, Z. Q. Wu, J. Fan, and Z. Y. Tang. Dendritic cell infiltration and prognosis of human hepatocellular carcinoma. *J Cancer Res Clin Oncol*, 132:293–301, 2006.
- [28] C. Carlberg. Genome-wide (over)view on the actions of vitamin d, 2014. ISSN 1664042X.
- [29] D. Chauss, T. Freiwald, R. McGregor, B. Yan, L. Wang, E. Nova-Lamperti, D. Kumar, Z. Zhang, H. Teague, E. E. West, K. M. Vannella, M. J. Ramos-Benitez, J. Bibby, A. Kelly, A. Malik, A. F. Freeman, D. M. Schwartz, D. Portilla, D. S. Chertow, S. John, P. Lavender, C. Kemper, G. Lombardi, N. N. Mehta, N. Cooper, M. S. Lionakis, A. Laurence, M. Kazemian, and B. Afzali. Autocrine vitamin d signaling switches off pro-inflammatory programs of th1 cells. *Nature Immunology*, 11 2021. ISSN 1529-2908. doi: 10.1038/s41590-021-01080-3. URL <https://www.nature.com/articles/s41590-021-01080-3>.
- [30] D. S. Chen and I. Mellman. Oncology meets immunology: The cancer-immunity cycle, 7 2013. ISSN 10747613.
- [31] E. Y. Chen, C. M. Tan, Y. Kou, Q. Duan, Z. Wang, G. V. Meirelles, N. R. Clark, and A. Ma’ayan. Enrichr: interactive and collaborative html5 gene list enrichment analysis tool, 2013. URL <http://amp.pharm.mssm.edu/Enrichr>.
- [32] J. Chen, C. C. Jiang, L. Jin, and X. D. Zhang. Regulation of pd-11: A novel role of

- pro-survival signalling in cancer. *Annals of Oncology*, 27:409–416, 2016.
- [33] X. Chen, R. J. Miragaia, K. N. Natarajan, and S. A. Teichmann. A rapid and robust method for single cell chromatin accessibility profiling. *Nature Communications*, 9, 12 2018. ISSN 20411723. doi: 10.1038/s41467-018-07771-0.
- [34] Y. Chen, R. A. Zander, X. Wu, D. M. Schauder, M. Y. Kasmani, J. Shen, S. Zheng, R. Burns, E. J. Taparowsky, and W. Cui. Batf regulates progenitor to cytolytic effector cd8+ t cell transition during chronic viral infection. *Nature Immunology*, 22:996–1007, 8 2021. ISSN 15292916. doi: 10.1038/s41590-021-00965-7.
- [35] Z. Chen, Z. Ji, S. F. Ngiow, S. Manne, Z. Cai, A. C. Huang, J. Johnson, R. P. Staupé, B. Bengsch, C. Xu, S. Yu, M. Kurachi, R. S. Herati, L. A. Vella, A. E. Baxter, J. E. Wu, O. Khan, J. C. Beltra, J. R. Giles, E. Stelekati, L. M. McLane, C. W. Lau, X. Yang, S. L. Berger, G. Vahedi, H. Ji, and E. J. Wherry. Tcf-1-centered transcriptional network drives an effector versus exhausted cd8 t cell-fate decision. *Immunity*, 51:840–855.e5, 11 2019. ISSN 10974180. doi: 10.1016/j.immuni.2019.09.013.
- [36] A. R. Cillo, C. H. Kürten, T. Tabib, Z. Qi, S. Onkar, T. Wang, A. Liu, U. Duvvuri, S. Kim, R. J. Soose, S. Oesterreich, W. Chen, R. Lafyatis, T. C. Bruno, R. L. Ferris, and D. A. Vignali. Immune landscape of viral- and carcinogen-driven head and neck cancer. *Immunity*, 52:183–199.e9, 1 2020. ISSN 10974180. doi: 10.1016/j.immuni.2019.11.014.
- [37] D. Clever, R. Roychoudhuri, M. G. Constantinides, M. H. Askenase, M. Sukumar, C. A. Klebanoff, R. L. Eil, H. D. Hickman, Z. Yu, J. H. Pan, D. C. Palmer, A. T. Phan, J. Goulding, L. Gattinoni, A. W. Goldrath, Y. Belkaid, and N. P. Restifo. Oxygen sensing by t cells establishes an immunologically tolerant metastatic niche. *Cell*, 166:1117–1131.e14, 8 2016. ISSN 10974172. doi: 10.1016/j.cell.2016.07.032.
- [38] L. Cong, F. A. Ran, D. Cox, S. Lin, R. Barretto, N. Habib, P. D. Hsu, X. Wu, W. Jiang, L. A. Marraffini, and F. Zhang. Multiplex genome engineering using crispr/cas systems. *Science*, 339:819–823, 2 2013. ISSN 10959203. doi: 10.1126/science.1231143.
- [39] M. R. Corces, A. E. Trevino, E. G. Hamilton, P. G. Greenside, N. A. Sinnott-Armstrong, S. Vesuna, A. T. Satpathy, A. J. Rubin, K. S. Montine, B. Wu, A. Kathiria, S. W. Cho, M. R. Mumbach, A. C. Carter, M. Kasowski, L. A. Orloff, V. I. Risca, A. Kundaje, P. A. Khavari, T. J. Montine, W. J. Greenleaf, and H. Y. Chang. An improved atac-seq protocol reduces background and enables interrogation of frozen tissues. *Nature*

## 6 REFERENCES

---

- Methods*, 14:959–962, 2017. ISSN 15487105. doi: 10.1038/nmeth.4396.
- [40] M. Cornberg, L. L. Kenney, A. T. Chen, S. N. Waggoner, S. K. Kim, H. P. Dienes, R. M. Welsh, and L. K. Selin. Clonal exhaustion as a mechanism to protect against severe immunopathology and death from an overwhelming cd8 t cell response. *Frontiers in Immunology*, 4, 2013. ISSN 16643224. doi: 10.3389/fimmu.2013.00475.
- [41] C. Courtemanche, I. Elson-Schwab, S. T. Mashiyama, N. Kerry, and B. N. Ames. Folate deficiency inhibits the proliferation of primary human cd8 + t lymphocytes in vitro. *The Journal of Immunology*, 173:3186–3192, 9 2004. ISSN 0022-1767. doi: 10.4049/jimmunol.173.5.3186.
- [42] D. Cyranoski. First trial of crispr in people, 2016.
- [43] N. R. Datta, S. G. Ordóñez, U. S. Gaipl, M. M. Paulides, H. Crezee, J. Gellermann, D. Marder, E. Puric, and S. Bodis. Local hyperthermia combined with radiotherapy and/or chemotherapy: Recent advances and promises for the future, 11 2015. ISSN 15321967.
- [44] M. Delacher, C. D. Imbusch, A. Hotz-Wagenblatt, J. P. Mallm, K. Bauer, M. Simon, D. Riegel, A. F. Rendeiro, S. Bittner, L. Sanderink, A. Pant, L. Schmidleithner, K. L. Braband, B. Echtenachter, A. Fischer, V. Giunchiglia, P. Hoffmann, M. Edinger, C. Bock, M. Rehli, B. Brors, C. Schmidl, and M. Feuerer. Precursors for nonlymphoid-tissue treg cells reside in secondary lymphoid organs and are programmed by the transcription factor batf. *Immunity*, 52:295–312.e11, 2 2020. ISSN 10974180. doi: 10.1016/j.immuni.2019.12.002.
- [45] H. Deveau, R. Barrangou, J. E. Garneau, J. Labonté, C. Fremaux, P. Boyaval, D. A. Romero, P. Horvath, and S. Moineau. Phage response to crispr-encoded resistance in streptococcus thermophilus. *Journal of Bacteriology*, 190:1390–1400, 2 2008. ISSN 00219193. doi: 10.1128/JB.01412-07.
- [46] S. Devkota. The road less traveled: Strategies to enhance the frequency of homology-directed repair (hdr) for increased efficiency of crispr/cas-mediated transgenesis, 9 2018. ISSN 1976670X.
- [47] L. DiCroce and K. Helin. Transcriptional regulation by polycomb group proteins, 10 2013. ISSN 15459993.
- [48] H. Dong, S. E. Strome, D. R. Salomao, H. Tamura, F. Hirano, D. B. Flies, P. C. Roche,

- J. Lu, G. Zhu, K. Tamada, V. a Lennon, E. Celis, and L. Chen. Tumor-associated b7-h1 promotes t-cell apoptosis: a potential mechanism of immune evasion. *Nature medicine*, 8:793–800, 2002.
- [49] M. E. Dudley, J. R. Wunderlich, T. E. Shelton, J. Even, and S. A. Rosenberg. Generation of tumor-infiltrating lymphocyte cultures for use in adoptive transfer therapy for melanoma patients, 2003.
- [50] A. Eberharter and P. B. Becker. Histone acetylation: a switch between repressive and permissive chromatin second in review series on chromatin dynamics, 2002.
- [51] M. A. ElTanbouly and R. J. Noelle. Rethinking peripheral t cell tolerance: checkpoints across a t cell's journey, 4 2021. ISSN 14741741.
- [52] C. F. D. EVALUATION and RESEARCH. Nivolumab. *Clinical Review*, 2014.
- [53] R. Fang, S. Preissl, Y. Li, X. Hou, J. Lucero, X. Wang, A. Motamedi, A. K. Shiau, X. Zhou, F. Xie, E. A. Mukamel, K. Zhang, Y. Zhang, M. M. Behrens, J. R. Ecker, and B. Ren. Comprehensive analysis of single cell atac-seq data with snapatac. *Nature Communications*, 12, 12 2021. ISSN 20411723. doi: 10.1038/s41467-021-21583-9.
- [54] D. F. A. Feinberg. Epigenetics at the crossroads of genes and the environment, 2015. URL <https://jamanetwork.com/>.
- [55] R. A. Fernandes, L. Su, Y. Nishiga, J. Ren, A. M. Bhuiyan, N. Cheng, C. J. Kuo, L. K. Picton, S. Ohtsuki, R. G. Majzner, S. P. Rietberg, C. L. Mackall, Q. Yin, L. R. Ali, X. Yang, C. S. Savvides, J. Sage, M. Dougan, and K. C. Garcia. Immune receptor inhibition through enforced phosphatase recruitment. *Nature*, 586:779–784, 10 2020. ISSN 14764687. doi: 10.1038/s41586-020-2851-2.
- [56] A. Finck, S. I. Gill, and C. H. June. Cancer immunotherapy comes of age and looks for maturity, 12 2020. ISSN 20411723.
- [57] C. Flamann, K. Peter, M. Kreutz, and H. Bruns. Regulation of the immune balance during allogeneic hematopoietic stem cell transplantation by vitamin d, 11 2019. ISSN 16643224.
- [58] B. Foglia, E. Novo, F. Protopapa, M. Maggiora, C. Bocca, S. Cannito, and M. Parola. Hypoxia, hypoxia-inducible factors and liver fibrosis, 7 2021. ISSN 20734409.
- [59] U. S. Food and D. Administration. Pembrolizumab. 2013.
- [60] J. Fourcade, Z. Sun, M. Benallaoua, P. Guillaume, I. F. Luescher, C. Sander, J. M.

## 6 REFERENCES

---

- Kirkwood, V. Kuchroo, and H. M. Zarour. Upregulation of tim-3 and pd-1 expression is associated with tumor antigen-specific cd8+ t cell dysfunction in melanoma patients. *Journal of Experimental Medicine*, 207:2175–2186, 9 2010. ISSN 00221007. doi: 10.1084/jem.20100637.
- [61] J. A. Fraietta, C. L. Nobles, M. A. Sammons, S. Lundh, S. A. Carty, T. J. Reich, A. P. Cogdill, J. J. Morrisette, J. E. DeNizio, S. Reddy, Y. Hwang, M. Gohil, I. Kulikovskaya, F. Nazimuddin, M. Gupta, F. Chen, J. K. Everett, K. A. Alexander, E. Lin-Shiao, M. H. Gee, X. Liu, R. M. Young, D. Ambrose, Y. Wang, J. Xu, M. S. Jordan, K. T. Marcucci, B. L. Levine, K. C. Garcia, Y. Zhao, M. Kalos, D. L. Porter, R. M. Kohli, S. F. Lacey, S. L. Berger, F. D. Bushman, C. H. June, and J. J. Melenhorst. Disruption of tet2 promotes the therapeutic efficacy of cd19-targeted t cells. *Nature*, 558:307–312, 6 2018. ISSN 14764687. doi: 10.1038/s41586-018-0178-z.
- [62] F. Franco, A. Jaccard, P. Romero, Y. R. Yu, and P. C. Ho. Metabolic and epigenetic regulation of t-cell exhaustion, 10 2020. ISSN 25225812.
- [63] T. F. Gajewski, H. Schreiber, and Y. X. Fu. Innate and adaptive immune cells in the tumor microenvironment, 2013. ISSN 15292908.
- [64] S. F. Gameiro, F. Ghasemi, J. W. Barrett, J. Koropatnick, A. C. Nichols, J. S. Mymryk, and S. M. Vareki. Treatment-naïve hpv+ head and neck cancers display a t-cell-inflamed phenotype distinct from their hpv- counterparts that has implications for immunotherapy. *Oncotmunology*, 7, 10 2018. ISSN 2162402X. doi: 10.1080/2162402X.2018.1498439.
- [65] J. Gao, L. Z. Shi, H. Zhao, J. Chen, L. Xiong, Q. He, T. Chen, J. Roszik, C. Bernatchez, S. E. Woodman, P. L. Chen, P. Hwu, J. P. Allison, A. Futreal, J. A. Wargo, and P. Sharma. Loss of ifn-?? pathway genes in tumor cells as a mechanism of resistance to anti-ctla-4 therapy. *Cell*, 167:397–404.e9, 2016.
- [66] D. G. Gennert, R. C. Lynn, J. M. Granja, E. W. Weber, M. R. Mumbach, Y. Zhao, Z. Duren, E. Sotillo, W. J. Greenleaf, W. H. Wong, A. T. Satpathy, C. L. Mackall, H. Y. Chang, R. S. Lo, and Y. Shen. Dynamic chromatin regulatory landscape of human car t cell exhaustion. doi: 10.1073/pnas.2104758118/-/DCSupplemental. URL <https://doi.org/10.1073/pnas.2104758118>.
- [67] H. E. Ghoneim, Y. Fan, A. Moustaki, H. A. Abdelsamed, P. Dash, P. Dogra,

- R. Carter, W. Awad, G. Neale, P. G. Thomas, and B. Youngblood. De novo epigenetic programs inhibit pd-1 blockade-mediated t cell rejuvenation. *Cell*, 170: 142–157.e19, 2017. ISSN 10974172. doi: 10.1016/j.cell.2017.06.007. URL <http://dx.doi.org/10.1016/j.cell.2017.06.007>.
- [68] A. S. Gokhale, A. Gangaplara, M. Lopez-Occasio, A. M. Thornton, and E. M. Shevach. Selective deletion of eos (ikzf4) in t-regulatory cells leads to loss of suppressive function and development of systemic autoimmunity. *Journal of Autoimmunity*, 105, 12 2019. ISSN 10959157. doi: 10.1016/j.jaut.2019.06.011.
- [69] H. Gonzalez, C. Hagerling, and Z. Werb. Roles of the immune system in cancer: from tumor initiation to metastatic progression. 2018. doi: 10.1101/gad.314617. URL <http://www.genesdev.org/cgi/doi/10.1101/gad.314617>.
- [70] J. M. Granja, M. R. Corces, S. E. Pierce, S. T. Bagdatli, H. Choudhry, H. Y. Chang, and W. J. Greenleaf. Archr is a scalable software package for integrative single-cell chromatin accessibility analysis. *Nature Genetics*, 53:403–411, 3 2021. ISSN 15461718. doi: 10.1038/s41588-021-00790-6.
- [71] A. Greiner, K. B. Müller, J. Hess, K. Pfeffer, H. K. Müller-Hermelink, and T. Wirth. Up-regulation of bob.1/obf.1 expression in normal germinal center b cells and germinal center-derived lymphomas. *American Journal of Pathology*, 156:501–507, 2000. ISSN 00029440. doi: 10.1016/S0002-9440(10)64754-2.
- [72] P. Gueguen, C. Metoikidou, T. Dupic, M. Lawand, C. Goudot, S. Baulande, S. Lameiras, O. Lantz, N. Girard, A. Seguin-Givelet, M. Lefevre, T. Mora, A. M. Walczak, J. J. Waterfall, and S. Amigorena. Contribution of resident and circulating precursors to tumor-infiltrating cd8 + t cell populations in lung cancer, 2021. URL <https://www.science.org>.
- [73] Z. S. Guo. The 2018 nobel prize in medicine goes to cancer immunotherapy (editorial for bmc cancer), 11 2018. ISSN 14712407.
- [74] J. R. Hamilton, C. A. Tsuchida, D. N. Nguyen, B. R. Shy, E. R. McGarrigle, C. R. S. Espinoza, D. Carr, F. Blaescheke, A. Marson, and J. A. Doudna. Targeted delivery of crispr-cas9 and transgenes enables complex immune cell engineering. *Cell Reports*, 35, 6 2021. ISSN 22111247. doi: 10.1016/j.celrep.2021.109207.
- [75] D. Hanahan. Hallmarks of cancer: New dimensions. *Cancer discovery*, 12:

## 6 REFERENCES

---

- 31–46, 1 2022. ISSN 2159-8290. doi: 10.1158/2159-8290.CD-21-1059. URL <http://www.ncbi.nlm.nih.gov/pubmed/35022204>.
- [76] D. Hanahan and R. A. Weinberg. The hallmarks of cancer. *Cell*, 100:57–70, 2000.
- [77] D. Hanahan and R. A. Weinberg. Hallmarks of cancer: The next generation. *Cell*, 144:646–674, 2011.
- [78] M. Hasmim, M. Z. Noman, J. Lauriol, H. Benlalam, A. Mallavialle, F. Rosselli, F. Mami-Chouaib, C. Alcaide-Loridan, and S. Chouaib. Hypoxia-dependent inhibition of tumor cell susceptibility to ctl-mediated lysis involves nanog induction in target cells. *The Journal of Immunology*, 187:4031–4039, 10 2011. ISSN 0022-1767. doi: 10.4049/jimmunol.1101011.
- [79] S. L. Hayward, C. D. Scharer, E. K. Cartwright, S. Takamura, Z. R. T. Li, J. M. Boss, and J. E. Kohlmeier. Environmental cues regulate epigenetic reprogramming of airway-resident memory cd8+ t cells. *Nature Immunology*, 21:309–320, 3 2020. ISSN 15292916. doi: 10.1038/s41590-019-0584-x.
- [80] S. Heinz, C. Benner, N. Spann, E. Bertolino, Y. C. Lin, P. Laslo, J. X. Cheng, C. Murre, H. Singh, and C. K. Glass. Simple combinations of lineage-determining transcription factors prime cis-regulatory elements required for macrophage and b cell identities. *Molecular Cell*, 38:576–589, 5 2010. ISSN 10972765. doi: 10.1016/j.molcel.2010.05.004.
- [81] S. Heinz, C. E. Romanoski, C. Benner, and C. K. Glass. The selection and function of cell type-specific enhancers. *Nature Reviews Molecular Cell Biology*, 16:144–154, 2015. ISSN 14710080. doi: 10.1038/nrm3949. URL <http://dx.doi.org/10.1038/nrm3949>.
- [82] K. E. H. I. Hellstrom. Cellular and humoral immunity to different types of neoplasms. *Nature*, 1968.
- [83] A. N. Henning, R. Roychoudhuri, and N. P. Restifo. Epigenetic control of cd8+ t cell differentiation. *Nature Reviews Immunology*, 2018. ISSN 1474-1733. doi: 10.1038/nri.2017.146. URL <http://www.nature.com/doifinder/10.1038/nri.2017.146>.
- [84] F. Himmelweit. The collected papers of paul ehrlich. *Pergamon Press*, pages 322–323, 1956.

- [85] D. Huang, J. Chen, L. Yang, Q. Ouyang, J. Li, L. Lao, J. Zhao, J. Liu, Y. Lu, Y. Xing, F. Chen, F. Su, H. Yao, Q. Liu, S. Su, and E. Song. Nkila Incrna promotes tumor immune evasion by sensitizing t cells to activation-induced cell death. *Nature Immunology*, 19:1112–1125, 10 2018. ISSN 15292916. doi: 10.1038/s41590-018-0207-y.
- [86] J. F. Hultquist, J. Hiatt, K. Schumann, M. J. McGregor, T. L. Roth, P. Haas, J. A. Doudna, A. Marson, and N. J. Krogan. Crispr–cas9 genome engineering of primary cd4 + t cells for the interrogation of hiv–host factor interactions. *Nature Protocols*, 14, 1 2019. ISSN 17502799. doi: 10.1038/s41596-018-0069-7.
- [87] P. C. Ikwegbue, P. Masamba, B. E. Oyinloye, and A. P. Kappo. Roles of heat shock proteins in apoptosis, oxidative stress, human inflammatory diseases, and cancer, 3 2018. ISSN 14248247.
- [88] S. J. Im, M. Hashimoto, M. Y. Gerner, J. Lee, H. T. Kissick, M. C. Burger, Q. Shan, J. S. Hale, J. Lee, T. H. Nasti, A. H. Sharpe, G. J. Freeman, R. N. Germain, H. I. Nakaya, H. H. Xue, and R. Ahmed. Defining cd8+ t cells that provide the proliferative burst after pd-1 therapy. *Nature*, 537:417–421, 2016. ISSN 14764687. doi: 10.1038/nature19330.
- [89] C. S. Jansen, N. Prokhnjevskaya, V. A. Master, M. G. Sanda, J. W. Carlisle, M. A. Bilén, M. Cardenas, S. Wilkinson, R. Lake, A. G. Sowalsky, R. M. Valanparambil, W. H. Hudson, D. McGuire, K. Melnick, A. I. Khan, K. Kim, Y. M. Chang, A. Kim, C. P. Filson, M. Alemozaffar, A. O. Osunkoya, P. Mullane, C. Ellis, R. Akondy, S. J. Im, A. O. Kamphorst, A. Reyes, Y. Liu, and H. Kissick. An intra-tumoral niche maintains and differentiates stem-like cd8 t cells. *Nature*, 576:465–470, 12 2019. ISSN 14764687. doi: 10.1038/s41586-019-1836-5.
- [90] E. C. Jenkins, M. Chattopadhyay, and D. Germain. Folding mitochondrial-mediated cytosolic proteostasis into the mitochondrial unfolded protein response, 9 2021. ISSN 2296634X.
- [91] T. I. Jensen, E. Axelgaard, and R. O. Bak. Therapeutic gene editing in haematological disorders with crispr/cas9, 6 2019. ISSN 13652141.
- [92] H. Jiang, R. Lei, S.-W. Ding, and S. Zhu. Skewer: a fast and accurate adapter trimmer for next-generation sequencing paired-end reads, 2014. URL <http://www.biomedcentral.com/1471-2105/15/182>.

## 6 REFERENCES

---

- [93] J. Jin, M. Sabatino, R. Somerville, J. R. Wilson, M. E. Dudley, D. F. Stroncek, and S. A. Rosenberg. Simplified method of the growth of human tumor infiltrating lymphocytes in gas-permeable flasks to numbers needed for patient treatment. *Journal of Immunotherapy*, 35:283–292, 4 2012. ISSN 15249557. doi: 10.1097/CJI.0b013e31824e801f.
- [94] M. Jinek, K. Chylinski, I. Fonfara, M. Hauer, J. A. Doudna, and E. Charpentier. A programmable dual-rna-guided dna endonuclease in adaptive bacterial immunity. URL <https://www.science.org>.
- [95] C. H. June, R. S. O’connor, O. U. Kawalekar, S. Ghassemi, and M. C. Milone. Car t cell immunotherapy for human cancer. URL <http://science.sciencemag.org/>.
- [96] A. Kallies, D. Zehn, and D. T. Utzschneider. Precursor exhausted t cells: key to successful immunotherapy?, 2 2020. ISSN 14741741.
- [97] E. Karkeni, S. O. Morin, B. B. Tayeh, A. Goubard, E. Josselin, R. Castellano, C. Fauriat, G. Guittard, D. Olive, and J. A. Nunès. Vitamin d controls tumor growth and cd8+ t cell infiltration in breast cancer. *Frontiers in Immunology*, 10, 2019. ISSN 16643224. doi: 10.3389/fimmu.2019.01307.
- [98] O. Khan, J. R. Giles, S. McDonald, S. Manne, S. F. Ngiew, K. P. Patel, M. T. Werner, A. C. Huang, K. A. Alexander, J. E. Wu, J. Attanasio, P. Yan, S. M. George, B. Bengsch, R. P. Staupé, G. Donahue, W. Xu, R. K. Amaravadi, X. Xu, G. C. Karakousis, T. C. Mitchell, L. M. Schuchter, J. Kaye, S. L. Berger, and E. J. Wherry. Tox transcriptionally and epigenetically programs cd8+ t cell exhaustion. *Nature*, 571:211–218, 7 2019. ISSN 14764687. doi: 10.1038/s41586-019-1325-x.
- [99] N. Khandelwal, M. Breinig, T. Speck, T. Michels, C. Kreutzer, A. Sorrentino, A. K. Sharma, L. Umansky, H. Conrad, I. Poschke, R. Offringa, R. König, H. Bernhard, A. Machlenkin, M. Boutros, and P. Beckhove. A highthroughput rna i screen for detection of immunecheckpoint molecules that mediate tumor resistance to cytotoxic t lymphocytes. *EMBO Molecular Medicine*, 7:450–463, 4 2015. ISSN 1757-4676. doi: 10.15252/emmm.201404414.
- [100] M. Kongsbak, T. B. Levring, C. Geisler, and M. R. von Essen. The vitamin d receptor and t cell function, 2013. ISSN 16643224.
- [101] R. D. Kornberg. Chromatin structure: A repeating unit of histones and dna. *Science*,

- 1974.
- [102] I. Korsunsky, N. Millard, J. Fan, K. Slowikowski, F. Zhang, K. Wei, Y. Baglaenko, M. Brenner, P. ru Loh, and S. Raychaudhuri. Fast, sensitive and accurate integration of single-cell data with harmony. *Nature Methods*, 16:1289–1296, 12 2019. ISSN 15487105. doi: 10.1038/s41592-019-0619-0.
- [103] S. Krishna, F. J. Lowery, A. R. Copeland, E. Bahadiroglu, R. Mukherjee, L. Jia, J. T. Anibal, A. Sachs, S. O. Adebola, D. Gurusamy, Z. Yu, V. Hill, J. J. Gartner, Y. F. Li, M. Parkhurst, B. Paria, P. Kvistborg, M. C. Kelly, S. L. Goff, G. Altan-Bonnet, P. F. Robbins, and S. A. Rosenberg. Stem-like cd8 t cells mediate response of adoptive cell immunotherapy against human cancer. URL <https://www.science.org>.
- [104] B. Langmead and S. L. Salzberg. Fast gapped-read alignment with bowtie 2. *Nature Methods*, 9:357–359, 4 2012. ISSN 15487091. doi: 10.1038/nmeth.1923.
- [105] Y. Larch, J. W. Lapointe, and R. D. Kornberg. Nucleosomes inhibit the initiation of transcription but allow chain elongation with the displacement of histones, 1987.
- [106] C. A. Lareau, L. S. Ludwig, C. Muus, S. H. Gohil, T. Zhao, Z. Chiang, K. Pelka, J. M. Verboon, W. Luo, E. Christian, D. Rosebrock, G. Getz, G. M. Boland, F. Chen, J. D. Buenrostro, N. Hacohen, C. J. Wu, M. J. Aryee, A. Regev, and V. G. Sankaran. Massively parallel single-cell mitochondrial dna genotyping and chromatin profiling. *Nature Biotechnology*, 39:451–461, 4 2021. ISSN 15461696. doi: 10.1038/s41587-020-0645-6.
- [107] R. C. Larson and M. V. Maus. Recent advances and discoveries in the mechanisms and functions of car t cells, 3 2021. ISSN 14741768.
- [108] Y. Lavin, D. Winter, R. Blecher-Gonen, E. David, H. Keren-Shaul, M. Merad, S. Jung, and I. Amit. Tissue-resident macrophage enhancer landscapes are shaped by the local microenvironment. *Cell*, 159:1312–1326, 12 2014. ISSN 10974172. doi: 10.1016/j.cell.2014.11.018.
- [109] C. Li, H. Mei, and Y. Hu. Applications and explorations of crispr/cas9 in car t-cell therapy. *Briefings in Functional Genomics*, 19:175–182, 5 2020. ISSN 20412657. doi: 10.1093/bfgp/elz042.
- [110] H. Li, A. M. van der Leun, I. Yofe, Y. Lubling, D. Gelbard-Solodkin, A. C. van Akkooi, M. van den Braber, E. A. Rozeman, J. B. Haanen, C. U. Blank, H. M. Horlings,

## 6 REFERENCES

---

- E. David, Y. Baran, A. Bercovich, A. Lifshitz, T. N. Schumacher, A. Tanay, and I. Amit. Dysfunctional cd8 t cells form a proliferative, dynamically regulated compartment within human melanoma. *Cell*, 176:775–789.e18, 2 2019. ISSN 10974172. doi: 10.1016/j.cell.2018.11.043.
- [111] B. Liu, X. Hu, K. Feng, R. Gao, Z. Xue, S. Zhang, Y. Zhang, E. Corse, Y. Hu, W. Han, and Z. Zhang. Temporal single-cell tracing reveals clonal revival and expansion of precursor exhausted t cells during anti-pd-1 therapy in lung cancer. *Nature Cancer*, 3: 108–121, 1 2022. ISSN 26621347. doi: 10.1038/s43018-021-00292-8.
- [112] L. Liu, C. Liu, L. Wu, Y. Yuan, M. Cheng, L. Xu, G. Dong, R. Li, Y. Liu, X. Wei, J. Xu, X. Chen, H. Lu, D. Chen, Q. Wang, Q. Zhou, X. Lin, G. Li, S. Liu, Q. Wang, H. Wang, J. L. Fink, Z. Gao, Y. Hou, S. Zhu, H. Yang, Y. Ye, F. Chen, C. Herrmann, R. Eils, Z. Shang, X. Xu, H. D. Science, V. Paleontology, and M. Sciences. Deconvolution of single-cell multi-omics layers reveals regulatory heterogeneity. *bioRxiv Genomics*, 2018. doi: 10.1101/316208. URL <http://biorxiv.org/cgi/content/short/316208v1>.
- [113] X. Liu, Y. Wang, H. Lu, J. Li, X. Yan, M. Xiao, J. Hao, A. Alekseev, H. Khong, T. Chen, R. Huang, J. Wu, Q. Zhao, Q. Wu, S. Xu, X. Wang, W. Jin, S. Yu, Y. Wang, L. Wei, A. Wang, B. Zhong, L. Ni, X. Liu, R. Nurieva, L. Ye, Q. Tian, X. W. Bian, and C. Dong. Genome-wide analysis identifies nr4a1 as a key mediator of t cell dysfunction. *Nature*, 567:525–529, 3 2019. ISSN 14764687. doi: 10.1038/s41586-019-0979-8.
- [114] X. P. Liu, K. R. Koehler, A. M. Mikosz, E. Hashino, J. R. Holt, and R. E. Dejonge. Manufacture of car-t cells in the body, 2017.
- [115] Y. Liu, N. Zhou, L. Zhou, J. Wang, Y. Zhou, T. Zhang, Y. Fang, J. Deng, Y. Gao, X. Liang, J. Lv, Z. Wang, J. Xie, Y. Xue, H. Zhang, J. Ma, K. Tang, Y. Fang, F. Cheng, C. Zhang, B. Dong, Y. Zhao, P. Yuan, Q. Gao, H. Zhang, F. X.-F. Qin, and B. Huang. Il-2 regulates tumor-reactive cd8+ t cell exhaustion by activating the aryl hydrocarbon receptor. *Nature Immunology*, 22:358–369, 3 2021. ISSN 15292916. doi: 10.1038/s41590-020-00850-9.
- [116] A. H. Long, W. M. Haso, J. F. Shern, K. M. Wanhainen, M. Murgai, M. Ingaramo, J. P. Smith, A. J. Walker, M. E. Kohler, V. R. Venkateshwara, R. N. Kaplan, G. H. Patterson, T. J. Fry, R. J. Orentas, and C. L. Mackall. 4-1bb costimulation ameliorates t cell

- exhaustion induced by tonic signaling of chimeric antigen receptors. *Nature Medicine*, 21:581–590, 6 2015. ISSN 1546170X. doi: 10.1038/nm.3838.
- [117] A. Loureiro and G. J. D. Silva. Crispr-cas: Converting a bacterial defence mechanism into a state-of-the-art genetic manipulation tool. *Antibiotics*, 8, 3 2019. ISSN 20796382. doi: 10.3390/antibiotics8010018.
- [118] R. C. Lynn, E. W. Weber, E. Sotillo, D. Gennert, P. Xu, Z. Good, H. Anbunathan, J. Lattin, R. Jones, V. Tieu, S. Nagaraja, J. Granja, C. F. de Bourcy, R. Majzner, A. T. Satpathy, S. R. Quake, M. Monje, H. Y. Chang, and C. L. Mackall. c-jun overexpression in car t cells induces exhaustion resistance. *Nature*, 576:293–300, 12 2019. ISSN 14764687. doi: 10.1038/s41586-019-1805-z.
- [119] J. Ma, B. Zheng, S. Goswami, L. Meng, D. Zhang, C. Cao, T. Li, F. Zhu, L. Ma, Z. Zhang, S. Zhang, M. Duan, Q. Chen, Q. Gao, and X. Zhang. Pd1hi cd8+ t cells correlate with exhausted signature and poor clinical outcome in hepatocellular carcinoma. *Journal for ImmunoTherapy of Cancer*, 7, 11 2019. ISSN 20511426. doi: 10.1186/s40425-019-0814-7.
- [120] A. Machlenkin, R. Uzana, S. Frankenburg, G. Eisenberg, L. Eisenbach, J. Pitcovski, R. Gorodetsky, A. Nissan, T. Peretz, and M. Lotem. Capture of tumor cell membranes by trogocytosis facilitates detection and isolation of tumor-specific functional ctls. *Cancer Research*, 68:2006–2013, 3 2008. ISSN 00085472. doi: 10.1158/0008-5472.CAN-07-3119.
- [121] L. K. MacKay, A. Rahimpour, J. Z. Ma, N. Collins, A. T. Stock, M. L. Hafon, J. Vega-Ramos, P. Lauzurica, S. N. Mueller, T. Stefanovic, D. C. Tschärke, W. R. Heath, M. Inouye, F. R. Carbone, and T. Gebhardt. The developmental pathway for cd103+ cd8+ tissue-resident memory t cells of skin. *Nature Immunology*, 14:1294–1301, 12 2013. ISSN 15292908. doi: 10.1038/ni.2744.
- [122] K. L. MacQuarrie, A. P. Fong, R. H. Morse, and S. J. Tapscott. Genome-wide transcription factor binding: Beyond direct target regulation, 4 2011. ISSN 01689525.
- [123] Z. Mao, M. Bozzella, A. Seluanov, and V. Gorbunova. Comparison of nonhomologous end joining and homologous recombination in human cells. *DNA Repair*, 7:1765–1771, 10 2008. ISSN 15687864. doi: 10.1016/j.dnarep.2008.06.018.
- [124] B. S. Marro, J. Zak, R. B. Zavareh, J. R. Teijaro, L. L. Lairson, and M. B. Oldstone.

## 6 REFERENCES

---

- Discovery of small molecules for the reversal of t cell exhaustion. *Cell Reports*, 29: 3293–3302.e3, 12 2019. ISSN 22111247. doi: 10.1016/j.celrep.2019.10.119.
- [125] E. McGowan, Q. Lin, G. Ma, H. Yin, S. Chen, and Y. Lin. Pd-1 disrupted car-t cells in the treatment of solid tumors: Promises and challenges, 1 2020. ISSN 19506007.
- [126] E. N. McNamee, D. K. Johnson, D. Homann, and E. T. Clambey. Hypoxia and hypoxia-inducible factors as regulators of t cell development, differentiation, and function. *Immunologic Research*, 55:58–70, 3 2013. ISSN 0257277X. doi: 10.1007/s12026-012-8349-8.
- [127] J. J. Melenhorst, G. M. Chen, M. Wang, D. L. Porter, C. Chen, M. A. Collins, P. Gao, S. Bandyopadhyay, H. Sun, Z. Zhao, S. Lundh, I. Pruteanu-Malinici, C. L. Nobles, S. Maji, N. V. Frey, S. I. Gill, L. Tian, I. Kulikovskaya, M. Gupta, D. E. Ambrose, M. M. Davis, J. A. Fraietta, J. L. Brogdon, R. M. Young, A. Chew, B. L. Levine, D. L. Siegel, C. Alanio, E. J. Wherry, F. D. Bushman, S. F. Lacey, K. Tan, and C. H. June. Decade-long leukaemia remissions with persistence of cd4+ car t cells. *Nature*, 2 2022. ISSN 0028-0836. doi: 10.1038/s41586-021-04390-6. URL <https://www.nature.com/articles/s41586-021-04390-6>.
- [128] G. Michlits, J. Jude, M. Hinterndorfer, M. de Almeida, G. Vainorius, M. Hubmann, T. Neumann, A. Schleiffer, T. R. Burkard, M. Fellner, M. Gijsbertsen, A. Traunbauer, J. Zuber, and U. Elling. Multilayered vbc score predicts sgrnas that efficiently generate loss-of-function alleles. *Nature Methods*, 17:708–716, 7 2020. ISSN 15487105. doi: 10.1038/s41592-020-0850-8.
- [129] A. N. Miliotou and L. C. Papadopoulou. Car t-cell therapy: A new era in cancer immunotherapy. *Current Pharmaceutical Biotechnology*, 19:5–18, 5 2018. ISSN 13892010. doi: 10.2174/1389201019666180418095526.
- [130] B. C. Miller, D. R. Sen, R. A. Aboody, K. Bi, Y. V. Virkud, M. W. LaFleur, K. B. Yates, A. Lako, K. Felt, G. S. Naik, M. Manos, E. Gjini, J. R. Kuchroo, J. J. Ishizuka, J. L. Collier, G. K. Griffin, S. Maleri, D. E. Comstock, S. A. Weiss, F. D. Brown, A. Panda, M. D. Zimmer, R. T. Manguso, F. S. Hodi, S. J. Rodig, A. H. Sharpe, and W. N. Haining. Subsets of exhausted cd8+ t cells differentially mediate tumor control and respond to checkpoint blockade. *Nature Immunology*, 20:326–336, 3 2019. ISSN 15292916. doi: 10.1038/s41590-019-0312-6.

- [131] G. P. Mognol, R. Spreafico, V. Wong, J. P. Scott-Browne, S. Togher, A. Hoffmann, P. G. Hogan, A. Rao, and S. Trifari. Exhaustion-associated regulatory regions in cd8<sup>hi</sup> tumor-infiltrating t cells. *Proceedings of the National Academy of Sciences*, 114:E2776–E2785, 2017. ISSN 0027-8424. doi: 10.1073/pnas.1620498114. URL <http://www.pnas.org/lookup/doi/10.1073/pnas.1620498114>.
- [132] F. J. Mojica, C. Díez-Villaseñor, J. García-Martínez, and E. Soria. Intervening sequences of regularly spaced prokaryotic repeats derive from foreign genetic elements. *Journal of Molecular Evolution*, 60:174–182, 2005. ISSN 00222844. doi: 10.1007/s00239-004-0046-3.
- [133] M. R. Mueller and A. Rao. Nfat, immunity and cancer: A transcription factor comes of age, 9 2010. ISSN 14741733.
- [134] K. Murphy and C. Weaver. *Janeway ' S 9 Th Edition*. 2016.
- [135] C. A. Musselman, M. E. Lalonde, J. Côté, and T. G. Kutateladze. Perceiving the epigenetic landscape through histone readers, 12 2012. ISSN 15459993.
- [136] P. Nenci and K. J. Harrington. The biology of cancer, 2 2020. ISSN 13654357.
- [137] H. Nishimura, Y. Agata, A. Kawasaki, M. Sato, S. Imamura, N. Minato, H. Yagita, T. Nakano, and T. Honjo. Developmentally regulated expression of the pd-1 protein on the surface of double-negative (cd4-cd8-) thymocytes. *International Immunology*, 8:773–780, 1996.
- [138] X. Nogues, D. Ovejero, M. Pineda-Moncusí, R. Bouillon, D. Arenas, J. Pascual, A. Ribes, R. Guerri-Fernandez, J. Villar-Garcia, A. Rial, C. Gimenez-Argente, M. L. Cos, J. Rodriguez-Morera, I. Campodarve, J. M. Quesada-Gomez, and N. Garcia-Giralt. Calcifediol treatment and covid-19-related outcomes. *Journal of Clinical Endocrinology and Metabolism*, 106:E4017–E4027, 10 2021. ISSN 19457197. doi: 10.1210/clinem/dgab405.
- [139] R. Noy and J. W. Pollard. Tumor-associated macrophages: From mechanisms to therapy, 7 2014. ISSN 10974180.
- [140] T. Okazaki and T. Honjo. Pd-1 and pd-1 ligands: From discovery to clinical application. *International Immunology*, 19:813–824, 2007.
- [141] T. Okazaki and J. Wang. Pd-1/pd-l pathway and autoimmunity. *Autoimmunity*, 38: 353–357, 2005.

## 6 REFERENCES

---

- [142] T. Okazaki, S. Chikuma, Y. Iwai, S. Fagarasan, and T. Honjo. A rheostat for immune responses: the unique properties of pd-1 and their advantages for clinical application. *Nature Immunology*, 14:1212–1218, 2013.
- [143] D. Osullivan, M. A. Stanczak, M. Villa, F. M. Uhl, M. Corrado, R. I. K. Geltink, D. E. Sanin, P. Apostolova, N. Rana, J. Edwards-Hicks, K. M. Grzes, A. M. Kabat, R. L. Kyle, M. Fabri, J. D. Curtis, M. D. Buck, A. E. Patterson, A. Regina, C. S. Field, F. Baixauli, D. J. Puleston, E. J. Pearce, R. Zeiser, and E. L. Pearce. Fever supports cd8 + effector t cell responses by promoting mitochondrial translation. doi: 10.1073/pnas.2023752118/-/DCSupplemental. URL <https://www.pnas.org/lookup/suppl/>.
- [144] F. Pan, H. Yu, E. V. Dang, J. Barbi, X. Pan, J. F. Grosso, D. Jinasena, S. M. Sharma, E. M. McCadden, D. Getnet, C. G. Drake, J. O. Liu, M. C. Ostrowski, and D. M. Pardoll. Eos mediates foxp3-dependent gene silencing in cd4+ regulatory t cells. *Science*, 325: 1142–1146, 2009. ISSN 00368075. doi: 10.1126/science.1176077.
- [145] D. M. Pardoll. The blockade of immune checkpoints in cancer immunotherapy. *Nature Reviews Cancer*, 12:252–264, 2012.
- [146] K. E. Pauken, M. A. Sammons, P. M. Odorizzi, S. Manne, J. Godec, O. Khan, A. M. Drake, Z. Chen, D. R. Sen, M. Kurachi, R. A. Barnitz, C. Bartman, B. Bengsch, A. C. Huang, J. M. Schenkel, G. Vahedi, W. N. Haining, S. L. Berger, and E. J. Wherry. Epigenetic stability of exhausted t cells limits durability of reinvigoration by pd-1 blockade. *Science*, 354:1160–1165, 2016. ISSN 10959203. doi: 10.1126/science.aaf2807.
- [147] K. Pelka, M. Hofree, J. H. Chen, S. Sarkizova, J. D. Pirl, V. Jorgji, A. Bejnood, D. Dionne, W. H. Ge, K. H. Xu, S. X. Chao, D. R. Zollinger, D. J. Lieb, J. W. Reeves, C. A. Fuhrman, M. L. Hoang, T. Delorey, L. T. Nguyen, J. Waldman, M. Klapholz, I. Wakiro, O. Cohen, J. Albers, C. S. Smillie, M. S. Cuoco, J. Wu, M. ju Su, J. Yeung, B. Vijaykumar, A. M. Magnuson, N. Asinovski, T. Moll, M. N. Goder-Reiser, A. S. Applebaum, L. K. Brais, L. K. DelloStritto, S. L. Denning, S. T. Phillips, E. K. Hill, J. K. Meehan, D. T. Frederick, T. Sharova, A. Kanodia, E. Z. Todres, J. Jané-Valbuena, M. Biton, B. Izar, C. D. Lambden, T. E. Clancy, R. Bleday, N. Melnitchouk, J. Irani, H. Kunitake, D. L. Berger, A. Srivastava, J. L. Hornick, S. Ogino, A. Rotem, S. Vigneau, B. E. Johnson, R. B. Corcoran, A. H. Sharpe, V. K. Kuchroo, K. Ng, M. Gi-

- annakis, L. T. Nieman, G. M. Boland, A. J. Aguirre, A. C. Anderson, O. Rozenblatt-Rosen, A. Regev, and N. Hacohen. Spatially organized multicellular immune hubs in human colorectal cancer. *Cell*, 184:4734–4752.e20, 9 2021. ISSN 10974172. doi: 10.1016/j.cell.2021.08.003.
- [148] L. A. Pennacchio, W. Bickmore, A. Dean, M. A. Nobrega, and G. Bejerano. Enhancers: Five essential questions, 4 2013. ISSN 14710056.
- [149] V. Petrova, M. Annicchiarico-Petruzzelli, G. Melino, and I. Amelio. The hypoxic tumour microenvironment, 1 2018. ISSN 21579024.
- [150] M. Philip and A. Schietinger. Cd8+ t cell differentiation and dysfunction in cancer. *Nature Reviews Immunology*, 7 2021. ISSN 1474-1733. doi: 10.1038/s41577-021-00574-3. URL <http://www.nature.com/articles/s41577-021-00574-3>.
- [151] M. Philip, L. Fairchild, L. Sun, E. L. Horste, S. Camara, M. Shakiba, A. C. Scott, A. Viale, P. Lauer, T. Merghoub, M. D. Hellmann, J. D. Wolchok, C. S. Leslie, and A. Schietinger. Chromatin states define tumour-specific t cell dysfunction and reprogramming. *Nature*, 545:452–456, 2017. ISSN 14764687. doi: 10.1038/nature22367. URL <http://dx.doi.org/10.1038/nature22367>.
- [152] S. Picelli, Åsa K. Björklund, B. Reinius, S. Sagasser, G. Winberg, and R. Sandberg. Tn5 transposase and tagmentation procedures for massively scaled sequencing projects. *Genome Research*, 24:2033–2040, 12 2014. ISSN 15495469. doi: 10.1101/gr.177881.114.
- [153] N. Plongthongkum, D. H. Diep, and K. Zhang. Advances in the profiling of dna modifications: Cytosine methylation and beyond, 10 2014. ISSN 14710064.
- [154] A. Poleshko, C. L. Smith, S. C. Nguyen, P. Sivaramakrishnan, K. G. Wong, J. I. Murray, M. Lakadamyali, E. F. Joyce, R. Jain, and J. A. Epstein. H3k9me2 orchestrates inheritance of spatial positioning of peripheral heterochromatin through mitosis. doi: 10.7554/eLife.49278.001. URL <https://doi.org/10.7554/eLife.49278.001>.
- [155] M. Poorebrahim, J. Melief, Y. P. de Coaña, S. L. Wickström, A. Cid-Arregui, and R. Kiessling. Counteracting car t cell dysfunction, 1 2021. ISSN 14765594.
- [156] A. D. Posey, O. U. Kawalekar, and C. H. June. Measurement of intracellular ions by flow cytometry. *Current Protocols in Cytometry*, 2015:9.8.1–9.8.21, 2015. ISSN 19349300. doi: 10.1002/0471142956.cy0908s72.

## 6 REFERENCES

---

- [157] C. Pourcel, G. Salvignol, and G. Vergnaud. Crispr elements in *Yersinia pestis* acquire new repeats by preferential uptake of bacteriophage DNA, and provide additional tools for evolutionary studies. *Microbiology*, 151:653–663, 3 2005. ISSN 13500872. doi: 10.1099/mic.0.27437-0.
- [158] M. D. Powell, K. A. Read, B. K. Sreekumar, and K. J. Oestreich. Ikaros zinc finger transcription factors: Regulators of cytokine signaling pathways and CD4<sup>+</sup> T helper cell differentiation, 2019. ISSN 16643224.
- [159] Y. Pritykin, J. van der Veecken, A. R. Pine, Y. Zhong, M. Sahin, L. Mazutis, D. Pe'er, A. Y. Rudensky, and C. S. Leslie. A unified atlas of CD8 T cell dysfunctional states in cancer and infection. *Molecular Cell*, 81:2477–2493.e10, 6 2021. ISSN 10974164. doi: 10.1016/j.molcel.2021.03.045.
- [160] A. R. Quinlan and I. M. Hall. BEDTools: A flexible suite of utilities for comparing genomic features. *Bioinformatics*, 26:841–842, 1 2010. ISSN 13674803. doi: 10.1093/bioinformatics/btq033.
- [161] M. Ramos-Casals, J. R. Brahmer, M. K. Callahan, A. Flores-Chávez, N. Keegan, M. A. Khamashta, O. Lambotte, X. Mariette, A. Prat, and M. E. Suárez-Almazor. Immune-related adverse events of checkpoint inhibitors, 12 2020. ISSN 2056676X.
- [162] E. Razeghian, M. K. Nasution, H. S. Rahman, Z. R. Gardanova, W. K. Abdelbasset, S. Aravindhan, D. O. Bokov, W. Suksatan, P. Nakhaei, S. Shariatzadeh, F. Marofi, M. Yazdanifar, S. Shamlou, R. Motavalli, and F. M. Khiavi. A deep insight into CRISPR/Cas9 application in CAR-T cell-based tumor immunotherapies, 12 2021. ISSN 17576512.
- [163] M. A. Reid, Z. Dai, and J. W. Locasale. The impact of cellular metabolism on chromatin dynamics and epigenetics, 11 2017. ISSN 14764679.
- [164] J. Ren, X. Liu, C. Fang, S. Jiang, C. H. June, and Y. Zhao. Multiplex genome editing to generate universal CAR T cells resistant to PD1 inhibition. *Clinical Cancer Research*, 23:2255–2266, 5 2017. ISSN 15573265. doi: 10.1158/1078-0432.CCR-16-1300.
- [165] K. Renner, K. Singer, G. E. Koehl, E. K. Geissler, K. Peter, P. J. Siska, and M. Kreutz. Metabolic hallmarks of tumor and immune cells in the tumor microenvironment. *Frontiers in Immunology*, 8:1–11, 2017. ISSN 16643224. doi: 10.3389/fimmu.2017.00248.
- [166] K. Renner, C. Bruss, A. Schnell, G. Koehl, H. M. Becker, M. Fante, A. N. Menevse,

- N. Kauer, R. Blazquez, L. Hacker, S. M. Decking, T. Bohn, S. Faerber, K. Evert, L. Aigle, S. Amslinger, M. Landa, O. Krijgsman, E. A. Rozeman, C. Brummer, P. J. Siska, K. Singer, S. Pektor, M. Miederer, K. Peter, E. Gottfried, W. Herr, I. Marchiq, J. Pouyssegur, W. R. Roush, S. F. Ong, S. Warren, T. Pukrop, P. Beckhove, S. A. Lang, T. Bopp, C. U. Blank, J. L. Cleveland, P. J. Oefner, K. Dettmer, M. Selby, and M. Kreutz. Restricting glycolysis preserves t cell effector functions and augments checkpoint therapy. *Cell Reports*, 29:135–150.e9, 10 2019. ISSN 22111247. doi: 10.1016/j.celrep.2019.08.068.
- [167] W. S. Reznikoff. Transposon tn5, 2008. ISSN 00664197.
- [168] A. Ribas. Antitumor activity in melanoma and anti-self responses in a phase i trial with the anti-cytotoxic t lymphocyte-associated antigen 4 monoclonal antibody cp-675,206. *Journal of Clinical Oncology*, 23:8968–8977, 2005.
- [169] J. L. Riley. Pd-1 signaling in primary t cells. 76:211–220, 2012.
- [170] D. R. Rodríguez-Rodríguez, R. Ramírez-Solís, M. A. Garza-Elizondo, M. D. L. Garza-Rodríguez, and H. A. Barrera-Saldaña. Genome editing: A perspective on the application of crispr/cas9 to study human diseases (review), 4 2019. ISSN 1791244X.
- [171] S. A. Rosenberg. Cancer immunotherapy. *The New England journal of medicine*, 10: 909–915, 2008.
- [172] M. SadeFeldman, K. Yizhak, S. L. Bjorgaard, J. P. Ray, C. G. de Boer, R. W. Jenkins, D. J. Lieb, J. H. Chen, D. T. Frederick, M. Barzily-Rokni, S. S. Freeman, A. Reuben, P. J. Hoover, A. C. Villani, E. Ivanova, A. Portell, P. H. Lizotte, A. R. Aref, J. P. Eliane, M. R. Hammond, H. Vitzthum, S. M. Blackmon, B. Li, V. Gopalakrishnan, S. M. Reddy, Z. A. Cooper, C. P. Paweletz, D. A. Barbie, A. Stemmer-Rachamimov, K. T. Flaherty, J. A. Wargo, G. M. Boland, R. J. Sullivan, G. Getz, and N. Hacohen. Defining t cell states associated with response to checkpoint immunotherapy in melanoma. *Cell*, 175:998–1013.e20, 11 2018. ISSN 10974172. doi: 10.1016/j.cell.2018.10.038.
- [173] A. T. Satpathy, J. M. Granja, K. E. Yost, Y. Qi, F. Meschi, G. P. McDermott, B. N. Olsen, M. R. Mumbach, S. E. Pierce, M. R. Corces, P. Shah, J. C. Bell, D. Jhuttly, C. M. Nemeč, J. Wang, L. Wang, Y. Yin, P. G. Giresi, A. L. S. Chang, G. X. Zheng, W. J. Greenleaf, and H. Y. Chang. Massively parallel single-cell chromatin landscapes of human immune cell development and intratumoral t cell exhaustion. *Nature Biotech-*

## 6 REFERENCES

---

- nology*, 37:925–936, 8 2019. ISSN 15461696. doi: 10.1038/s41587-019-0206-z.
- [174] P. A. Savage, S. Malchow, and D. S. Leventhal. Basic principles of tumor-associated regulatory t cell biology, 1 2013. ISSN 14714906.
- [175] N. E. Scharping, D. B. Rivadeneira, A. V. Menk, P. D. Vignali, B. R. Ford, N. L. Rittenhouse, R. Peralta, Y. Wang, Y. Wang, K. DePeaux, A. C. Poholek, and G. M. Delgoffe. Mitochondrial stress induced by continuous stimulation under hypoxia rapidly drives t cell exhaustion. *Nature Immunology*, 22:205–215, 2 2021. ISSN 15292916. doi: 10.1038/s41590-020-00834-9.
- [176] A. N. Schep, B. Wu, J. D. Buenrostro, and W. J. Greenleaf. Chromvar: Inferring transcription-factor-associated accessibility from single-cell epigenomic data. *Nature Methods*, 14:975–978, 10 2017. ISSN 15487105. doi: 10.1038/nmeth.4401.
- [177] A. Schietinger, M. Philip, V. E. Krisnawan, E. Y. Chiu, J. J. Delrow, R. S. Basom, P. Lauer, D. G. Brockstedt, S. E. Knoblaugh, G. J. Hämmerling, T. D. Schell, N. Garbi, and P. D. Greenberg. Tumor-specific t cell dysfunction is a dynamic antigen-driven differentiation program initiated early during tumorigenesis. *Immunity*, 45:389–401, 2016. ISSN 10974180. doi: 10.1016/j.immuni.2016.07.011.
- [178] C. Schmidl, M. Delacher, J. Huehn, and M. Feuerer. Epigenetic mechanisms regulating t-cell responses, 9 2018. ISSN 10976825.
- [179] A. J. Schoenfeld and M. D. Hellmann. Acquired resistance to immune checkpoint inhibitors, 4 2020. ISSN 18783686.
- [180] K. Schumann, S. Lin, E. Boyer, D. R. Simeonov, M. Subramaniam, R. E. Gate, G. E. Haliburton, C. J. Ye, J. A. Bluestone, J. A. Doudna, and A. Marson. Generation of knock-in primary human t cells using cas9 ribonucleoproteins. *Proceedings of the National Academy of Sciences of the United States of America*, 112:10437–10442, 8 2015. ISSN 10916490. doi: 10.1073/pnas.1512503112.
- [181] A. C. Scott, F. Dündar, P. Zumbo, S. S. Chandran, C. A. Klebanoff, M. Shakiba, P. Trivedi, L. Menocal, H. Appleby, S. Camara, D. Zamarin, T. Walther, A. Snyder, M. R. Femia, E. A. Comen, H. Y. Wen, M. D. Hellmann, N. Anandasabapathy, Y. Liu, N. K. Altorki, P. Lauer, O. Levy, M. S. Glickman, J. Kaye, D. Betel, M. Philip, and A. Schietinger. Tox is a critical regulator of tumour-specific t cell differentiation. *Nature*, 571: 270–274, 7 2019. ISSN 14764687. doi: 10.1038/s41586-019-1324-y.

- [182] A. Seki and S. Rutz. Optimized rnp transfection for highly efficient cri spr/cas9-mediated gene knockout in primary t cells. *Journal of Experimental Medicine*, 215: 985–997, 3 2018. ISSN 15409538. doi: 10.1084/jem.20171626.
- [183] D. R. Sen, J. Kaminski, R. A. Barnitz, M. Kurachi, U. Gerdemann, K. B. Yates, H. W. Tsao, J. Godec, M. W. LaFleur, F. D. Brown, P. Tonnerre, R. T. Chung, D. C. Tully, T. M. Allen, N. Frahm, G. M. Lauer, E. J. Wherry, N. Yosef, and W. N. Haining. The epigenetic landscape of t cell exhaustion. *Science*, 354:1165–1169, 12 2016. ISSN 10959203. doi: 10.1126/science.aae0491.
- [184] H. Seo, J. Chen, E. González-Avalos, D. Samaniego-Castruita, A. Das, Y. H. Wang, I. F. López-Moyado, R. O. Georges, W. Zhang, A. Onodera, C. J. Wu, L. F. Lu, P. G. Hogan, A. Bhandoola, and A. Rao. Tox and tox2 transcription factors cooperate with nr4a transcription factors to impose cd8+ t cell exhaustion. *Proceedings of the National Academy of Sciences of the United States of America*, 116:12410–12415, 6 2019. ISSN 10916490. doi: 10.1073/pnas.1905675116.
- [185] V. Shankaran, H. Ikeda, a T Bruce, J. M. White, P. E. Swanson, L. J. Old, and R. D. Schreiber. Ifngamma and lymphocytes prevent primary tumour development and shape tumour immunogenicity. *Nature*, 410:1107–1111, 2001.
- [186] C. Shen, D. Nettleton, M. Jiang, S. K. Kim, and J. A. Powell-Coffman. Roles of the hif-1 hypoxia-inducible factor during hypoxia response in caenorhabditis elegans. *Journal of Biological Chemistry*, 280:20580–20588, 5 2005. ISSN 00219258. doi: 10.1074/jbc.M501894200.
- [187] J. J. Sherba, S. Hogquist, H. Lin, J. W. Shan, D. I. Shreiber, and J. D. Zahn. The effects of electroporation buffer composition on cell viability and electro-transfection efficiency. *Scientific Reports*, 10, 12 2020. ISSN 20452322. doi: 10.1038/s41598-020-59790-x.
- [188] H. Shin, S. D. Blackburn, A. M. Intlekofer, C. Kao, J. M. Angelosanto, S. L. Reiner, and E. J. Wherry. A role for the transcriptional repressor blimp-1 in cd8+ t cell exhaustion during chronic viral infection. *Immunity*, 31:309–320, 8 2009. ISSN 10747613. doi: 10.1016/j.immuni.2009.06.019.
- [189] I. Siddiqui, K. Schaeuble, V. Chennupati, S. A. F. Marraco, S. Calderon-Copete, D. P. Ferreira, S. J. Carmona, L. Scarpellino, D. Gfeller, S. Pradervand, S. A. Luther,

## 6 REFERENCES

---

- D. E. Speiser, and W. Held. Intratumoral tcf1 + pd-1 + cd8 + t cells with stem-like properties promote tumor control in response to vaccination and checkpoint blockade immunotherapy. *Immunity*, 50:195–211.e10, 1 2019. ISSN 10974180. doi: 10.1016/j.immuni.2018.12.021.
- [190] D. R. Simeonov and A. Marson. Crispr-based tools in immunity. 2019. doi: 10.1146/annurev-immunol-042718. URL <https://doi.org/10.1146/annurev-immunol-042718->.
- [191] D. R. Simeonov, B. G. Gowen, M. Boontanrart, T. L. Roth, J. D. Gagnon, M. R. Mumbach, A. T. Satpathy, Y. Lee, N. L. Bray, A. Y. Chan, D. S. Lituiev, M. L. Nguyen, R. E. Gate, M. Subramaniam, Z. Li, J. M. Woo, T. Mitros, G. J. Ray, G. L. Curie, N. Naddaf, J. S. Chu, H. Ma, E. Boyer, F. V. Gool, H. Huang, R. Liu, V. R. Tobin, K. Schumann, M. J. Daly, K. K. Farh, K. M. Ansel, C. J. Ye, W. J. Greenleaf, M. S. Anderson, J. A. Bluestone, H. Y. Chang, J. E. Corn, and A. Marson. Discovery of stimulation-responsive immune enhancers with crispr activation. *Nature*, 549:111–115, 9 2017. ISSN 14764687. doi: 10.1038/nature23875.
- [192] Y. Simoni, E. Becht, M. Fehlings, C. Y. Loh, S. L. Koo, K. W. W. Teng, J. P. S. Yeong, R. Nahar, T. Zhang, H. Kared, K. Duan, N. Ang, M. Poidinger, Y. Y. Lee, A. Larbi, A. J. Khng, E. Tan, C. Fu, R. Mathew, M. Teo, W. T. Lim, C. K. Toh, B. H. Ong, T. Koh, A. M. Hillmer, A. Takano, T. K. H. Lim, E. H. Tan, W. Zhai, D. S. Tan, I. B. Tan, and E. W. Newell. Bystander cd8+t cells are abundant and phenotypically distinct in human tumour infiltrates. *Nature*, 557:575–579, 2018. ISSN 14764687. doi: 10.1038/s41586-018-0130-2.
- [193] A. H. Smits, F. Ziebell, G. Joberty, N. Zinn, W. F. Mueller, S. Clauder-Münster, D. Eberhard, M. F. Savitski, P. Grandi, P. Jakob, A. M. Michon, H. Sun, K. Tessmer, T. Bürckstümmer, M. Bantscheff, L. M. Steinmetz, G. Drewes, and W. Huber. Biological plasticity rescues target activity in crispr knock outs. *Nature Methods*, 16: 1087–1093, 11 2019. ISSN 15487105. doi: 10.1038/s41592-019-0614-5.
- [194] E. A. Stadtmauer, J. A. Fraietta, M. M. Davis, A. D. Cohen, K. L. Weber, E. Lancaster, P. A. Mangan, I. Kulikovskaya, M. Gupta, F. Chen, L. Tian, V. E. Gonzalez, J. Xu, I. young Jung, J. J. Melenhorst, G. Plesa, J. Shea, T. Matlawski, A. Cervini, A. L. Gaymon, S. Desjardins, A. Lamontagne, J. Salas-Mckee, A. Fesnak, D. L. Siegel, B. L.

- Levine, J. K. Jadowsky, R. M. Young, A. Chew, W. T. Hwang, E. O. Hexner, B. M. Carreno, C. L. Nobles, F. D. Bushman, K. R. Parker, Y. Qi, A. T. Satpathy, H. Y. Chang, Y. Zhao, S. F. Lacey, and C. H. June. Crispr-engineered t cells in patients with refractory cancer. *Science*, 367, 2 2020. ISSN 10959203. doi: 10.1126/science.aba7365.
- [195] H. Sung, J. Ferlay, R. L. Siegel, M. Laversanne, I. Soerjomataram, A. Jemal, and F. Bray. Global cancer statistics 2020: Globocan estimates of incidence and mortality worldwide for 36 cancers in 185 countries. *CA: A Cancer Journal for Clinicians*, 71: 209–249, 5 2021. ISSN 0007-9235. doi: 10.3322/caac.21660.
- [196] P. A. Szabo, H. M. Levitin, M. Miron, M. E. Snyder, T. Senda, J. Yuan, Y. L. Cheng, E. C. Bush, P. Dogra, P. Thapa, D. L. Farber, and P. A. Sims. Single-cell transcriptomics of human t cells reveals tissue and activation signatures in health and disease. *Nature Communications*, 10, 12 2019. ISSN 20411723. doi: 10.1038/s41467-019-12464-3.
- [197] A. Tarasov, A. J. Vilella, E. Cuppen, I. J. Nijman, and P. Prins. Sambamba: fast processing of ngs alignment formats. doi: 10.5281/zenodo.13200. URL <http://picard.sourceforge.net/>.
- [198] S. Technologies. Genome editing with direct cas9 rnp delivery design considerations, 2018. URL <https://www.stemcell.com/design-considerations-for-the-arcitect-crispr-cas9-genome-editing-system.html>.
- [199] P. I. Thakore, A. M. D’Ippolito, L. Song, A. Safi, N. K. Shivakumar, A. M. Kabadi, T. E. Reddy, G. E. Crawford, and C. A. Gersbach. Highly specific epigenome editing by crispr-cas9 repressors for silencing of distal regulatory elements. *Nature Methods*, 12:1143–1149, 12 2015. ISSN 15487105. doi: 10.1038/nmeth.3630.
- [200] L. Thomas. On immunosurveillance in human cancer. *Yale Journal of Biology and Medicine*, 55:329–333, 1982.
- [201] D. D. Thommen, V. Koelzer, P. Herzig, A. Roller, M. Trefny, A. Kiialainen, J. Hanhart, C. Schill, C. Hess, S. S. Prince, M. Wiese, D. Lardinois, P. Ho, C. Klein, V. Karanikas, K. Mertz, T. Schumacher, and A. Zippelius. A transcriptionally and functionally distinct pd-1 + cd8 + t cell pool with predictive potential in non-small cell lung cancer treated with pd-1 blockade. *Nature Medicine*, 2018. ISSN 1078-8956. doi: 10.1038/s41591-018-0057-z. URL <http://dx.doi.org/10.1038/s41591-018-0057-z>.

## 6 REFERENCES

---

- [202] D. S. Thommen. The first shall (be) last: Understanding durable t cell responses in immunotherapy, 1 2019. ISSN 10974180.
- [203] S. L. Topalian, C. G. Drake, and D. M. Pardoll. Immune checkpoint blockade: A common denominator approach to cancer therapy. *Cancer Cell*, 27:451–461, 2015.
- [204] M. Trebak and J. P. Kinet. Calcium signalling in t cells, 3 2019. ISSN 14741741.
- [205] G. Ureña-Bailén, A. Lamsfus-Calle, A. Daniel-Moreno, J. Raju, P. Schlegel, C. Seitz, D. Atar, J. S. Antony, R. Handgretinger, and M. Mezger. Crispr/cas9 technology: Towards a new generation of improved car-t cells for anticancer therapies. *Briefings in Functional Genomics*, 19:191–200, 5 2020. ISSN 20412657. doi: 10.1093/bfgp/elz039.
- [206] D. T. Utzschneider, S. S. Gabriel, D. Chisanga, R. Gloury, P. M. Gubser, A. Vasanthakumar, W. Shi, and A. Kallies. Early precursor t cells establish and propagate t cell exhaustion in chronic infection. *Nature Immunology*, 21:1256–1266, 10 2020. ISSN 15292916. doi: 10.1038/s41590-020-0760-z.
- [207] G. Vahedi, Y. Kanno, Y. Furumoto, K. Jiang, S. C. Parker, M. R. Erdos, S. R. Davis, R. Roychoudhuri, N. P. Restifo, M. Gadina, Z. Tang, Y. Ruan, F. S. Collins, V. Sartorelli, and J. J. O’Shea. Super-enhancers delineate disease-associated regulatory nodes in t cells. *Nature*, 520:558–562, 4 2015. ISSN 14764687. doi: 10.1038/nature14154.
- [208] D. vanDijk, R. Sharma, J. Nainys, K. Yim, P. Kathail, A. J. Carr, C. Burdziak, K. R. Moon, C. L. Chaffer, D. Pattabiraman, B. Bieri, L. Mazutis, G. Wolf, S. Krishnaswamy, and D. Pe’er. Recovering gene interactions from single-cell data using data diffusion. *Cell*, 174:716–729.e27, 7 2018. ISSN 10974172. doi: 10.1016/j.cell.2018.05.061.
- [209] S. A. Vardhana, M. A. Hwee, M. Berisa, D. K. Wells, K. E. Yost, B. King, M. Smith, P. S. Herrera, H. Y. Chang, A. T. Satpathy, M. R. van den Brink, J. R. Cross, and C. B. Thompson. Impaired mitochondrial oxidative phosphorylation limits the self-renewal of t cells exposed to persistent antigen. *Nature Immunology*, 21:1022–1033, 9 2020. ISSN 15292916. doi: 10.1038/s41590-020-0725-2.
- [210] S. Venkatesh and J. L. Workman. Histone exchange, chromatin structure and the regulation of transcription, 3 2015. ISSN 14710080.
- [211] M. D. Vesely, M. H. Kershaw, R. D. Schreiber, and M. J. Smyth. Natural innate and adaptive immunity to cancer. *Annual review of immunology*, 29:235–271, 2011.

- [212] M. VonGamm, A. Schaub, A. N. Jones, C. Wolf, G. Behrens, J. Lichti, K. Essig, A. Macht, J. Pircher, A. Ehrlich, K. Davari, D. Chauhan, B. Busch, W. Wurst, R. Feederle, A. Feuchtinger, M. H. Tschöp, C. C. Friedel, S. M. Hauck, M. Sattler, A. Geerlof, V. Hornung, V. Heissmeyer, C. Schulz, M. Heikenwalder, and E. Glasmacher. Immune homeostasis and regulation of the interferon pathway require myeloid-derived regnase-3. *Journal of Experimental Medicine*, 216:1700–1723, 2019. ISSN 15409538. doi: 10.1084/jem.20181762.
- [213] C. H. Waddington. Canalization of development and the inheritance of acquired characters. *Nature*, 1942.
- [214] C. H. Waddington. The epigenotype. 1942. *International journal of epidemiology*, 41: 10–13, 2 2012. ISSN 14643685. doi: 10.1093/ije/dyr184.
- [215] J. Wang, H. Sun, Q. Zeng, X. J. Guo, H. Wang, H. H. Liu, and Z. Y. Dong. Hpv-positive status associated with inflamed immune microenvironment and improved response to anti-pd-1 therapy in head and neck squamous cell carcinoma. *Scientific Reports*, 9, 12 2019. ISSN 20452322. doi: 10.1038/s41598-019-49771-0.
- [216] E. W. Weber, M. V. Maus, and C. L. Mackall. The emerging landscape of immune cell therapies, 4 2020. ISSN 10974172.
- [217] E. W. Weber, K. R. Parker, E. Sotillo, R. C. Lynn, H. Anbunathan, J. Lattin, Z. Good, J. A. Belk, B. Daniel, D. Klysz, M. Malipatlolla, P. Xu, M. Bashti, S. Heitzeneder, L. Labanieh, P. Vandriss, R. G. Majzner, Y. Qi, K. Sandor, L. C. Chen, S. Prabhu, A. J. Gentles, T. J. Wandless, A. T. Satpathy, H. Y. Chang, and C. L. Mackall. Transient rest restores functionality in exhausted car-t cells through epigenetic remodeling. *Science*, 372, 4 2021. ISSN 10959203. doi: 10.1126/science.aba1786.
- [218] E. J. Wherry and M. Kurachi. Molecular and cellular insights into t cell exhaustion, 8 2015. ISSN 14741741.
- [219] W. A. Whyte, D. A. Orlando, D. Hnisz, B. J. Abraham, C. Y. Lin, M. H. Kagey, P. B. Rahl, T. I. Lee, and R. A. Young. Master transcription factors and mediator establish super-enhancers at key cell identity genes. *Cell*, 153:307–319, 4 2013. ISSN 10974172. doi: 10.1016/j.cell.2013.03.035.
- [220] M. Xydia, R. Rahbari, E. Ruggiero, I. Macaulay, M. Tarabichi, R. Lohmayer, S. Wilkening, T. Michels, D. Brown, S. Vanuytven, S. Mastitskaya, S. Laidlaw, N. Grabe,

## 6 REFERENCES

---

- M. Pritsch, R. Fronza, K. Hexel, S. Schmitt, M. Müller-Steinhardt, N. Halama, C. Domschke, M. Schmidt, C. von Kalle, F. Schütz, T. Voet, and P. Beckhove. Common clonal origin of conventional t cells and induced regulatory t cells in breast cancer patients. *Nature Communications*, 12, 12 2021. ISSN 20411723. doi: 10.1038/s41467-021-21297-y.
- [221] T. Yamauchi, T. Hoki, T. Oba, V. Jain, H. Chen, K. Attwood, S. Battaglia, S. George, G. Chatta, I. Puzanov, C. Morrison, K. Odunsi, B. H. Segal, G. K. Dy, M. S. Ernststoff, and F. Ito. T-cell cx3cr1 expression as a dynamic blood-based biomarker of response to immune checkpoint inhibitors. *Nature Communications*, 12, 12 2021. ISSN 20411723. doi: 10.1038/s41467-021-21619-0.
- [222] F. Yan, D. R. Powell, D. J. Curtis, and N. C. Wong. From reads to insight: A hitchhiker's guide to atac-seq data analysis, 2 2020. ISSN 1474760X.
- [223] R. Yang, S. Cheng, N. Luo, R. Gao, K. Yu, B. Kang, L. Wang, Q. Zhang, Q. Fang, L. Zhang, C. Li, A. He, X. Hu, J. Peng, X. Ren, and Z. Zhang. Distinct epigenetic features of tumor-reactive cd8+ t cells in colorectal cancer patients revealed by genome-wide dna methylation analysis. *Genome Biology*, 21, 12 2019. ISSN 1474760X. doi: 10.1186/s13059-019-1921-y.
- [224] T. Yao, P. Shooshtari, and S. M. Haeryfar. Leveraging public single-cell and bulk transcriptomic datasets to delineate mait cell roles and phenotypic characteristics in human malignancies. *Frontiers in Immunology*, 11, 7 2020. ISSN 16643224. doi: 10.3389/fimmu.2020.01691.
- [225] J. H. Yearley, C. Gibson, N. Yu, C. Moon, E. Murphy, J. Juco, J. Lunceford, J. Cheng, L. Q. M. Chow, T. Y. Seiwert, M. Handa, J. E. Tomassini, and T. McClanahan. Pd-l2 expression in human tumors: Relevance to anti-pd-1 therapy in cancer. *Clinical Cancer Research*, 23:3158–3167, 2017.
- [226] K. E. Yost, A. T. Satpathy, D. K. Wells, Y. Qi, C. Wang, R. Kageyama, K. L. McNamara, J. M. Granja, K. Y. Sarin, R. A. Brown, R. K. Gupta, C. Curtis, S. L. Bucktrout, M. M. Davis, A. L. S. Chang, and H. Y. Chang. Clonal replacement of tumor-specific t cells following pd-1 blockade. *Nature Medicine*, 25:1251–1259, 8 2019. ISSN 1546170X. doi: 10.1038/s41591-019-0522-3.
- [227] M. D. Young, T. J. Mitchell, F. A. V. Braga, M. G. B. Tran, B. J. Stewart, J. R. Fer-

- dinand, G. Collord, R. A. Botting, D.-M. Popescu, K. W. Loudon, R. Vento-Tormo, E. Stephenson, A. Cagan, S. J. Farndon, M. D. C. Velasco-Herrera, C. Guzzo, N. Richez, L. Mamanova, T. Aho, J. N. Armitage, A. C. P. Riddick, I. Mushtaq, S. Farrell, D. Rampling, J. Nicholson, A. Filby, J. Burge, S. Lisgo, P. H. Maxwell, S. Lindsay, A. Y. Warren, G. D. Stewart, N. Sebire, N. Coleman, M. Haniffa, S. A. Teichmann, M. Clatworthy, and S. Behjati. Single-cell transcriptomes from human kidneys reveal the cellular identity of renal tumors. URL <http://science.sciencemag.org/>.
- [228] M. M. Zhan. From monoclonal antibodies to small molecules: The development of inhibitors targeting the pd-1/pd-l1 pathway. *Drug Discovery Today*, 21:1027–1036, 2016.
- [229] Y. Zhang, T. Liu, C. A. Meyer, J. Eeckhoute, D. S. Johnson, B. E. Bernstein, C. Nussbaum, R. M. Myers, M. Brown, W. Li, and X. S. Shirley. Model-based analysis of chip-seq (macs). *Genome Biology*, 9, 9 2008. ISSN 14747596. doi: 10.1186/gb-2008-9-9-r137.
- [230] Y. Zhang, H. Chen, H. Mo, X. Hu, R. Gao, Y. Zhao, B. Liu, L. Niu, X. Sun, X. Yu, Y. Wang, Q. Chang, T. Gong, X. Guan, T. Hu, T. Qian, B. Xu, F. Ma, Z. Zhang, and Z. Liu. Single-cell analyses reveal key immune cell subsets associated with response to pd-l1 blockade in triple-negative breast cancer. *Cancer cell*, 10 2021. ISSN 1878-3686. doi: 10.1016/j.ccell.2021.09.010. URL <http://www.ncbi.nlm.nih.gov/pubmed/34653365>.
- [231] C. Zheng, L. Zheng, J. K. Yoo, H. Guo, Y. Zhang, X. Guo, B. Kang, R. Hu, J. Y. Huang, Q. Zhang, Z. Liu, M. Dong, X. Hu, W. Ouyang, J. Peng, and Z. Zhang. Landscape of infiltrating t cells in liver cancer revealed by single-cell sequencing. *Cell*, 169:1342–1356.e16, 6 2017. ISSN 10974172. doi: 10.1016/j.cell.2017.05.035.
- [232] L. Zheng, S. Qin, W. Si, A. Wang, B. Xing, R. Gao, X. Ren, L. Wang, X. Wu, J. Zhang, N. Wu, N. Zhang, H. Zheng, H. Ouyang, K. Chen, Z. Bu, X. Hu, J. Ji, and Z. Zhang. Pan-cancer single-cell landscape of tumor-infiltrating t cells. *Science*, 374, 12 2021. ISSN 0036-8075. doi: 10.1126/science.abe6474. URL <https://www.science.org/doi/10.1126/science.abe6474>.
- [233] B. H. Zinselmeyer, S. Heydari, C. Sacristán, D. Nayak, M. Cammer, J. Herz, X. Cheng, S. J. Davis, M. L. Dustin, and D. B. McGavern. Pd-1 promotes immune exhaustion by

## 6 REFERENCES

---

inducing antiviral t cell motility paralysis. *Journal of Experimental Medicine*, 210:757–774, 2013. ISSN 00221007. doi: 10.1084/jem.20121416.

# 7 Appendix

## 7.1 List of Abbreviations

Activation Induced Cell Death	AICD
Antigen Presenting Cells	APCs
Assay for Transposase-Accessible Chromatin using sequencing	ATAC-seq
Basal Cell Carcinoma	BCC
Chimeric Antigen Receptor T cells	CAR T cells
Chromatin immunoprecipitation	ChIP
Clear Cell Renal Cell Carcinoma	ccRCC
Cluster of Differentiation	CD
Colorectal Carcinoma	CRC
Clustered Regularly Interspaced Short Palindromic Repeats	CRISPR
CRISPR associated protein 9	Cas9
CRISPR RNA	crRNAs
Cycle threshold	ct
Cytotoxic T-lymphocyte-associated protein 4	CTLA4
Cytotoxic T lymphocytes	CTLs
DNase I hypersensitive sites sequencing	DNase-seq
Fluorescence-Activated Cell Sorting	FACS
Fluorescence Minus One	FMO
United States Food and Drug Administration	FDA
Fraction of Reads in Peaks	FRIP
Gene Regulatory Element	GRE

## 7. APPENDIX

---

Hepatocellular Carcinoma	HCC
Homology Directed Repair	HDR
Head and Neck Squamous Cell Carcinoma	HNSCC
Human Papillomavirus	HPV
Heat Shock Factor 1	HSF1
Heat Shock Protein	HSP
Immune checkpoint blockade	ICB
Immune checkpoint therapy	ICT
INsertion or DELetions	INDELs
Immunotherapy	IT
Lymphocyte-activation gene 3	LAG3
Lymphocytic choriomeningitis virus	LCMV
Lymphoid Enhancer Binding Factor 1	LEF1
Mucosa associated invariant T cells	MAIT cells
Melanoma-associated antigen recognized by T cells	MART-1
Myeloid derived suppressor cells	MDSCs
Major histocompatibility complex	MHC
Micrococcal nuclease digestion with deep sequencing	MNase-seq
messenger RNA	mRNA
Nuclear factor of activated T cells	NFAT
Non-homologous end joining	NHEJ
Nuclear receptor subfamily 4	NR4A
Protospacer-Adjacent Motifs	PAMs
Peripheral blood mononuclear cell	PBMC
Programmed death-ligand 1	PD-L1
Programmed death-ligand 2	PD-L2
Programmed cell death protein 1	PD1
Reverse crosslinking buffer	RCB
Renal Cell Carcinoma	RCC
Ribonucleoprotein complex	RNP

Reactive oxygen species	ROS
Single-cell ATAC-seq	scATAC-seq
Squamous Cell Carcinoma	SCC
Single-cell RNA sequencing	scRNA-seq
T-box	Tbx
T cell factor 1	TCF1
T cell receptor	TCRs
Transcription factor	TF
Tumor-infiltrating lymphocyte	TIL
T-cell immunoglobulin and mucin-domain containing-3	TIM3
Tumor microenvironment	TME
Thymocyte selection-associated high mobility group box protein	TOX
Trans-activating RNA	tracrRNA
Regulatory T cells	Tregs
Transcription start site	TSS
Uniform Manifold Approximation and Projection	UMAP
Vitamin D receptor	VDR

## 7.2 List of Units

°C	degree Celcius
g	gram or gravitational acceleration (9.80665 m/s <sup>2</sup> )
h	hour
min	minute
s	second
l	liter
m	meter
M	molar concentration in mol l <sup>-1</sup>
t	time
T	temperature

## 7.3 List of Dimensions

k	kilo (10 <sup>3</sup> )
m	milli (10 <sup>-3</sup> )
μ	micro (10 <sup>-6</sup> )
n	nano (10 <sup>-9</sup> )
p	pico (10 <sup>-12</sup> )
f	femto (10 <sup>-15</sup> )

## 7.4 List of Figures

2.1	The hallmarks of cancer . . . . .	6
2.2	The cancer immunity cycle . . . . .	8
2.3	Differentiation models of CD8+ TILs . . . . .	11
2.4	Model of epigenetic regulation of T cell dysfunction . . . . .	13
2.5	Schematic of immune checkpoint therapy . . . . .	15
2.6	CAR T cell therapy . . . . .	17
2.7	Epigenetic mechanisms driving T cell dysfunction . . . . .	21
2.8	Representative workflow and output of plate-based single cell ATAC-seq . . .	24
2.9	Schematic of genome editing via CRISPR/Cas9 . . . . .	26
3.1	Gating strategy . . . . .	47
4.1	Establishment of plate-based scATAC-seq . . . . .	66
4.2	Study setup . . . . .	68
4.3	Comparison of scATAC-seq protocols . . . . .	69
4.4	Quality control and filter application of scATAC-seq data . . . . .	70
4.5	Sorting strategy . . . . .	71
4.6	Functional characterization of patient samples . . . . .	72
4.7	Phenotypical characterization of patient samples . . . . .	73
4.8	Clustering and UMAP embedding of all single-cell chromatin profiles . . . . .	75
4.9	Cluster identification via gene activity of marker genes . . . . .	76
4.10	Cluster identification via projection of published signatures . . . . .	78
4.11	Variability of chromatin accessibility among T cell states . . . . .	80
4.12	Differential TF motif accessibility between T cell states . . . . .	81
4.13	Detection of tissue-specific TF motifs . . . . .	83
4.14	Entity-harmonized analysis of the TIL chromatin landscape . . . . .	86
4.15	Evaluation of developmental relationship between cell states . . . . .	88
4.16	Entity-shared core trajectory to terminal CD8 <sup>+</sup> TIL dysfunction . . . . .	90
4.17	Selection of putative target genes . . . . .	92
4.18	Table of putative target genes . . . . .	93

## 7. APPENDIX

---

4.19 Chromatin accessibility and expression of exhaustion markers . . . . .	95
4.20 Chromatin accessibility at target loci and expression of targets VDR and EOS	96
4.21 Workflow of CRISPR/Cas9 in TIL209 using the Neon™ or the Nucleofector™	98
4.22 Test of CRISPR conditions using the Neon™ . . . . .	99
4.23 Target KO using the Neon™ . . . . .	100
4.24 Test of 4D-Nucleofector™ conditions and comparison with Neon™ . . . . .	101
4.25 Evaluation of gRNA performance . . . . .	102
4.26 Methods of KO evaluation . . . . .	104
4.27 Ca <sup>2+</sup> flux measurement in genome edited TIL209 . . . . .	106
4.28 Real-time cytotoxicity assay to analyze killing capacity of genome edited TIL209	108
4.29 VDR and EOS staining in primary TILs from HCC and RCC patients . . . . .	110

## 7.5 List of Tables

3.1	Laboratory consumables . . . . .	29
3.2	Laboratory equipment . . . . .	30
3.3	Reagents, chemicals and media . . . . .	31
3.4	Buffer and media . . . . .	34
3.5	Cell lines . . . . .	35
3.6	Primary human samples . . . . .	35
3.7	Antibodies . . . . .	36
3.8	Fluorescent molecules . . . . .	38
3.9	Kits . . . . .	38
3.10	Oligonucleotides . . . . .	39
3.11	Software and algorithms . . . . .	41

## 7.6 Acknowledgments

In the first place, I want to express my gratitude to my group leader and 'real' supervisor Christian Schmidl. He gave me the chance to work on this exciting project, and even though I experienced tough times in the lab, he did not stop to believe in my skills. He gave me the opportunity to get at least a glimpse into bioinformatic analysis. The discussions with you and the excitement for science you always show inspired me. Thank you for all your input, your highly valued help and last but not least for revising my thesis. Further, I want to thank my supervisor Michael Rehli for giving valuable input to the project and helping with sequencing problems, demultiplexing and ChIP establishment. Thank you for your time and support! I would like to thank Hinrich Abken for being my examiner and for all the interesting insights into the CAR world. Thank you Gernot Längst for mentoring my PhD project, for being my examiner and for all the valuable input you added to the project. Moreover, I want to thank Udo Gaipf, who was my Master's Thesis supervisor and my mentor during my time as a PhD student. He started to nourish my interest in cancer immunotherapy and gave me the confidence to actually start a PhD.

I further wish to thank the patients who generously provided their samples and made this project possible in the first place. In addition, I want to thank Peter Siska, Jens Werner, Ines Ugele and Katrin Singer for sharing the precious patient samples with us. I am grateful for the collaboration and the discussions.

Furthermore, I want to thank the NGS core team members, especially Johanna, Nick and Claudia for their help with sequencing and demultiplexing. I also want to give credits to the members of the sorting facility, especially to Irina and Rüdiger who spend many hours to sort my cells and did a great job there.

Of course I will never forget the hearty welcome Manu and Brigitte gave me. I loved the time with you in the lab and outside the lab, all the laughter and your funny stories made my time with you memorable. I also would like to thank Lukas for his help and for starting the CRISPR adventure together with me in our lab. Many hours would have been really boring without your black humor. Of course I want to thank our Spanish and Italian sunshines Elena and Marianna, not only for their great food, but also for lively discussions inside the lab and much fun outside the lab. A big thank you to Meike, my lovely Bachelor's student! Your help

and your funny stories were very appreciated and helped me through the ups and downs of CRISPR experiments. I would like to thank the whole immunology group for a great time with you and for always helping me whenever I needed support. Christina, Kathrin, Sandra and Severin I am so happy to have met you and to have you as my friends. Thank you for all adventures I already experienced with you, and for your patience with my bavarian skills ;) Further, I would like to thank Susanne from AG Jantsch who helped me with the  $\text{Ca}^{2+}$  flux experiments, and Ayse and Julian who helped me with the Incucyte analysis software. Of course I want to thank my beloved parents, my sisters (I love you), my grandma Mimi, my partners family and all my friends for being there, for believing in me and supporting me whenever I needed it. Last but not least I want to thank my partner Manuel. Thank you for your love, your constant support, trust and patience (and for your help with a couple of LateX problems ;)).

Vielen Dank für all eure Unterstützung und für die schöne Zeit!